UNIVERSIDAD NACIONAL AUTÓNOMA DE MÉXICO
Posgrado en Ciencia e Ingeniería de Materiales

SYNTHESIS OF HYBRID MATERIALS DERIVED FROM ORGANOSILICATE PRECURSORS

TESIS

QUE PARA OPTAR POR EL GRADO DE
DOCTOR EN CIENCIA E INGENIERÍA DE MATERIALES

PRESENTA:
MIRIAM DE JESÚS VELÁSQUEZ HERNÁNDEZ

TUTOR PRINCIPAL
DR. VOJTECH JANCIK
INSTITUTO DE QUÍMICA

MIEMBROS DEL COMITÉ TUTOR

DR. HERIBERTO PFEIFFER PEREA
INSTITUTO DE INVESTIGACIONES EN MATERIALES

DR. EDILSO REGUERA RUIZ
CICATA-IPN

CIUDAD UNIVERSITARIA, CIUDAD DE MÉXICO, ENERO 2018

Universidad Nacional Autónoma de México

Centro Conjunto de Investigación en Química Sustentable
UAEM-UNAM

Posgrado en Ciencia e Ingeniería de Materiales

SYNTHESIS OF HYBRID MATERIALS DERIVED FROM ORGANOSILICATE PRECURSORS

T H E S I S

SUBMITTED TO ATTAIN THE DEGREE OF
DOCTOR IN MATERIALS SCIENCE AND ENGINEERING

PRESENTED BY

Miriam de Jesús Velásquez Hernández

supervisor
Dr. Vojtech Jancik

supervisor commitee

Dr. Heriberto Pfeiffer Perea   Dr. Edilso Reguera Ruiz

Ciudad de México   January, 2018

SYNTHESIS OF HYBRID MATERIALS DERIVED FROM ORGANOSILICATE PRECURSORS

by

Miriam de Jesús Velásquez Hernández

Thesis submitted to attain the degree of

DOCTOR IN MATERIALS SCIENCE AND ENGINEERING

at the

CENTRO CONJUNTO DE INVESTIGACIÓN EN QUÍMICA SUSTENTABLE
UAEM-UNAM

UNIVERSIDAD NACIONAL AUTÓNOMA DE MÉXICO

Ciudad de México. January, 2018

Este trabajo está dedicado a mis padres y mis abuelos;
los cuales han sido un claro ejemplo
de pasión, entrega y sabiduría
para alcanzar el éxito en la vida.

. . . Sometido a los golpes del destino
mi cabeza está ensangrentada, pero erguida.
. . . No importa cuán estrecho sea el portal,
cuán cargada de castigos la sentencia,
Soy el amo de mi destino;
Soy el capitán de mi alma.
— WILLIAM ERNEST HENLEY

Acknowledgements

Contents

List of Figures

List of Tables

List of Abbreviations

AcO$^-$	—	Acetate
ASA	—	Acetoxysilylalkoxide
Ar	—	Aryl
ATR	—	Attenuated total reflectance
Calcd	—	Calculated
δ	—	Chemical shift
COFs	—	Covalent-organic frameworks
dec	—	Decomposition
DABCO	—	1,4-diazabicyclo[2.2.2]ocatne
DMSO	—	Dimethyl sulfoxide
DFT	—	Density functional theory
D4R	—	Double four ring
d	—	Doublet
dq	—	Doublet of quartets
EI-MS	—	Electron ionization mass spectroscopy
equiv	—	Equivalent
EtO	—	Ethoxy
Et	—	Ethyl
FT	—	Fourier transform
GC-MS	—	Gas chromatography mass spectrometry
X	—	Halogen

h	—	hours
HBD	—	hydrogen-bond donor
HOFs	—	Hydrogen-bonded organic frameworks
HB	—	Hydrogen-bonding
IR	—	Infrared
m/z	—	Mass-to-charge ratio
M.p.	—	Melting point
MOFs	—	Metal-organic frameworks
MeO	—	Methoxy
Me	—	Methyl
min	—	Minutes
m	—	Multiplet
nBuO	—	n-Butoxy
nPrO	—	n-Propoxy
NMR	—	Nuclear magnetic resonance
ORMOSILs	—	Organically Modified Silicates
ppm	—	Parts per million
Ph	—	Phenyl
POSS	—	Polyhedral oligomeric silsesquioxanes
PXRD	—	Powder X-ray diffraction
QTAIM	—	Quantum theory atoms in molecules
SCXRD	—	Single crystal X-ray diffraction
s	—	Singlet
SC	—	Styrene carbonate
SO	—	Styrene oxide
t-BuOH	—	$tert$-Butanol
TADDOL	—	(4R,5R)-2,2-dimethyl-$\alpha, \alpha, \alpha', \alpha'$-tetraphenyldioxolane-4,5-dimethanol
TBAI	—	Tetrabutylammonium iodide
THF	—	Tetrahydrofuran
TMS	—	Tetramethylsilane

TGA	—	Thermogravimetric analysis
3D	—	Three dimensional
4,4'-bpe	—	4,4'-vinylenedipyridine
t	—	Triplet
2D	—	Two dimensional
$\tilde{\nu}$	—	Wave number
w	—	Weak
0D	—	Zero dimensional

Declaration

I hereby declare that the dissertation entitled **Synthesis of Hybrid Materials Derived From Organosilicate Precursors** is a bonafide record of the research work carried out by me with the assistance of Dr. Aaron Torres Huerta, who synthesized the majority of borosilicate compounds, and he also contributed actively in the synthesis of some organosilanol compounds. Additionally, this work was developed under the supervision and guidance of Prof. Dr. Vojtech Jancik; in the laboratory of Inorganic Chemistry 1, at the Centro Conjunto de Investigación en Química Sustentable UAEM-UNAM. The results presented herein are original, and they have not been submitted earlier in any other institution for the award of a degree diploma or title.

I also declare that the results included in this thesis has been published in two indexed journals. Moreover, these results were presented at the following national and international conferences:

1. 20th International Symposium on Homogeneous Catalysis (ISHCXX), which was held from 10th to 15th July 2016 in Kyoto, Japan.

2. 51st Annual meeting of the Mexican Society of Chemistry A. C. (Pachuca 2016)

3. Internal symposium of the CCIQS UAEM-UNAM.

Signature

_____
Miriam de Jesús Velásquez Hernández

List of compounds

Organosilyl derivatives
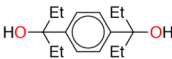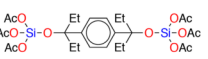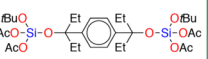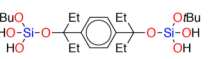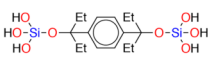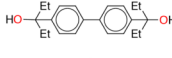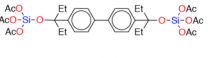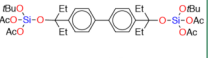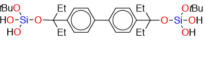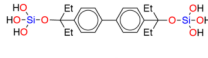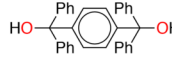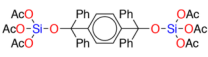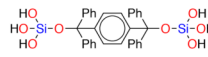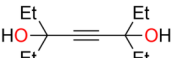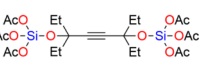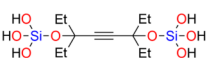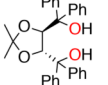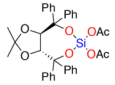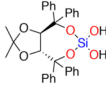
Alcohol	bis(triacetoxysilyl) alkoxides	bis(diacetoxysilyl) alkoxides	Organo(bis-silanediols)	Organo(bis-silanetriols)
1	BTA1	BDA1	D1	T1
2	BTA2	BDA2	D2	T2
3	BTA3			T3
4	BTA4			T4
	mono(triacetoxysilyl) alkoxides	mono(diacetoxysilyl) alkoxides	Organo (mono-silanediols)	Organo (mono-silanetriols)
5	MTA5	MDA5	D5	T5
6	MDA6		D6	

Figure 0.1. List of compounds Chapter 2

Hydrogen-bonded organic frameworks (HOFs)
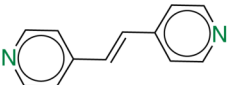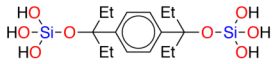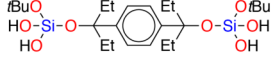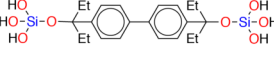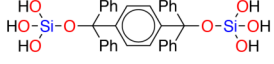
	1,4-diazabicyclo[2.2.2]octane DABCO (**a**)	trans-1,2-Bis(4-pyridyl)ethylene 4,4'-bpe (**b**)
HT1a compound	**HT1a**	**HT1b**
HD1a compound	**HD1a**	**HD1b**
HT2a compound	**HT2a**	**HT2b**
HT3b compound		**HT3b**

Figure 0.2. List of compounds Chapter 3

Cyclic and cage borosilicates

BS1 **BS2** **BS3** **BS4** **BS5**
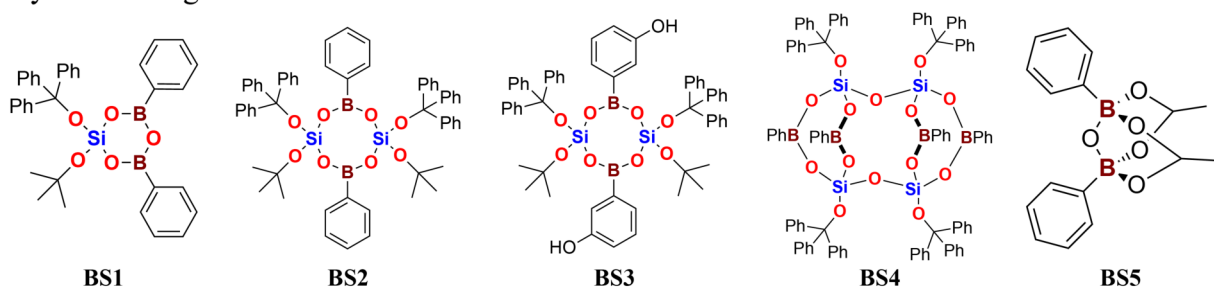
Figure 0.3. List of compounds Chapter 4

SYNTHESIS OF HYBRID MATERIALS DERIVED FROM ORGANOSILICATE PRECURSORS

by

Miriam de Jesús Velásquez Hernández

Abstract

Single-source molecular precursors based on organosilanols have attracted a new wave of interest due to their synergistic properties, which arise from the adjustable organic moiety and the remarkable hydrogen-bonding (HB) capabilities of the Si–OH groups. Such features make them attractive candidates as discrete building blocks for the *Bottom-up* synthesis of ordered hybrid organic-inorganic materials. Additionally, more recently, organosilanols have also been successfully applied as organocatalysts in the HB activation of nucleophiles. Nevertheless, the wider use of such compounds has been hampered by the lack of a cost-efficient and eco-friendly methodology for their synthesis; as well as their limited stability towards condensation.

In this context, the primary purpose of this study consists on the development of an alternative approach for the synthesis of molecular organosilylated precursors. Additionally, the performance of these precursors as organocatalysts in the synthesis of molecular models of hybrid borosilicate materials was explored. Thus, this dissertation is divided in three main sections.

The first part is focussed on the synthesis of acetoxysilylalkoxides (ASA), which are readily prepared by the reaction of $Si(OAc)_4$ in the presence of stoichiometric amounts of suitable bulky tertiary alcohol (**1**–**6**) to afford the corresponding acetoxysilylalkoxides $(AcO)_3Si–O–R–O–Si(OAc)_3$ (**BTA1** to **BTA4**), $(Ph_3CO)Si(OAc)_3$ (**MTA5**) and κ^2-O,O'-$(Si(OAc)_2)$-(*4R,5R*)-TADDOLate (**MDA6**). In the presence of one or two equivalents of *t*-BuOH, selected mono- and bis-triacetoxysilylalkoxides **MTA5**, **BTA1** and **BTA2**, respectively, are converted to the corresponding mono- and bis(diacetoxysilyl)alkoxides $(t$-BuO$)(Ph_3CO)Si(OAc)_2$ (**MDA5**) or $(AcO)_2(t$-BuO$)Si–O–R–O–Si(Ot$-Bu$)(OAc)_2$ (**BDA1** and **BDA2**, respectively). Subsequently, the ASA precursors were hydrolyzed in an aqueous medium to generate air-stable organosilanols with tailored hydrogen-bonding capabilities: $(HO)_{3-n}(t$-BuO$)_n$Si–O–R–O–Si(Ot-Bu$)_n(OH)_{3-n}$ (n = 0 for **T1** to **T4**; and n = 1 for **D1** and **D2**), $(t$-BuO$)_n(Ph_3CO)Si(OH)_{3-n}$ (n = 0 for **T5**; and n = 1 for **D5**) and κ^2-O,O'-$(Si(OH)_2)$-(*4R,5R*)-TADDOLate (**D6**).

Additionally, the hydrogen-bonding based organocatalytic performance of selected organosilanols **T1**, **D1**, **T5**, **D5** and **D6** in the cycloaddition of CO_2 to styrene oxide, in the presence of TBAI as co-catalyst was explored. Quantitative conversions and excellent selectivity under mild reaction conditions (60 °C and 1 atmosphere of CO_2) were observed, and these results reveal

how both, the steric and electronic environment of the silicate center, affect the organocatalytic efficiency of such precursors.

On the other hand, the second part of this thesis, takes further advantage of the HB capabilities of selected organosilanols, with an organic bridging group on the synthesis of hydrogen-bonded organic frameworks (HOFs) with supramolecular arrangements exhibiting 1D, 0D porosity or non-porous structures.

Such hybrid organic-inorganic materials were readily obtained by co-crystallization of the organosilanols $(HO)_{3-n}(t\text{-}BuO)_nSi\text{–}O\text{–}R\text{–}O\text{–}Si(Ot\text{-}Bu)_n(OH)_{3-n}$ (n = 0 for **T1**, **T2** and **T3**; n = 1 for **D1**) in the presence of two equivalents of rigid organic diamines such as DABCO (**a**) and 4,4'-bpe (**b**). These Lewis bases participate in highly directional SiO–H$\cdots$N interactions resulting in the formation of the corresponding hydrogen-bonded supramolecular networks with either 1:1 (**HT1b** and **HD1b**) or 2:1 (**HT1a**, **HD1a**, **HT2a**, **HT2b** and **HT3b**) diamine:alkoxysilanol stoichiometric ratio. This study revealed that the structural features exhibited by each HOF are determined by the relative basicity of the selected diamine, the size of the organic *spacer*, and the steric environment around the silicon center.

Finally, in the third part of this work, the known reactivity of the acetoxysilyl moieties Si–OAc toward reagents with OH groups, such as water and alcohols; prompted us to study the condensation reactions between phenylboronic acid derivatives and acetoxysilylalkoxides **MDA5** and **MTA5** affording the corresponding molecular borosilicates. Thus, the condensation of the phenylboronic or 3-hydroxyphenylboronic acid with diacetoxysilylalkoxide **MDA5** $(t\text{-}BuO)(Ph_3CO)Si(OAc)_2$ leads to the formation of borosilicates $(t\text{-}BuO)(Ph_3CO)Si\{(\mu\text{-}O)BPh\}_2$ $(\mu\text{-}O)$(**BS1**), $\{(t\text{-}BuO)(Ph_3CO)Si(\mu\text{-}O)BPh(\mu\text{-}O)\}_2$ (**BS2**), and $\{(t\text{-}BuO)(Ph_3CO) Si(\mu\text{-}O)B(3\text{-}HOPh)(\mu\text{-}O)\}_2$ (**BS3**), with cyclic inorganic B_2SiO_3 or $B_2Si_2O_4$ cores, respectively. On the other hand, the reaction of the phenylboronic acid with triacetoxysilylalkoxide $(Ph_3CO)Si(OAc)_3$ in 3:2 ratio resulted in the formation of a cage-like structure $\{(Ph_3CO)Si(\mu\text{-}O)_2BPh(\mu\text{-}O)\}_2$ (**BS4**) with $B_4Si_4O_{10}$ core. These molecules represent to the best of our knowledge the first examples of cyclic molecular borosilicates containing SiO_4 units.

On the basis of the results obtained in this thesis, it was found that the use of ASA precursors, offers a straightforward scalable and cost-efficient synthetic pathway towards the synthesis of organosilanols and borosilicate compounds. This pathway eliminates the main disadvantages of the current synthetic methods, such as large quantities of organic solvent, the use of a base, and long reaction times. Additionally, this allows a stepwise tuning of the steric and electronic environment of the silicate center. The precise control of the number of OH groups attached to each silicon atom, as well as their Brønsted acidity, and consequently, their hydrogen bonding capabilities.

Introduction

The development of new synthetic strategies to obtain molecular entities, capable of combining in one discrete precursor the apparently dissimilar properties of organic and inorganic moieties, has been an emerging issue, not only in the field of synthetic chemistry but also in materials science.[1] Owing to the hybrid organic-inorganic character of such molecular precursors; they exhibit superior properties compared with those observed in their pure counterparts.[2]

Organosililated compounds, particularly organochlorosilanes and organoalkoxysilanes derivatives $R_nSiX_{(4-n)}$ (n = 1–3; X = Cl or OR'), are among the most widely studied molecular precursors for hybrid systems. This is mainly due to the fact, that these compounds contain labile Si–Cl and Si–OR' groups, that can be readily hydrolyzed, esterified and polymerized, in the presence of water, alcohols, and other Si–OH groups. This feature makes them ideal candidates as molecular building blocks in the synthesis of functional hybrid materials, with applications in heterogeneous catalysis, in the design of chemosensors, and in the fabrication of coatings with optical activity, among others.[3]

Another kind of organosililated precursors that have attracted a new wave of interest are the organosilanol derivatives $R_{(4-n)}Si(OH)_n$ (n = 2, 3). These can be understood as the hydrolyzed counterparts of the chloro- and alkoxysilane derivatives. The importance of organosilanols resides in the synergy between the easily adjustable organic moiety and the remarkable hydrogen-bonding capabilities of the Si–OH moieties.

Consequently, this amphiphilic character enhances the versatility of the organosilanols in comparison to other organosilyl derivatives, and opens the possibilities for their application in a wider range of areas; such as the development of eco-friendly surfactants based on organosilanetriols,[4] molecular recognition,[5–10] hazardless organocatalysts for the activation of elec-

trophiles,[11–15] and the construction of long-range ordered hybrid materials.[16–20]

However, despite the above-mentioned promising applications; wider use of organosilanols is hampered by their limited stability, high costs, and synthetic difficulties. Traditionally, the synthesis of silanols is based on the hydrolysis of organochlorosilanes. This method requires the use of stoichiometric amounts of water, HCl scavengers (usually amines) and large quantities of organic solvent.[16,21–23]

Therefore, to tackle this problem, we pursued a new eco-friendly synthesis of molecular organosilanols with modulated hydrogen-bonding capabilities. Such capabilities were tested in practical applications such as in the organocatalytic conversion of CO_2 and styrene oxide into styrene carbonate under mild reaction conditions; in the construction of hydrogen-bonded organic frameworks (HOFs) with modulated porosity.

Additionally, we took a further advantage of the reactivity of the ASA precursors to apply them in the synthesis of cyclic and cage-like molecular borosilicates. Such compounds result attractive because borosilicate scaffolds represent suitable candidates as molecular models for the design of more complex reticular networks. In fact, Yaghi and co-workers showed that using designed borosilicate molecular clusters and applying reticular chemistry principles; it is possible to predict the structure of microcrystalline Covalent Organic Frameworks (COFs).[24] However, in order to achieve an accurate prediction, it is important to study the kinetic and thermodynamic aspects determining the formation of desired morphologies.

Chapter 1

Background

1.1 Silicon-based single-source precursors

One of the most widely studied types of precursors for the synthesis of hybrid organic-inorganic materials are the organosilylated compounds; particularly organochlorosilanes and organo-alkoxysilanes derivatives,[25] mainly because they are either easy-to-synthesize or commercially available. Moreover, these compounds present high molecular versatility, which comes from the endless variety of the functional organic groups that can be attached to the silicon atom through Si–C, Si–O or Si–N covalent bonds.

This organic moieties can be found either as terminal or a bridging groups between the silicon centers ($R_nSiX_{(4-n)}$ or $(X)_3Si–R–Si(X)_3$, n = 1–3; R = organic group; X = Cl, OH or OR') and can be varied in length, rigidity, geometry, and functionality.[26–29]

1.1.1 Organically modified chloro- and alkoxysilanes

Most of the early investigations on ORganically MOdified SILicates (ORMOSILs) as a type of hybrid organic-inorganic materials are based, principally, on the hydrolysis and condensation of mono- and bis-silylated derivatives, mainly trichloro- and trialkoxysilanes ($R_nSiX_{(4-n)}$ or $(X)_3Si–R–Si(X)_3$, n = 1–3; X = Cl, OEt or OMe).[3,26,27,30–35] One of the attractive features of working with such kind of compounds is the relative ease with which the monomers can be prepared.[36]

One of the most commonly used approaches for the synthesis of such monomers is the

hydrosilylation reaction.[28] This method consists of the addition of the H–Si bond, present in trichlorosilanes or trialkoxysilanes, across carbon-carbon, carbon-oxygen or carbon-nitrogen unsaturated bonds. Notwithstanding the versatility of this synthetic approach to affords a wide variety of functional organosilylated derivatives, this methodology is limited to unsaturated organic moieties. Furthermore, ordinarily, this reaction takes place under catalytic conditions; where the most common catalysts are based on noble metal compounds such as Karstedt's ($C_{24}H_{54}O_3Pt_2Si_6$) or Spier's (H_2PtCl_6) catalysts.[37–39]

An alternative route for the synthesis of trichlorosilane and trialkoxysilane compounds consists in the cross-coupling reaction between a suitable tetrafunctional silane derivative, and an organometallic reagent. The latter can be easily prepared by the metallation of alkynyl or aryl precursors, using either Grignard or lithium-halogen exchange reactions.[30,36,40]

Sol-gel method: reactivity of organochlorosilanes and organoalkoxysilanes

As mentioned earlier, chloro- and alkoxysilyl- derivatives have been widely studied as molecular building blocks in the synthesis of functional materials because they exhibit a remarkable tendency to undergo polycondensation reactions through the formation of Si–O–Si siloxane bonds under mild reaction conditions.

In general, such bonds can be formed following three main pathways (I) by the hydrolysis and condensation of either chloro- or alkoxysilyl groups (this is the well-known sol-gel method), (II) by nonhydrolytic reactions, or (III) Piers-Rubinsztajn reactions.[16,21–23]

These pathways, eventually lead to the formation of hyper-cross linked organically functionalized siloxane networks commonly known as silsesquioxanes, due to the fact that the tetra-coordinated silicon atoms, in such materials, are capable to form up to three siloxane bonds where each oxygen atom is shared between two silicon atoms leading to 1.5 (sesqui) oxygens per silicon atom.[26]

Among the aforementioned methodologies for the synthesis of silsesquioxanes, the most widely studied is the hydrolytic sol-gel method, since this approach not only involves mild reaction conditions; but also permits tailoring the morphology of the resultant material in thin films or fibers, as well as bulk porous and non-porous materials.[2,23]

The hydrolytic sol-gel processing of trichloro- and trialkoxysilanes can be understood as

4

a series of stages: hydrolysis, condensation, gelation, aging, and drying.[22,26] The hydrolysis involves the formation of organosilanol species, mixing a mono- or bis-silylated precursor with at least 1.5 or 3 equivalents of water; respectively. Nevertheless, the extreme reactivity of trichlorosilane derivatives towards water gives rise to the formation of heterogeneous mixtures at the early stages of the sol-gel process, due to the rapid formation of oligosilsesquioxanes which precipitates before the mixing is completed. Moreover, although the production of one equivalent of hydrogen chloride for each equivalent of hydrolyzed Si–Cl group, makes the reaction thermodynamically favorable; this fact limits the application of chlorosilyl- derivatives to those systems that are stable under acidic conditions.[1]

On the other hand, the hydrolysis of trialkoxysilanes is orders of magnitude slower than their trichlorosilane analogues.[22,28] Consequently, in the case of trialkoxysilanes, this process is typically performed in the presence of acidic or basic catalysts. Additionally, the rate of such process also decreases as the steric bulk of the alkoxide group increases. In this context, it has been shown that the relative rate of the first hydrolysis step for the most common alkoxysilanes follows this reactivity trend MeO $>>$ EtO $>$ n-PrO $>$ n-BuO.[3]

Additionally, the electronic and steric effects of the functional organic group (R) attached to the trialkoxysilyl moiety play a major role in the hydrolysis and condensation processes. For example, under acidic conditions, electron-donating substituents increase the rates of hydrolysis and condensation in related to the observed in the pure tetra-alkoxysilanes, whereas under the same conditions, the electron-withdrawing substituents decrease the rate of such processes.[3]

The hydrolysis and condensation processes of organosilylated precursors occur simultaneously in a complicated sequence of nonconsecutive pathways, where the relative rate of such overlapping processes are highly sensitive to the imposed pH conditions. Consequently, the "sol" obtained under acid-catalyzed conditions contains many small particles and oligomers; while under basic catalysis only few larger particles are formed. Subsequent cross-linking and aggregation of such particles eventually results in the formation of the final polymeric network. The moment at which the viscosity of this polymeric fluid increases sharply is called the "gel" point. Finally, after the gelation this silica matrix goes through an evolution stage commonly called aging.[16,22]

1.1.2 Synthesis of polyhedral oligomeric silsesquioxanes (POSS) and spherosilicates

Although monosilylated derivatives $RSiX_3$ (X = Cl or OR') have three potentially reactive groups available for the formation of an infinite network of siloxane bonds, the polymerization of such derivatives rarely achieves the "gel" point. This fact may be due to the tendency of such compounds to form cycles and small oligomers at the early stages of the hydrolysis process.[33,41,42] Nevertheless, due to the presence of the organic pendant group, such monosilylated precursors $RSiX_3$ (X = Cl, OR') are suitable candidates for applications that involve surface modifications, coating or immobilization.[2,3,35]

On the other hand, mono- trichlorosilyl- and trialkoxysilyl- derivatives have also been extensively used in the synthesis of polyhedral oligomeric silsesquioxanes (POSS) and spherosilicates. These, unlike the branched polysilsesquioxanes, are based on a finite number of siloxane bonds. Accordingly, such compounds exhibit cage-like discrete structures formed by polycyclic silsesquioxane core $[-SiO_{3/2}]_n$; where n = 6, 8, 10, 12.[41,43–48] Although both spherosilicates and POSS share the polyhedral silicate cage $[-SiO_{3/2}]_n$ as a common structural element, the major difference between them resides uniquely in the type of substituent attached to the silicon vertices. While in POSS the "n" peripheral groups are strictly organic, in sphereosilicates, this position is ocuppied by siloxy groups [**Fig**.1.1 and **Fig**.1.3]. Therefore, in accordance with the conventional ^{29}Si NMR nomenclature used for silicate and siloxide type compounds, the POSS and spherosilicates can be represented as T_n and Q_n, respectively, where the most available and widely used polyhedral compounds are T_8 and Q_8; the later is also commonly described as a double-four-ring D4R [**Fig**. 1.1].
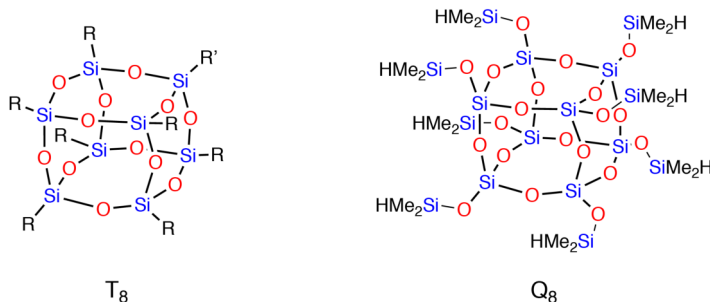
Figure 1.1. Cubic polyhedral organosylilated compounds T_8 and Q_8.

Even though both of the aforementioned polyhedral compounds share the same Si_8O_{12} structural cores, their synthesis follows different routes. Typically, the synthesis of POSS [−$SiO_{3/2}]_n$ is achieved by a controlled hydrolysis and condensation of either $RSiCl_3$ or $RSi(OR')_3$ derivatives in non-nucleophilic solvents.[49] The presence of bulky substituents in such precursors forces the formation of discrete polyhedral oligomers rather than extended polymeric networks. In fact, certain bulky groups may lead to the formation of incompletely condensed *closo* structures $R_7Si_7O_9(OH)_3$.[44,45] The latter can be further functionalized reacting the remaining Si–OH groups with a less bulky organosilylated precursor $R'SiCl_3$, closing the cube of the final structure $R'R_7Si_8O_{12}$ [**Scheme** 1.1].
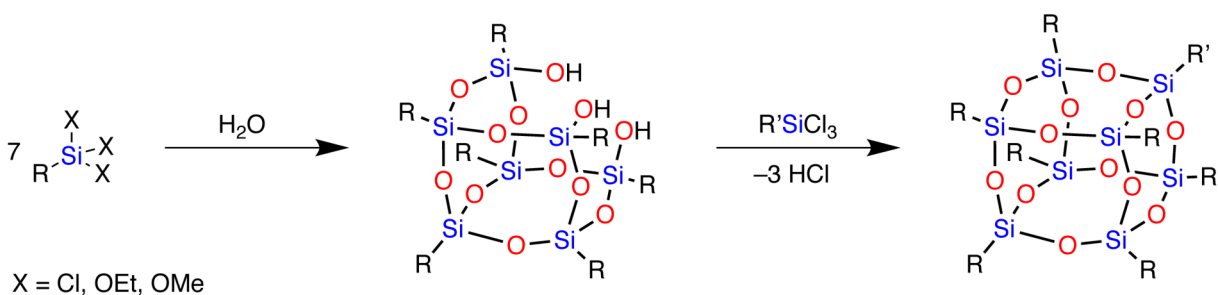
Scheme 1.1. Synthesis of functionalized T_8 POSS.

Moreover, Unno *et al.* reported an alternative method for the synthesis of octasilsesquioxane "Janus-cube", a nanometer-scale Janus particle, obtained by the cross-coupling reaction between two square siloxanes; one sodium tetrasilanoxide, and one cyclic tetrafluorosiloxane [**Scheme** 1.2].[50]
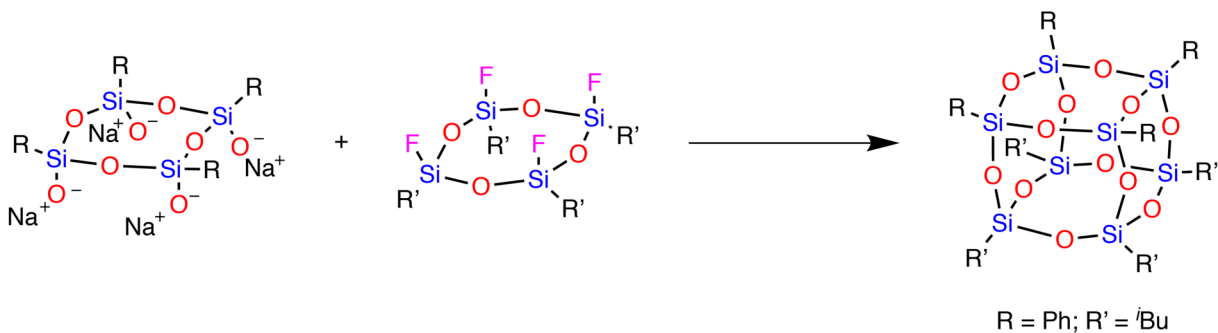
Scheme 1.2. Synthesis of a Janus-cube through the cross-coupling of cyclic siloxane derivatives.

The spherosilicates $[O–SiO_{3/2}]_n^{n-}$ are commonly prepared by the hydrolysis of trialkoxysilane precursors $RSi(OR')_3$ in an aqueous solution of tetramethylammonium hydroxide to afford a discrete polyhedral silicate core. Subsequently, the anionic oxidic surface of the polyhedral silicate reacts in the presence of suitable silylating agents such as $HSi(CH_3)_2Cl$ and $(CH_2=CH)Si(CH_3)_2Cl$ to afford $[Si_8O_{12}][OSi(CH_3)_2H]_8$ and $[Si_8O_{12}][OSi(CH_3)_2(CH=CH_2)]_8$; respectively [Scheme 1.3]. [45,48,51–53]
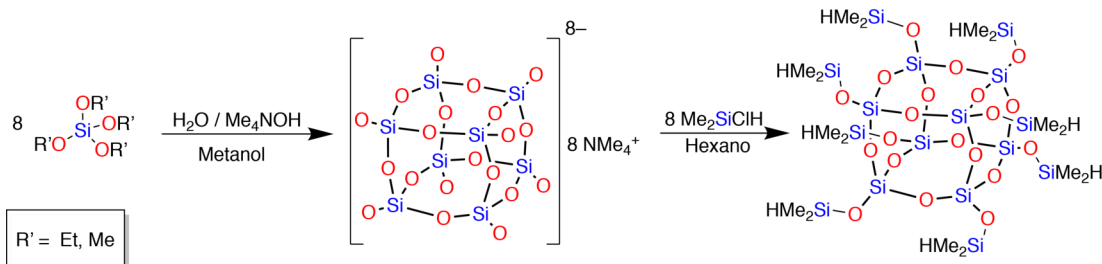
Scheme 1.3. Synthesis of D4R spherosilicate.

Overall, the versatility of the aforementioned synthetic procedures to obtain POSS and spherosilicates allows the incorporation of almost any organic functional groups. In addition, some POSS and spherosilicates have been successfully studied by SC-XRD, and their molecular structures reveal that the well-defined 3-dimensional silica core Si_8O_{12} has a size around 0.5 and 0.7 nm. Consequently, such discrete entities can be considered to be sub-nanometer particles with applications in the synthesis of nanocomposite materials. Furthermore, the aforementioned D4R silicate cluster $[SiO_{5/2}]_8^{8-}$ has been successfully applied as a molecular model, because it mimics the surfaces of larger silica particles [Scheme 1.3]. [54,55]

All these attributes make the POSS and spherosilicates ideal candidates in the construction of hybrid organic-inorganic materials with a wide range of applications; such as catalysis,[43,54] nanocomposites,[47] biomaterials,[47] light-emitting diode materials,[56] among others.[44]

1.1.3 Bridged polysilsesquioxanes obtained from chlorosilyl- and alkoxysilyl-molecular precursors

Conversely to the observed in monosilylated precursors, the sol-gel polymerization of organosilyl derivatives with organic bridging group permits a rapid formation of an infinite siloxane network reaching easily the "gel" point. Therefore, such monomeric precursors allow the construction of amorphous hyper-cross-linked bridged polysilsesquioxanes, where the organic part comprises from 40 to 60 wt percent of the bulk material.[34]

This *Bottom-up* synthetic approach for the construction of hybrid organic-inorganic materials circumvents the commonly observed phase segregation problems during the polymerization process. In fact, the organic groups are an integral part of the network architecture.[31,57]

A great variety of such organic substituents have been used to manipulate the physical and chemical properties of the hybrid materials.[27,32,58,59] They range from rigid arylenic and acetylenic moieties[23,29,30,36] to flexible alkylenes,[33] as well as functionalized linkers such as amines,[31] ethers, sulfides, phosphines, and even organometallic compounds [**Fig**. 1.2].[36,60]
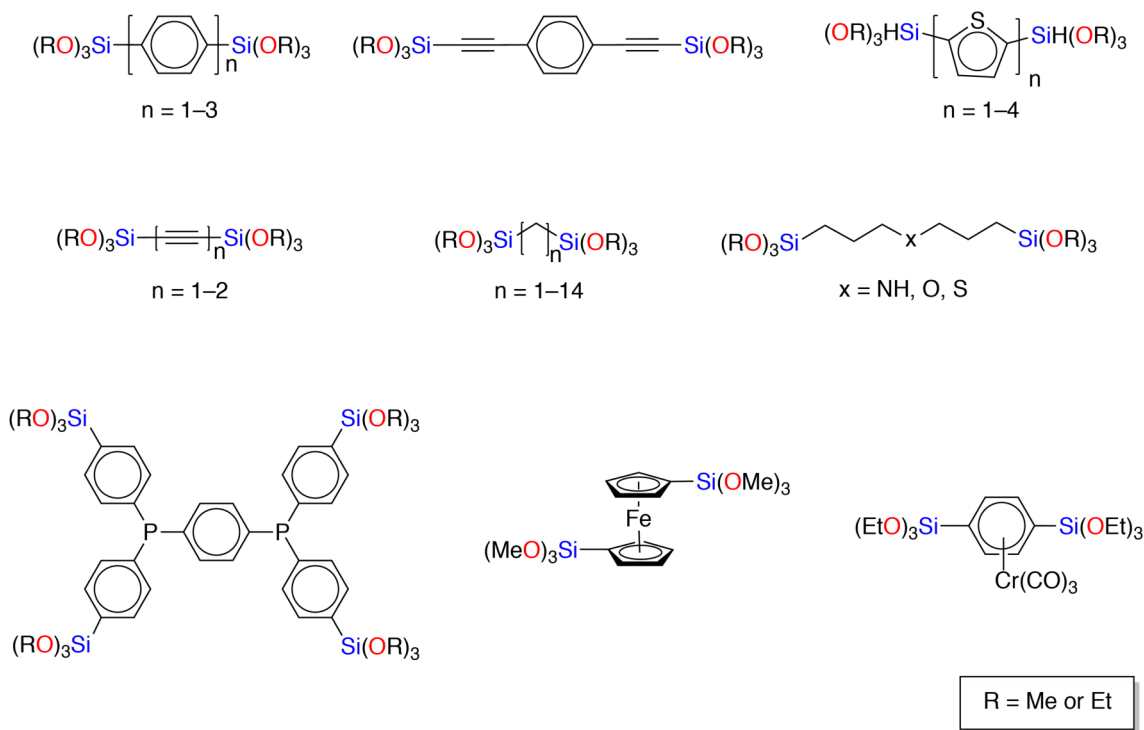
Figure 1.2. Some examples of bis-(trialkoxysilyl)- derivatives with organic bridging groups $(R'O)_3Si–R–Si(OR')_3$.

However, in bulk sol-gel polymerization, the influence of the organic bridging group on the long-range order is diminished by the poor control over the hydrolysis and condensation processes, which occur concurrently. Hence, the resulting bridged polysilsesquioxanes are amorphous solids that exhibit fractal dimensions.[22]

Nevertheless, Corriu and Kuroda demonstrated that under well-controlled conditions, the hydrolysis of organosilyl- derivatives to the corresponding organosilanol derivatives could be achieved, suppressing the polycondensation process.[16–18,61,62] This method leads to the formation of ordered mesostructures due to the presence of hydrophilic Si–OH groups which are prone to self-assembly.

1.1.4 Molecular organosilanols

Functionalized silanols could be understood as derivatives of the orthosilicic acid H_4SiO_4, where an organic residue has substituted one or more OH groups $R_nSi(OH)_{(4-n)}$ (n = 1–3), as the silicon atom, unlike its lighter homologue carbon, is capable of stabilizing more than one hydroxyl group on the same silicon center.[63–65] Nonetheless, a strong steric protection and precise control over the reaction conditions are mandatory to avoid the condensation of the geminal silanediols and silanetriols to oligo- or polysiloxanes.[64]

The vast majority of the literature reports only the synthesis and use of organosilanols with less than three hydroxyl groups attached to the same silicon atom $R_nSi(OH)_{(4-n)}$ (n = 2 or 3). This fact may be explained with regard to the relative stability of such compounds, which decreases with the number of hydroxyl groups attached to the same silicon atom. Thus, both, organosilanols and organosilanediols, are synthetically more accessible than silanetriol-based derivatives [**Fig**. 1.3].

R
Si
R   R
OH

R
Si—OH
R   OH

R
Si
HO   OH
OH

R'   R'
HO–Si–R–Si–OH
R'   R'

Monosilanol   **Silanediol**   **Silanetriol**   **Disilanol**

R = Me, Et, *t*-Bu, *n*-Bu

R = Ar
R' = Me or Et

R'   R'
HO–Si–R–Si–OH
HO   OH

HO   OH
HO–Si–R–Si–OH
HO   OH

R   O   R
Si   Si
R   O   R
OH   OH

R   O   R
Si   Si
HO   OH
OH   OH

Bis(silanediol)   **Bis(silanetriol)**   **Dihydroxydisiloxane**   **Tetrahydroxydisiloxane**

R = Ar
R' = Me or Et

R = *t*-BuO

R = Me, Et, *n*-Pr, Ph

Cyclic siloxane based silanols   **Silsesquioxane based silanols**

R' = C_4H_8NO
R = Ph

R = C_5H_9

Figure 1.3. General structures of some representative organosilanols reported in the literature.

Recently, organosilanols have attracted a new wave of interest due to the synergy between the remarkable hydrogen-bonding capabilities of the Si–OH groups, and the easily adjustable organic moiety. Therefore, a vast variety of molecular organosilanols have been extensively investigated in a wide range of applications; such as, in the synthesis of hybrid organic-inorganic materials with a long-range order obtained by the cross-coupling reaction between organosilanol derivatives,[16–20] environmentally friendly surfactants based on organosilanetriols,[4] in molecular recognition,[5–10] as well as unique bioisosteres, that do not have stable carbon analogues, improving the advance of new therapeutic agents.[66,67] Moreover, more recently, organosilanediols have been applied in enantioselective hydrogen-bond donor catalysis (HBD).[11–15] Finally, discrete $RO_nSi(OH)_{(4-n)}$ (n = 2, 3) organosilicates with a silicon atom immediately coordinated

to four oxygen atoms as in silica materials, have been used by Copéret and co-workers in the preparation of molecular models to understand the local active sites on the surface of heterogeneous catalysts.[68] However, despite the above-mentioned promising applications, wider use of organosilanols is hampered by their limited stability, high commercial price and synthetic difficulties. Current synthetic approaches involve the controlled hydrolysis of chlorosilyl- and alkoxysilyl- derivatives; as well as, the oxidation of silanes. However, these methods suffer from selectivity.

Synthetic methods to obtain molecular organosilanols

Traditionally, the synthesis of organosilanols is based on the controlled hydrolysis of organochlorosilanes $R_nSiCl_{(4-n)}$ (n = 1–3), which requires the use of stoichiometric amounts of water and large quantities of organic solvent. Furthermore, this methodology requires the use of HCl scavengers, usually amines, since even when traces of residual HCl or an excess of the base are present, rapid condensation of the SiOH moieties into Si–O–Si siloxane bridges takes place.[63,64] This is especially crucial in the case of organosilanetriols, which are much more prone to undergo polycondensation than the analogous silanols and silanediols.[16,69]

Thus, to avoid the formation of undesirable condensation byproducts, a precise control over the reaction conditions is mandatory, since the relative rates of the overlapping hydrolysis and condensation processes are dependant on the pH, solvent, temperature, concentration, and the equivalents of water (R_w=[H$_2$O]/[Si–OR]) in the reaction media.[22]

In this context, it has been shown that the chemical nature of the organosilyl- derivatives plays an important role in the formation and stability of the corresponding organosilanol derivatives, where the condensation process is retarded in the case of organosilylated precursors with bulky organic groups.[70,71] This effect was evidenced by Roesky and co-workers[63,64] in consisting on a study about the relative stability of a series of *N*-substituted silanetriols [2,6-*i*-Pr$_2$C$_6$H$_3$N(SiMe$_3$)Si(OH)$_3$], and [2,4,6-Me$_3$C$_6$H$_3$N(SiMe$_3$)Si(OH)$_3$], [2,6-Me$_2$C$_6$H$_3$N(SiMe$_3$)Si(OH)$_3$], where they modulated the steric hindrance of the organic pendant group. The highest stability was observed in the case of the compound with the isopropyl groups in the ortho positions of the aromatic ring. Nevertheless, it should be pointed out, that it was necessary to block the nitrogen atom with a bulky SiMe$_3$ group, in all of these compounds in order to

stabilize the silanetriol moiety. Similarly, Kuroda and co-workers reported the synthesis of stable mono-silanetriols ROSi(OH)$_3$ (R = Adamantyl, 3-ethyl-3-pentyl), through the controlled hydrolysis of chlorosilyl derivatives, where the bulky pendant group is attached to the silicon center *via* an O–Si bond [**Fig**. 1.4].[71]

R = *i*-Pr; R' = H
R = Me; R' = H
R = Me; R' = Me
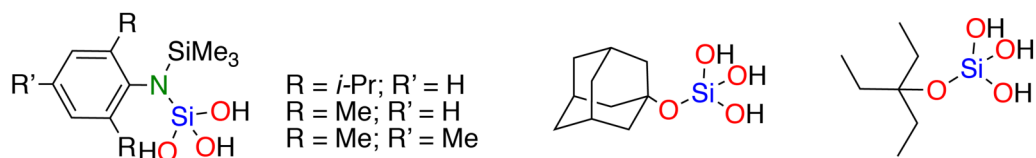
Figure 1.4. Mono-silanetriols stabilized by bulky pendant groups.

Although the controlled hydrolysis of chlorosilyl derivatives enables to isolate stable mono-silanetriols, this approach results inadequate for the synthesis of bis-silanetriols, as the latter present a greater number of reactive Si–OH groups. This enhances its probability to undergo polymerization. Consequently, alkoxysilane derivatives (R$_n$SiOR'$_{(4-n)}$; R' = Me, Et; n = 1–3) were proposed as an alternative since the alcohols formed during the hydrolysis do not accelerate the condensation of silanols. Nonetheless, this hydrolysis proceeds in a biphasic medium (diethyl ether/water) under acidic catalysis and requires in some cases extremely long reaction times (up to 34 days!), which always result in a partial condensation and thus product loss [**Scheme** 1.4].[19,69]
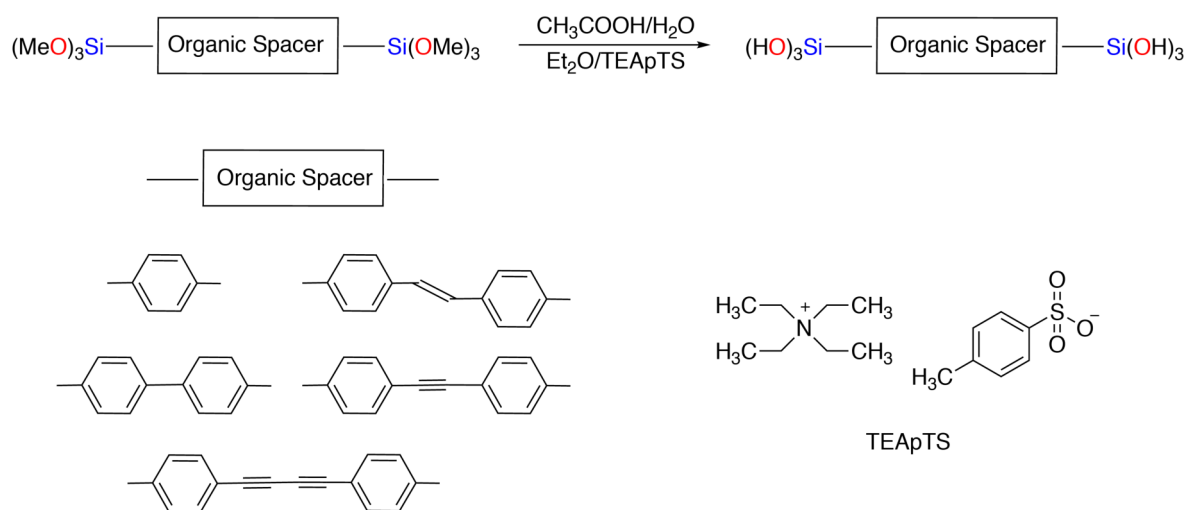
Scheme 1.4. Synthetic route to stable organo-bis(silanetriols).

13

1.1.5 Applications of hydrogen-bonding properties of organosilanols

Applications of mono-organosilanols in organocatalysis and molecular recognition

Hydrogen-bonded functional groups such as alcohols, amides, carboxylic, boronic and phosphonic acids have been applied in sensing, organocatalysis, and molecular recognition.[72,73] In this context, silanediols with the $Si(OH)_2$ moiety result attractive for these applications, due to their impressive HB abilities. Consequently, Kondo and co-workers used fluorescence spectroscopy to show that silanediol derivatives, bearing 1-naphthyl, 9-anthyl, and 1-pyrenyl organic groups, can be applied in anion recognition upon the addition of biologically relevant anions, such as acetate [**Scheme** 1.5]. Clearly, the close location of the two Si–OH groups play an important role in the cooperative binding of the anion in these systems.[5,6,10] Therefore, the stability of the $Si(OH)_2$ moieties toguether with their Brønsted acidity make them unique in the chemical recognition and electrophilic activation.
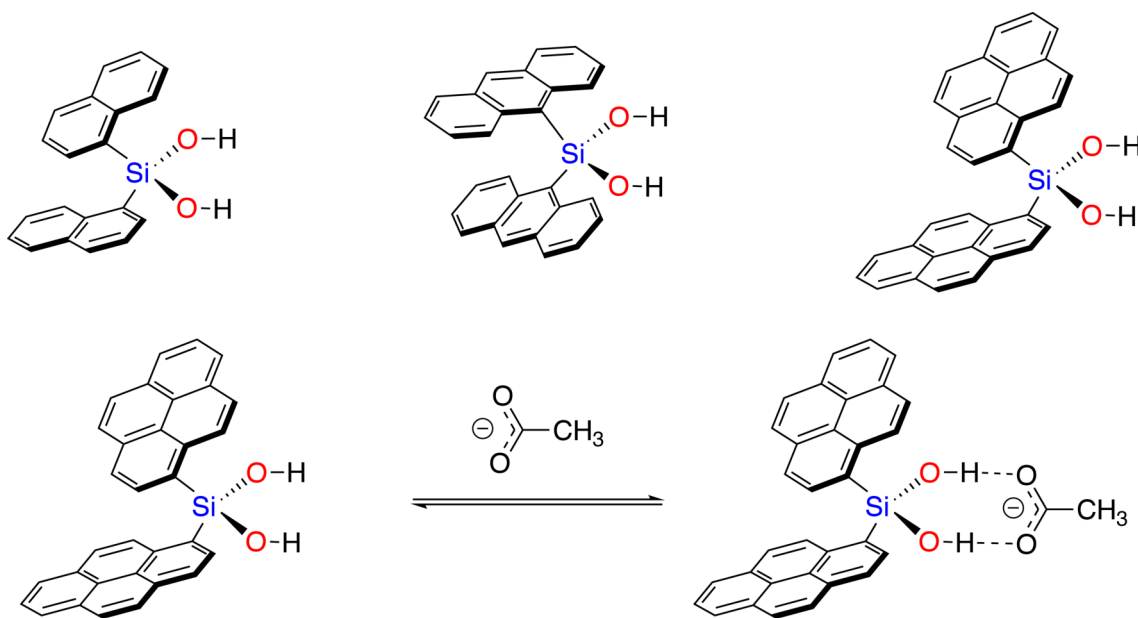
Scheme 1.5. Silanediol-based anion receptors studied by Kondo and co-workers.[5]

However, it is noteworthy, that silanediols also exhibit dual donor and acceptor properties, leading to self-recognition and formation of dimeric active species. In this realm, Franz and co-workers studied the importance of such cooperative hydrogen-bonding effects in the silanol-acidification and their implications in silanediol-assisted organocatalysis. Accordingly, to evaluate the Hydrogen-bond-donor HBD organocatalytic performance of such compounds, one of the most studied reactions is the Friedel-Crafts addition of indole to activated nitroalkenes. This reaction is an important C–C bond-forming reaction, regularly, catalyzed by silica gel. From these results, it was concluded that the cooperative hydrogen-bonding enhances the acidity of the external protons in the dimeric cycle and by consequence, allows a stronger activation of electrophiles and provides a new mode of activation for catalysts design [**Scheme** 1.6].[11,14]
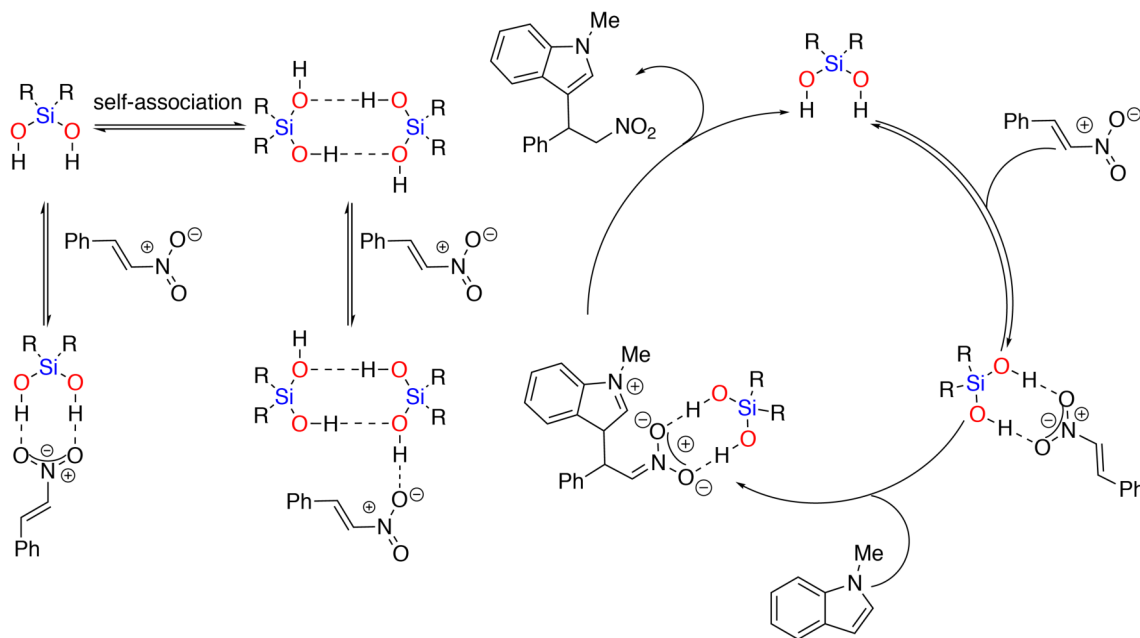
Scheme 1.6. Proposed modes of hydrogen-bonding activation of nitrostyrene by organosilanol compounds and proposed catalytic cycle in the addition of indole to nitrostyrene.

15

More recently, Mattson *et al.* demonstrated that the HBD catalytic properties of organosilanediols could also be extended on the metal-free CO_2 fixation through the coupling reaction of the later with epoxides to form the corresponding cyclic carbonates. In general, these compounds find applications as high-boiling polar aprotic solvents, as electrolytes in batteries and they are raw materials for the preparation of polymers.[12,15] However, the carbon atom in CO_2 is present in its most oxidized state, which results in high stability and low reactivity. Consequently, harsh reaction conditions involving high temperatures and pressures are necessary for CO_2 conversion.[74] Therefore, the development of metal-free efficient catalysts to overcome the high reaction barrier is of high interest for academia and industry, since they are usually significantly more cost-efficient and less toxic than the traditionally used metal-based catalysts.

In this context, it was shown that the bis(1-naphthyl)silanediol in the presence of tetrabutylammonium iodide (TBAI) as co-catalyst provides a new platform for the conversion of CO_2 and epoxides to carbonates under mild reaction conditions [**Scheme** 1.7].[12]
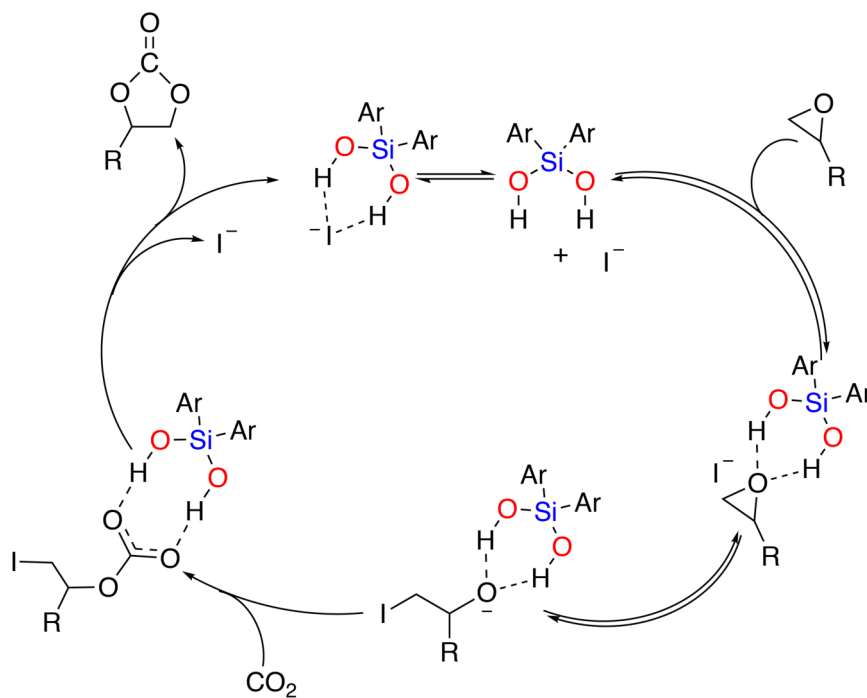
Scheme 1.7. Proposed reaction pathway for the catalytic cycloaddition of CO_2 to epoxides to form the corresponding organic carbonates.

16

Moreover, the binary catalytic system silanediol/TBAI has been described by Cokoja *et al.* as a *"potential metal-free system which bridges the gap between organocatalytic and metal containing catalysts".*[74]

The proposed reaction pathway begins with the initial activation of the epoxide by the dual HB interaction with the silanediol. Subsequently, the epoxide undergoes ring-opening upon the nucleophilic attack of the iodide anion to afford the corresponding alkoxide which is also stabilized by the HB interaction with the $Si(OH)_2$ moiety. The latter reacts with CO_2 to produce an HB-stabilized intermediate. Finally, the completion of the catalytic cycle occurs upon intramolecular ring formation yielding the cyclic carbonate and regenerating the iodide and silanediol.

Applications of organosilanols in the synthesis of ordered hybrid materials

One of the most widely explored applications of monosilanols with long alkyl chains as organic pendant group is in the construction of hybrid organic-inorganic materials with lamellar morphologies. For example, Kuroda and co-workers have developed a wide range of polysilsesquioxane based materials with a great variety of morphologies from lamellar nanocomposites to worm-like mesostructures.[16,17]

The synthesis of multilayered hybrids is, regularly, carried out via hydrolysis of alkyltriethoxysilanes, $C_nH_{(2n+1)}Si(OEt)_3$ (n = 12, 14, 16 and 18) to produce the corresponding alkylsilanetriols $C_nH_{(2n+1)}Si(OH)_3$ (n = 12, 14, 16 and 18). These amphiphilic molecules are prone to self-organization directed by the HB interactions between the Si–OH moieties and also by the weak interactions between the hydrophobic alkyl chains to give rise to supramolecular self-assembled layers.[17,18] Subsequently, these preordered structures can be converted to a polycondensed lamellar nanocomposite materials through thermal treatment [**Scheme** 1.8].
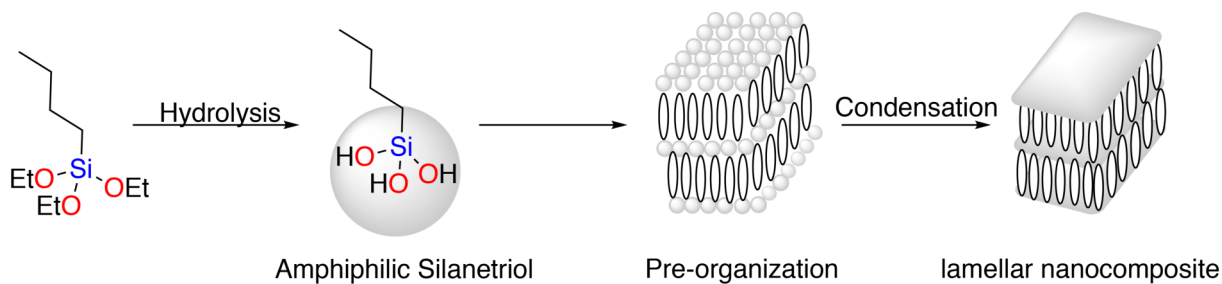
Scheme 1.8. Formation of lamellar structures by self-assembly of organosilanetriols.

Similarly, in regard to bis-silanols with an organic bridging group, the presence of multiple $Si(OH)_n$ moieties in the same molecular building block permits the "self-directed" assembly processes directed principally by HB interactions between the hydrophilic Si–OH moieties. This fact gives rise to a new class of ordered functional materials where the organic functionality is an integral part of the bulk material.[20,61,62,75] This improvement in the long-range order was evidenced by the structural differences between those materials obtained from bis-trimethoxysilanes $(MeO)_3Si–R–Si(OMe)_3$ as molecular building blocks and those obtained from their hydrolyzed counterparts $(HO)_3Si–R–Si(OH)_3$, where the latter exhibit a higher degree of organization at nano-metric scale [**Scheme** 1.9].
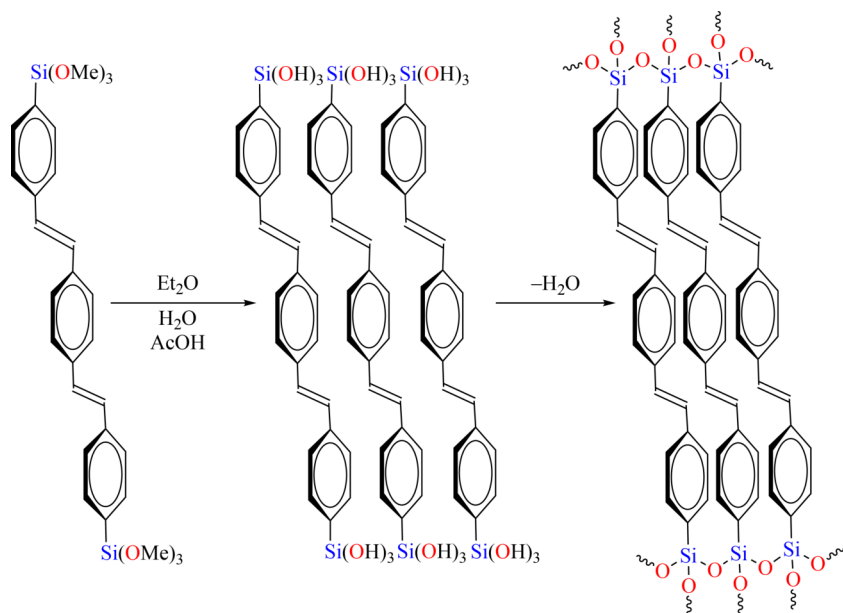
Scheme 1.9. Formation of ordered polysilsesquioxanes via hydrogen-bonding interactions between monomeric species.

1.2 Hydrogen-bonded organic frameworks (HOFs): A new class of porous crystalline materials

The development of novel porous solids has attracted considerable attention in academia and industry; as they have found application in a wide range of technological areas, such as gas storage and separation processes, heterogeneous catalysis, drug delivery, and conductivity. Porous materials are found in several kinds of structural manifestations, ranging from crystalline solids such as zeolites, Metal-Organic Frameworks (MOFs) and Hydrogen-bonded organic frameworks (HOFs) to amorphous carbons [**Fig**. 1.5].[76]

Among crystalline systems, the most widely studied porous materials are zeolites.[77] These are pure inorganic aluminosilicate materials with well defined arrangements. This feature confers them robustness, and consequently high thermal and mechanical stability making them suitable candidates for applications in high-temperature processes such as the catalytic cracking of hydrocarbons.[78]

By contrast, MOFs, which constitute a second broad class of crystalline porous solids, exhibit superior structural flexibility; since such kind of materials lies at the intersection between inorganic and organic structures and in which the metal centers act as nodes interconnected by organic linkers through coordinative bonds. Consequently, the cavity size in this kind of materials can be easily modulated by alteration of the length of the organic linkers. This particular feature makes MOFs a far more versatile class of porous materials than inorganic zeolites.[79–81]

In the same way, more recently, Hydrogen-bonded Organic Frameworks (HOFs), another group of flexible porous materials based on organic building blocks, has taken some relevance, because these metal-free reticular frameworks exhibit low density, as a result of the use of light elements.[82,83]

Certainly, compared with Zeolites and MOFs, HOFs can be readily synthesized using mild reaction conditions through the self-assembly of the molecular tectons directed primarily by intermolecular HB interactions and followed by weaker secondary contacts such as $\pi\cdot\cdot\cdot\pi$ interactions which enables the straightforward regeneration of the porous material by a simple recrystallization process.[84–87]

Nevertheless, the hydrogen bonds in such materials are much weaker than the ionic and coordinative bonds present in zeolites and MOFs, respectively. Hence, unlike the later, HOFs are less robust materials.[84,88]
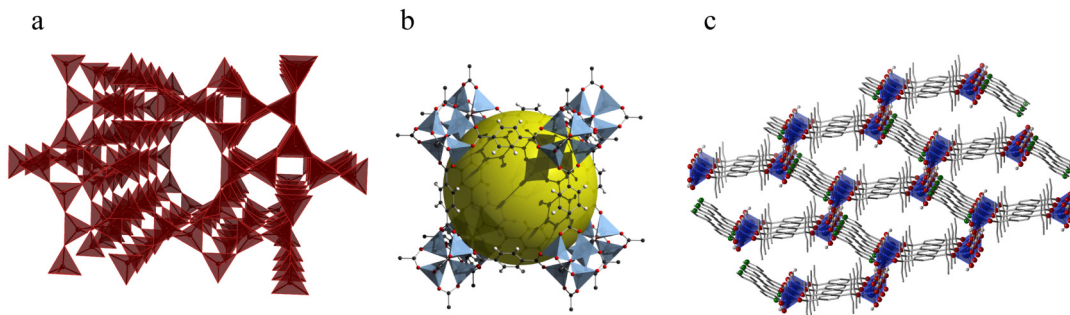
Figure 1.5. Crystal structures of key families of porous solids. (a) terranovaite-type zeolite; (b) IRMOF-1; (c) HOF.[89,90]

Therefore, it is much more difficult and challenging to stabilize porous HOFs when compared with MOFs, since they tend to collapse after the release of guest solvent molecules. Regardless of this limitation, some progress has been made to stabilize such porous structures, thus HOFs with permanent extrinsic porosity were established around 2010.[84–86,91]

In fact, Chen *et al.* demonstrated that some porous functionalized HOFs even exhibit superior properties in highly selective separation of challenging gas mixtures such as C_2H_2/C_2H_4, C_2H_2/CO_2, and fluorocarbons. In such materials, the porous structure and functionality can be easily modulated by subtle changes in the molecular building blocks and the crystallization conditions.[84,86,91]

Regularly, such building blocks include a wide variety of neutral organic compounds with hydrogen-bonding capabilities such as alcohols, carboxylic and boronic acids, imidazole, pyrazole or other amino-heterocyclic compounds. Nevertheless, charged constituents, such as carboxylate salts, organosulfates, and organophosphates have been used in the formation of ionic networks directed by reinforced charge-assisted hydrogen bonds increasing the stability of the final material.

Notwithstanding the extensive research focuses on HOFs, a vast majority of literature reports the synthesis of single-component HOFs, restricting their design regarding the molecular constituents. Furthermore, this synthesis sometimes requires the use of solvothermal conditions

to afford an open porous network.[85]

By contrast, the synthesis of multicomponent HOFs by the self-assembly of complementary tectons, following a molecular recognition approach, takes advantage of crystal engineering to achieve a balanced interplay between the complementary donating/accepting functional groups. Consequently, following this approach, the intermolecular interactions can be optimized and balanced.

In this context, to achieve a fine structural control of the resulting co-crystalline material, it is essential to known the kinetic and thermodynamic aspects that determine the formation of robust synthons formed by interactions between complementary tectons, which in turn, govern the nucleation process.[92,93]

Within the most extensively studied multicomponent HB networks are those formed by donor/acceptor HB interactions between carboxylic groups and amines or amides, because, these O–H⋯N interactions offer directionality and strength. More recently, to improve both of the aforementioned features, the use of molecular tectons with stronger acid moieties such as organophosphonic and organosulfonic acid derivatives was proposed, as in the presence of organic amides they afford highly directional interactions which allow fine control over the molecular organization in the resulting structure.[94]

On the other hand, the presence of additional groups with HB capabilities (=O, –OH), on the central sulfur $-SO_3H$ or phosphorus $-PO_3H_2$ atoms, respectively, enriches their supramolecular chemistry regarding hydrogen bond network generation, in comparison with carboxylates. Besides, due to the tetrahedral geometry of the central atom, these molecular building blocks exhibit higher conformational flexibility than carboxylic groups with trigonal planar geometry. Nevertheless, the high polarity of organophosphonic and organosulfonic acid derivatives limits considerably their solubility in organic solvents. Therefore, they are used in a form of sodium salts due to their low stability in a free state. Consequently, these facts have hampered the wider use of such compounds as molecular building blocks.[95]

As an alternative, it is well known that molecular organosilanetriols are isoelectronic with the corresponding organophosphonic and organosulfonic acid derivatives. Additionally, all of them also share the same tetrahedral geometry around the central atom. Moreover, organosilanetriols present some advantages over organophosphonic and organosulfonic acid derivatives.

First, organosilanetriols are much less acidic and less polar, therefore they present higher solubility in organic solvents, and they do not dissociate under the reaction conditions. Additionally, they contain one more HB donor hydroxyl group attached to the silicon atom. In this context, Murugavel and Pietching showed that sterically hindered molecular mono(organosilanetriols) represent a good alternative in the formation of diamine/silanetriol co-crystals. However, it should be noted that only mono(organosilanetriols) were used as molecular tectons for the formation of supramolecular arrangements. Thus, to the best of our knowledge, there are no reports on the use of bridged organo-bis(silanetriols) as molecular building blocks for the construction of multicomponent HOFs, mainly due to their lower stability towards polycondensation reaction than their monosilanetriol analogues.[96,97] Nonetheless, evaluating all these considerations stable bridged organosilanetriols should be powerful tectons that would open new possibilities in the synthesis of porous networks.

1.3   Organoborosilicates: Molecular models of extended networks

As was mentioned earlier, the hybrid character of MOFs and HOFs confer them unique properties such as flexibility and functionality. Nonetheless, the relatively weak coordinative bonds and hydrogen bonding interactions in MOFs and HOFs, respectively, represent the major drawback for the extended use of such materials particularly in those applications that require high thermal stability.

This problem has been addressed in making Covalent organic frameworks (COFs), which are a new class of porous materials composed of lightweight elements (B, C, N, O, Si) linked by strong covalent bonds. Consequently, such materials combine the flexibility with the strength of the covalent bonds, leading to robust materials. However, linking organic molecules by covalent bonds to form extended reticular networks typically generates amorphous materials, which limits the elucidation of the structural arrangement of COFs and does not allow a precise control of their functionality.[98]

To overcome this "Crystallization problem" it is important to find the optimal thermodynamic and kinetic conditions under which the formation of covalent linkage is reversible, and

the reaction rate is on a time scale that allows for self-correction of defects. Thus, in reticular chemistry, this goal was initially achieved through the condensation reactions to form C–N, B–O, and B–O–Si covalent linkages, where the stoichiometric quantity of water generated in the process allows the modulation of the reaction's equilibrium leading to the formation of ordered materials.[98]

In this way, COF-300 was obtained by the imine condensation of aldehyde and amine linkers;[99] whereas, COF-1 was prepared by the self-condensation of 1,4-phenylenediboronic acid.[100] Additionally, boronic acids can also react with catechols to form extended networks, as in COF-5 and COF-105,[100,101] or with silanols to form borosilicate bonds as in the case of COF-202.[24]

It should be pointed out that those COFs obtained from boronic acid derivatives are of special interest because the boron sites can interact strongly with Lewis base guests such as ammonia, which make them ideal candidates for the storage of this corrosive reagent.[102] However, in general, all of these COFs are obtained as microcrystalline powders and until now large COF single crystals remain rare. Consequently, the structural characterization of such materials requires the simulation of the powder X-ray diffraction pattern using preconceived molecular clusters as models to predict the experimental patterns.[98]

The structural elucidation of COFs using calculated models and PXRD analysis has many limitations. For example, PXRD patterns give little information about stacking sequence of layers in two-dimensional COFs. Additionally, to assure an accurate prediction of the resultant structure under certain conditions; it is important to have a deeper knowledge about the kinetic and thermodynamic aspects that determine the formation of preferred morphologies in the molecular clusters used as models.

In this context, despite the fact that borosilicate scaffolds represent suitable candidates as molecular models for the design of more complex reticular networks, they have been investigated only marginally. The main reasons are: I) a limited number of commercially available silanols, II) difficult structural modification of these compounds, III) in the case of dichlorosilanes, the use of highly basic reaction conditions to neutralize the hydrochloric acid generated and IV) limited reactivity of the Si–C bonds in the siloxanes.

The most common structurally characterized molecular borosilicates exhibit the formation of six-, eight-, ten- or twelve-membered cyclic cores based on B–O–Si units, where the

23

eight-membered $B_2Si_2O_4$ rings are the most common [**Fig**. 1.6].[103] It is noteworthy that the formation of the smaller or bigger rings requires the use of predesigned precursors such as $ClSi(R)_2OSi(R)_2Cl$ or $HOSi(R)_2OSi(R)_2OSi(R)_2OH$.[104] However, only a handful of such compounds have been reported so far. Additionally, few cage-like structures with $B_2Si_6O_9$, $B_3Si_2O_6$ and $B_4Si_4O_{10}$ inorganic cores are also known and are based either on boric ($B(OSiPh_2O$-$SiPh_2O)_3B$) or boronic acids (t-BuOSi{O(BR)O}$_3$Sit-Bu or (t-BuOSi)$_4$(BR)$_4$O$_{10}$; R = organic group) and silanols with Si–C bond [**Fig**. 1.6].[105]

Finally, to the best of our knowledge, reports of structurally characterized borosilicates containing SiO_4 units are limited to few acyclic derivatives of [{(t-BuO)$_3$SiO}$_2$BOH].[106,107]
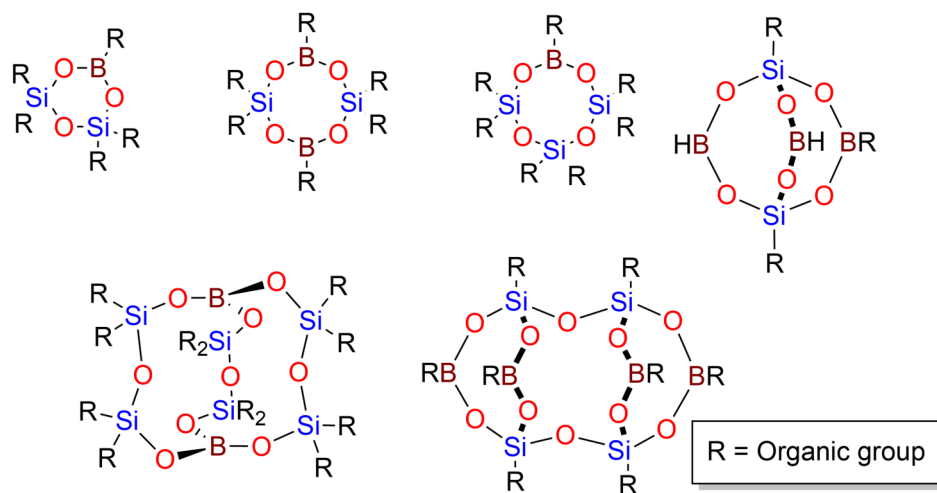
Figure 1.6. Structurally characterized cyclic and cage molecular borosilicates.

Hypothesis

In this work, it is intended to evaluate the viability of the use of ASA precursors in the synthesis of stable mono- and bis(organosilanols), under mild and eco-friendly reaction conditions. Also, ASA compounds are more stable and easier to handle than their chlorosilanes analogues but at the same time still more reactive than alkoxysilanes, due to the better-leaving group ability of the acetate ion AcO^-. Furthermore, taking into account that the condensation rate of alkylsilanetriols in aqueous media has a minimum at a pH of 4.5; we hypothesize that the acetic acid formed during the hydrolysis of the ASA precursors might, in fact, stabilize the desired silanols avoiding the formation of condensation byproducts.

Additionally, we consider that by tuning the steric hindrance around the silicon center it is possible to modulate the HB capabilities of the $Si–(OH)_n$ (n = 2, 3) moieties. Therefore, this might have important consequences in the organocatalytic performance of the obtained organosilanols. This assumption, can be evaluated by using the organosilanols, for the metal-free catalytic conversion of CO_2 to styrene carbonate under mild reaction conditions.

Moreover, by virtue of the hydrogen bonding capabilities of Si–OH moieties. We also envisioned the use of bridged organosilanols as molecular tectons, which in the presence of rigid organic diamines, might afford higher order co-crystalline structures. The supramolecular arrangement obtained can be directed by the highly directional hydrogen bonding interaction between the acid Si–OH moieties and the organic amines.

Finally, given the reactivity of the acetoxysilyl groups Si–OAc in the presence of compounds with anchored hydroxyl groups, such as organic alcohols or water, to lead the esterification Si–OR and hydrolysis Si–OH products, respectively.

It was suggested testing the reactivity of monoacetoxysilyl derivatives in the presence of

phenylboronic acid derivatives, with the purpose to achieve the formation of the corresponding discrete borosilicates; which in principle could mimic the structure and morphology of more complex borosilicate-based materials.

Objectives

General Objective

- Design and synthesis of organosilyl precursors with easily modulated organic moieties attached to one or two $-Si(OX)_n$ (X = OAc or H; n = 2 or 3) cores and their application in organocatalysis, and as molecular building blocks for the synthesis of porous hybrid materials and discrete organoborosilicates.

Particular Objectives

- Synthesis of mono- and bis(acetoxysilylalkoxides) (ASA) $((t\text{-BuO})_n(\text{RO})Si(OAc)_{3-n}$ and $(\text{AcO})_{3-n}(t\text{-BuO})_n Si\text{–O–R–O–}Si(Ot\text{-Bu})_n(OAc)_{3-n}$; n = 0 or 1) from the reaction between bulky tertiary alcohols and $Si(OAc)_4$.

- Synthesize stable organosilanediols and organosilanetriols with a pendant or bridging organic groups and modulated hydrogen bonding capabilities, by hydrolysis of the ASA precursors in aqueous media.

- Evaluate the organocatalytic properties of the organosilanols in the conversion of CO_2 into cyclic carbonates under mild reaction conditions.

- Explore the stability of the organosilanediols and organosilanetriols with bridging organic groups as molecular tectons in the synthesis of multifunctional porous HOFs directed by the strong interaction with rigid organic amines.

- Synthesis of discrete cyclic- and cage-like borosilicates from the ASA precursors in the presence of phenylboronic acid derivatives.

Chapter 2

Organosilanols: Organocatalytic conversion of CO$_2$

Pohl and Osterholtz determined that the condensation rate of alkylsilanetriols in aqueous media has a minimum at the pH of 4.5, that is just slightly lower than the pK_a of the acetic acid (4.76 at 25 °C) [**Fig. 2.1**].[108] Therefore, the acetoxysilylalkoxides (ASA), prepared from Si(OAc)$_4$ and bulky tertiary alcohols as organic moiety, seem as ideal precursors for the preparation of stable molecular organosilanols, as the acetic acid formed during the hydrolysis of ASA precursors might allow us to control the protic conditions in the reaction media, which improve the stabilization of the Si–(OH)$_n$ moieties, avoiding the formation of undesirable condensation by-products.

Figure 2.1. Plot of condensation rate of organosilanetriols versus pH, representing the minimum in hydrolysis kinetics near pH = 5.

Additionally, a further advantage of this method is that the acetic acid is biodegradable and it is much less corrosive than the HCl that is released during the hydrolysis process of the chlorosilane derivatives.

2.1 Results and discussion

2.1.1 Synthesis and characterization

The bis(triacetoxysilyl)alkoxides $(AcO)_3Si–O–R–O–Si(OAc)_3$ were prepared following a synthetic approach previously developed in our research group.[109] Thus, tertiary diols (**1–4**) were reacted with two equivalents of $Si(OAc)_4$, as a silicon source, to yield the corresponding **BTA1–BTA4** ASA precursors. Similarly, for the synthesis of bis(diacetoxysilyl)alkoxides $(AcO)_2(t\text{-}BuO)Si–O–R–O–Si(Ot\text{-}Bu)(OAc)_2$ (**BDA1** and **BDA2**) the compounds **BTA1** and **BTA2** were further reacted with two equivalents of t-BuOH to substitute one AcO^- group in each silicate moiety by t-BuO group [**Scheme** 2.1].
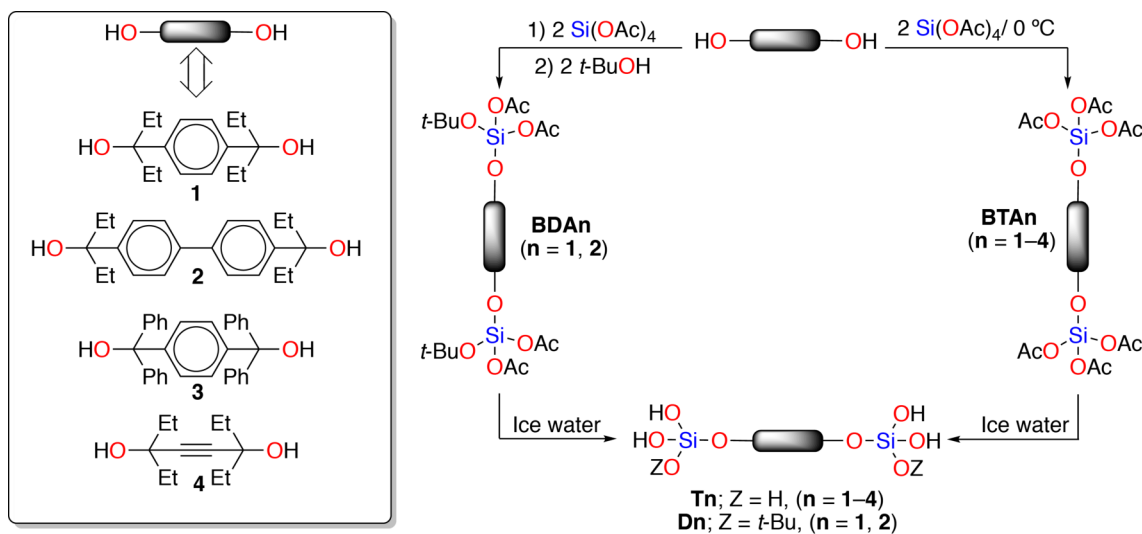
Scheme 2.1. Synthesis of bis(acetoxysilyl)alkoxides and their correspoinding organo-bis(silanetriols) and organo-bis(silanediols).

Following an analogous method, the synthesis of mono(acetoxysilyl)alkoxides was accomplished by the reaction of either Ph_3COH (**5**) or (4R,5R)-TADDOL (**6**) (TADDOL = (4R,5R)-2,2-dimethyl-$\alpha, \alpha, \alpha', \alpha'$-tetraphenyldioxolane-4,5-dimethanol) with one equivalent of $Si(OAc)_4$ to yield the corresponding mono(triacetoxylsilyl)-triphenylmethanolate (**MTA5**) and the cyclic chiral κ^2-O,O'-$(Si(OAc)_2)$-(*4R,5R*)-TADDOLate (**MDA6**). Subsequently, **MTA5** can be directly reacted with one equivalent of t-BuOH to yield the corresponding mono(diacetoxysilyl)alkoxide (**MDA5**) [**Scheme** 2.2].
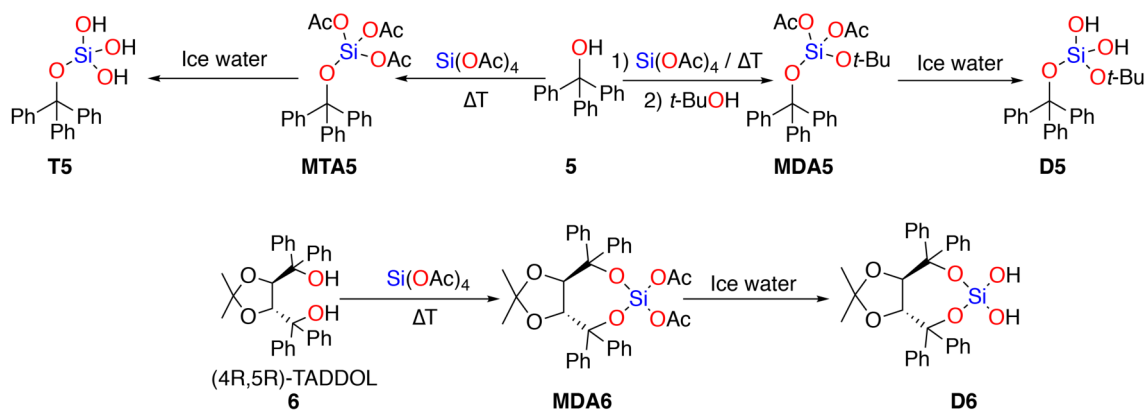
Scheme 2.2. Synthesis of mono(acetoxysilyl)alkoxides and their corresponding mono(silanols).

It is noteworthy, that the synthesis of the ASA compounds from the alcohols **3**, **5**, and **6** requires reflux in toluene to achieve the full conversion towards the ASA compounds. This fact can be explained by a higher steric hindrance around the hydroxyl groups of these tertiary alcohols compared with the rest of the alcohols used in this work.

The aforementioned synthetic approach for the synthesis of organosilylated precursors represents a straightforward way to easily modulate the steric environment around the silicon centers. Additionally, this allows an efficient control of the number of acetate groups attached to each silicon atom. With the exception of **BDA1** and **BDA2**, which are colorless oils, all the ASA derivatives were isolated as off-white crystalline powders that are soluble in polar organic solvents.

The formation of the ASA compounds was confirmed by ^{1}H and ^{13}C NMR spectroscopy (^{1}H: δ 1.52–2.14 ppm, ^{13}C: δ 21.9–23.0 for CH$_3$COO$^-$ and δ 167.7–168.6 ppm for C=O). Additionally, in the IR spectra of the ASA compounds the bands associated with the C=O stretching vibration are shifted to lower wavenumbers ($\tilde{\nu}$ 1739–1752 cm^{-1}) in comparison to those in Si(OAc)$_4$ ($\tilde{\nu}$ 1760 cm^{-1}). Afterwards, the solid ASA compounds presented above were suspended directly in ice-cold water and stirred for 2–15 min to obtain the corresponding mono- and bis-silanols. In the case of **MDA5**, ammonia was added to accelerate the hydrolysis rate, whereas in the case of oily ASA derivatives **BDA1** and **BDA2**, a mixture of water and ethylacetate was used to prevent the oily compounds from sticking to the glass walls during the hydrolysis.

The corresponding molecular organosilicates containing silanol groups OSi(OH)$_n$ (n = 2, 3)

were filtered off as a white solids in good yields (**T1**–**T5**, **D1**, **D2**, **D5**, and **D6**) [**Scheme** 2.1 and **Scheme**. 2.2]. The silanols were fully characterized by ^{1}H, ^{13}C, ^{29}Si NMR and IR spectroscopy, elemental analysis, and mass spectrometry. In addition, the molecular structures of most of them were determined by single crystal X-ray diffraction. The retention of organic moieties in the molecular silanols after the hydrolysis process was confirmed by elemental analysis and NMR spectroscopy (^{1}H and ^{13}C) where the signals corresponding to the organic moieties remained present; while those for the acetate groups, were essentially absent. The signals corresponding to the OH groups appear, in the ^{1}H spectra, in the range of δ 5.90–6.89 ppm (*see Experimental section*).

Furthermore, the corresponding normalized integrals match with the number of the OH groups expected for each silanol. Additionally, the absence of any condensation by-products in the silanols was also corroborated by the lack of the band corresponding to the siloxane Si–O–Si bridge ($\tilde{\nu}$ 1060–1220 cm^{-1}) in their IR spectra.[110]

It should be pointed out that all silanediols are soluble in polar organic solvents and toluene, whereas their silanetriol analogues are soluble only in highly polar solvents such as DMSO and only sparingly in THF. This can be explained by a higher acidity of the OH moieties in the silanetriol group and, thus, higher strength of the present hydrogen bonds (*vide infra*). These inductive effects, associated the with substituents such as OH and OR in organosilanol compounds, are further supported by ^{29}Si NMR spectroscopy, where the signals of the silanols shifted up-field with each consecutive substitution of the OH moiety by OR groups $Si(OH)_4$ ([29]Si: δ –72 ppm), $ROSi(OH)_3$ ([29]Si: δ –78.3 to –81.0 ppm), $(RO)(tBuO)Si(OH)_2$ ([29]Si: δ –83.8 to –91.2 ppm) [**Fig**. 2.2]. Moreover, in the IR spectra, the shift of the broad band attributed to OH groups in **D1**, **D2**, and **D5** ($\tilde{\nu}$ 3373, 3331 and 3381 cm^{-1}) to upper wavenumber compared to the respective silanetriol analogues **T1**, **T2** and **T5** ($\tilde{\nu}$ 3143, 3300 and 3312 cm^{-1}), evidences the influence of the number of OH groups attached to the same silicon center on the strength of the hydrogen bond interactions in the solid state. This behavior was further supported by X-ray structural analysis. Finally, these findings seem to have important implications in the relative catalytic activity of the organosilanols in the metal-free conversion of CO_2 (*vide infra*).
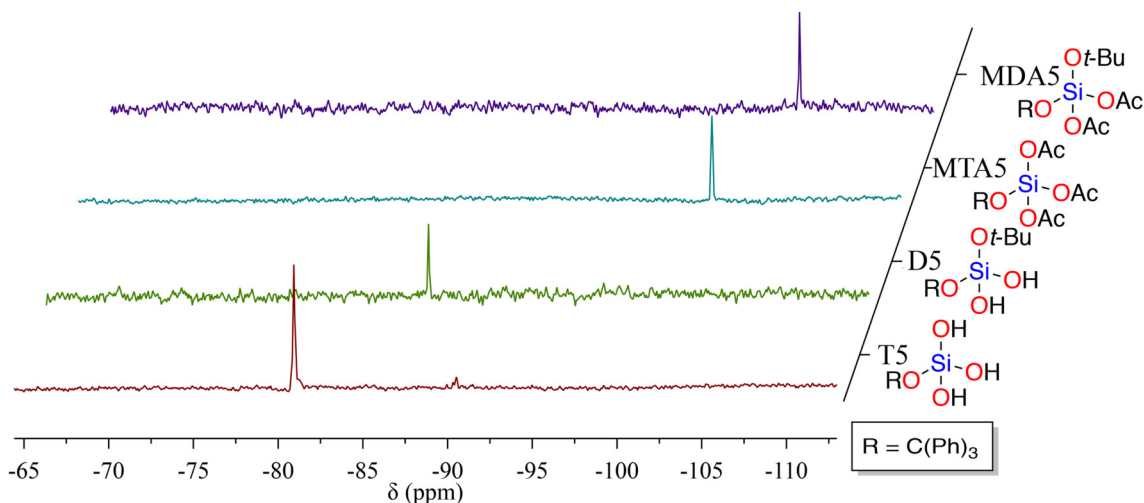
Figure 2.2. ^{29}Si NMR signals shifted up-field upon substitution of the –OH moiety by –OR groups.

2.1.2 X-ray structural analysis

The molecular structures of the acetoxylsilylalkoxides **BTA1**, **BTA4**, **MTA5**, **MDA5** and **MDA6**, silanediols **D1**, **D2**, **D5** and **D6**; as well as the mono-silanetriol **T5**, were determined by single crystal X-ray diffraction. Crystals suitable for X-ray diffraction studies were obtained either from saturated toluene (**BTA1**, **BTA4**), THF (**MTA5**, **MDA5**, **MDA6**, **D1**, **D2** and **T5**), or CH$_2$Cl$_2$ (**D5**, **D6**) solutions at –24 °C. Besides, crystals of compound **D5** were also obtained from a saturated DMSO solution by slow evaporation at room temperature. Although the bis(silanediols) **D1** and **D2** can be easily crystallized, their analogous bis(silanetriols) **T1** and **T2** always precipitate as microcrystalline powders and all attempts to grow suitable crystals for their analysis by single crystal X-ray diffraction failed. This behavior was also observed for the rest of organo-bis(silanetriols) (**T3** and **T4**). This fact can be explained by the strong tendency exhibited by the oragano-bis(silanetriols) to undergo self-condensation, when they are kept in solution for extended periods of time. Nonetheless, Murugavel *et al.* demonstrated that mono(silanetriols) could be successfully stabilized in the presence of organic diamines by the formation of Si–OH$\cdots$N adducts.[96,97] Therefore, to obtain suitable single crystals, **T1**, **T2** and **T3** were co-crystallized with organic diamines; whereas in the case of **T4** it was not possible to obtain any co-crystal, because the organic bridging group in this compound is easily hydrolyzable in solution (*see Chapter 3*).
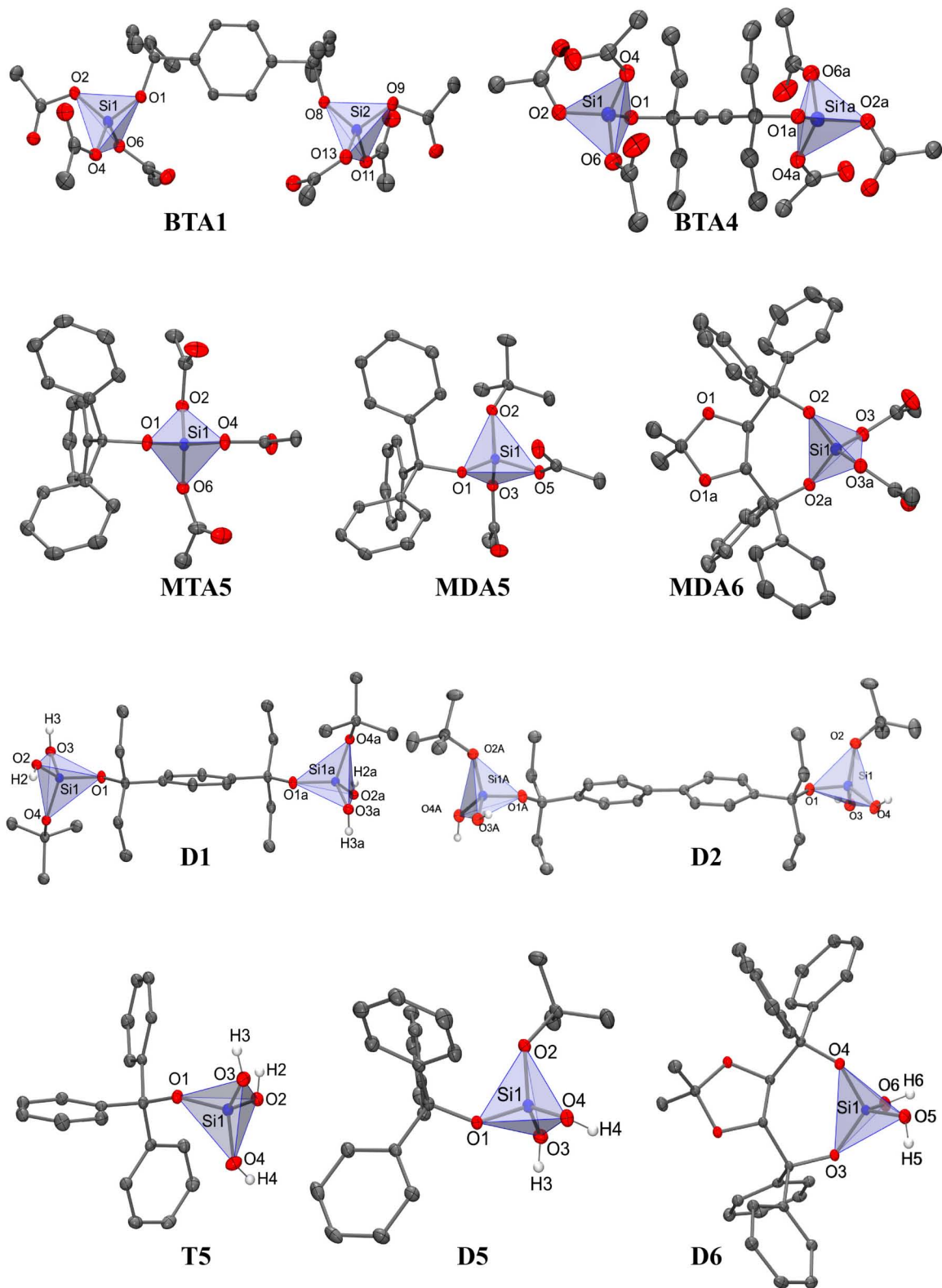
Figure 2.3. Crystal structures of acetoxysilylalkoxides and organosilanols. Thermal ellipsoids are set at 50 % probability level and carbon bound hydrogen atoms were omitted for the sake of clarity.

Compounds **BTA4**, **MTA5**, **MDA5**, **D1** and **D5·H₂O** crystallized in the triclinic $P\bar{1}$ space group, compounds **MDA6** and **D6** in the orthorhombic $P2_12_12_1$ space group, while the rest of the compounds crystallized in monoclinic space groups: C2 (**BTA1**), $P2_1$/n (**T5**) or C2/c (**D5·DMSO** and **D1**). The asymmetric unit contains half a molecule (**BTA4**, **MDA6**, **MDA5**, **D2**) one molecule (**MTA5**, **D1**, **T5**, **D5**, **D6**) or one molecule of the corresponding organosilyl derivative plus one solvent molecule: THF (**T5**), DMSO (**D5·DMSO**), H₂O (**D5·H₂O**) or CH₂Cl₂ (**D6**).

In all compounds, the Si(OX)₄ (X = OAc, H or organic group) unit has a distorted tetrahedral geometry with angles ranging from 99.34(6)° to 116.06(6)°. The Si–O bond distances are only slightly influenced by the different substituents; hence, the values for the Si–O(C) (1.578(2)–1.641(1) Å), Si–OAc (1.640(1)–1.654(1) Å) and Si–OH bonds (1.607(1)–1.632(1) Å) fall in a very narrow range. However, the Si–OAc bond lengths are always slightly longer (0.03 Å) than the corresponding Si–OH distances.

	Si–O$_{Ac}$	Si–O$_{spacer}$	Si–O$_{tBu}$	Si–OH	<O-Si-O	<O-Si-O
mono- and bis(triacetoxylsilyl)alkoxides						
MTA5	1.642(1)	1.590(1)	–	–	114.09(5)	100.84(4)
BTA1	1.648(2)	1.578(2)	–	–	114.14(13)	104.06(13)
BTA4	1.640(1)	1.588(1)	–	–	114.72(7)	102.35(7)
mono(diacetoxylsilyl)alkoxides						
MDA5	1.654(1)	1.608(1)	1.597(1)	–	114.83(4)	103.24(4)
MDA6	1.642(1)	1.611(1)	–	–	116.06(6)	99.34(6)
mono- and bis(dihydroxysilyl)alkoxides						
D6·CH₂Cl₂	–	1.616(1)	–	1.608(1)	112.01(6)	105.35(6)
D5·DMSO	–	1.628(1)	1.676(1)	1.617(1)	113.05(5)	103.47(5)
D5·H₂O	–	1.618(1)	1.637(1)	1.620(1)	113.68(6)	106.59(6)
D1	–	1.613(1)	1.641(1)	1.607(1)	112.83(4)	106.90(4)
D2	–	1.606(1)	1.611(1)	1.632(1)	112.83(7)	106.90(7)
mono(trihydroxysilyl)alkoxides						
T5·THF	–	1.618(1)	–	1.624(1)	113.82(5)	104.17(6)

Table 2-1. Selected bond distances (Å) and angles (°) for acetoxysilylalkoxides and organosilanols.

These values are comparable to those in related silicate based silanols (Si–O(C) 1.608–1.612 Å, Si–OH 1.592–1.625 Å, O–Si–O 104.7–112.4°) [Ph₂Si(μ-O)Si(OH)₂(μ-O)]₂, Me₂Si[(μ-

O)SiMe$_2$(μ-O)]$_2$Si(OH)$_2$, [(t-BuO)$_3$Si(μ-O)Si(OH)$_2$](μ-O), and [(Mes*O)$_2$Si(OH)$_2$]·2THF.[111–114]

While the acetates are isolated molecules in the crystal, the silanols form higher order supramolecular networks, directed by the self-association between adjacent molecules through strong hydrogen-bonding interactions. In this context, five different hydrogen-bonding patterns (**I**–**V**) were observed, as a function of the steric bulk of the organic groups and the number of OH groups per silicon atom that regulates the degree of self-association [**Fig**. 2.4].
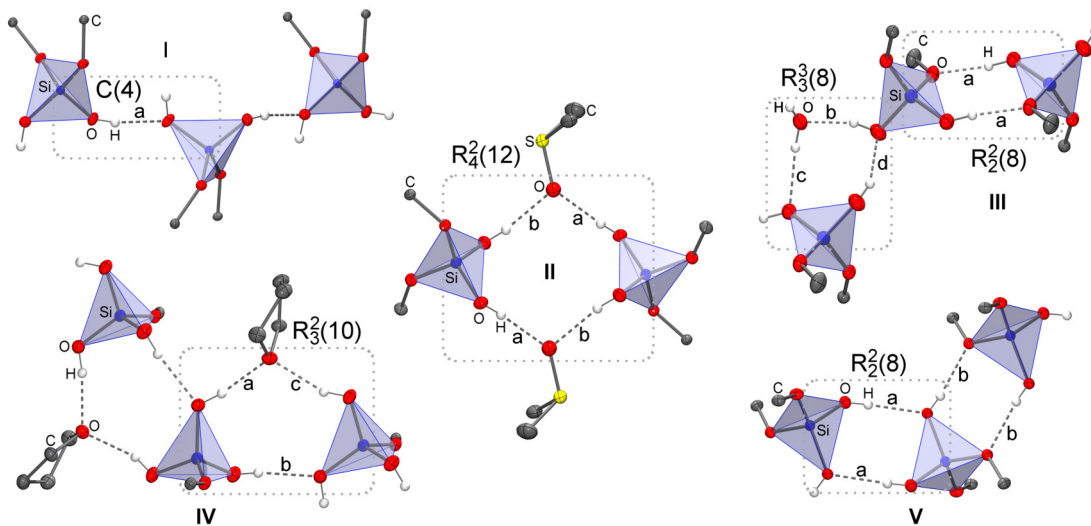
Figure 2.4. Hydrogen-bonding patterns found in compounds **D6** (I), **D5**·DMSO (II), **D5**·H$_2$O (III), **T5** (IV) and **D1** (V).

Compound	H-bond	D–H (Å)	H···A (Å)	D···A (Å)	<DHA (º)	Symmetry code
D1	O(2)–H(2)···O(4)	0.81(1)	1.91(1)	2.715(1)	171.6(2)	−x+1,−y+1,−z
	O(3)–H(3)···O(2)	0.82(1)	1.92(1)	2.721(1)	169.0(2)	−x+2,−y+1,−z
D2	O(3)–H(3)···O(3)	0.82(2)	1.91(2)	2.697(2)	160(4)	−x+1,y,−z+3/2
	O(3)–H(3)···O(4)	0.82(2)	1.92(2)	2.745(2)	176(5)	−x+1,−y+1,−z+1
	O(4)–H(4)···O(3)	0.82(2)	1.93(2)	2.745(2)	178(5)	−x+1,−y+1,−z+1
	O(4)–H(4)···O(4)	0.80(2)	2.04(3)	2.745(2)	147(5)	−x+1,y,-z+1/2
D5·DMSO	O(3)–H(3)···O(5)	0.82(1)	1.96(2)	2.773(1)	170.7(2)	−x+1/2,−y+3/2,−z+1
	O(4)–H(4)···O(5)	0.81(1)	1.89(2)	2.678(1)	167.2(2)	−x+1/2,−y+3/2,−z+1
D5·H$_2$O	O(3)–H(3)···O(5)	0.86(2)	1.77(2)	2.600(3)	161.0(5)	−x+1,−y+1,−z+1
	O(4)–H(4)···O(2)	0.86(2)	1.88(2)	2.731(2)	172.0(2)	−x+1,−y+1,−z+1
	O(5)–H(5)···O(4)	0.82(2)	2.06(2)	2.870(3)	168.0(4)	−x+2,−y+1,−z+1
D6	O(5)–H(5)···O(6)	0.81(2)	1.94(2)	2.744(2)	171.0(2)	x+1/2,−y+3/2,−z+1
T5	O(2)–H(2)···O(5)	0.83(1)	1.85(2)	2.670(2)	170.0(2)	−x+1,y+1/2,−z+3/2
	O(3)–H(3)···O(2)	0.83(1)	2.08(1)	2.908(2)	173.0(2)	−x+1,y+1/2,−z+3/2
	O(4)–H(4)···O(5)	0.83(1)	1.99(3)	2.780(3)	158.0(2)	−x+1,y−1/2,−z+3/2

Table 2-2. Selected bond distances (Å), angles (°) and geometric parameters for the hydrogen-bonds in the compounds **D1**, **D2**, **D5**·DMSO, **D5**·H$_2$O, **D6**, **T5**.

In this study, the TADDOL derivative **D6** contains the bulkiest organic group, which resulted in the formation of only a single hydrogen-bond derived by the self-association between adjacent molecules [**Fig**. 2.4, motif **I**]; where the proton from one Si–OH group coordinates to the oxygen atom from the second Si–OH group belonging to a neighboring molecule of **D6** and the proton of this accepting OH group is also involved in an C–H$\cdots\pi$ interaction. Consequently, the aforementioned self-assembly between adjacent **D6** molecules leads to the formation of 1D infinite chain; which propagates parallel to the crystallographic a-axis and can be described according the graph set theory as C(4) [**Fig**. 2.5].
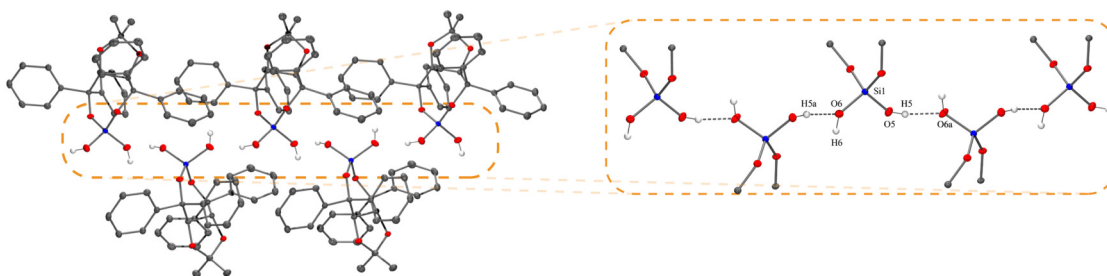
Figure 2.5. Supramolecular chain formed by the self-association between adjacent **D6** molecules.

In the case of **D5**·H_2O, the characteristic Si–OH$\cdots$H homodimer ring pattern $R_2^2(8)$ usually found in organosilanediol structures is present [**Fig**. 2.4, motif **III**]. In this solvatomorphic structure, **D5** crystallize as hydrate, where the water molecule play the role of a "molecular glue" to interconnect these $R_2^2(8)$ synthons through the formation of the ring motif $R_3^3(8)$ to afford a hydrogen bonded extended network [**Fig**. 2.6 (b)].

By contrast, in the other solvatomorph of **D5**, two molecules of DMSO were included in the structure and these break the strong Si–OH$\cdots$H interaction of the homodimer $R_2^2(8)$ to give an heterosynthon formed by discrete solvated rings $R_4^2(12)$ [**Fig**. 2.4, motif **II**]; where the oxygen atom in DMSO acts as hydrogen-bond acceptor suppressing the formation of an extended network [**Fig**. 2.6 (a)].
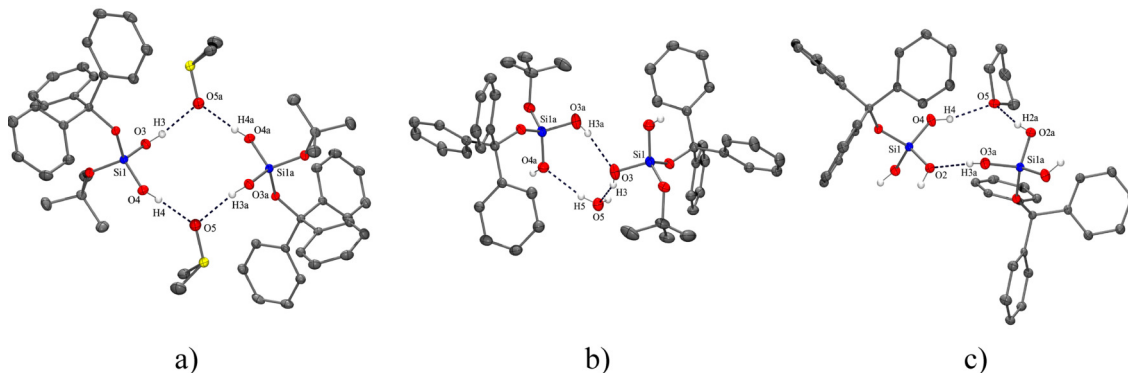
Figure 2.6. Molecular structures of **D5**·DMSO (a), **D5**·H$_2$O (b), and **T5**·THF (c).

In **T5**, the *t*-BuO group present in **D5** is replaced by a third OH group leading to a higher acidity and lower steric protection around the silicon center [**Fig**. 2.6 (c)]. Accordingly, **T5** presents a modulated equilibrium between solvent interaction and self-association through (Si–OH···O–Si) hydrogen-bonding. Hence, the THF breaks one of the two hydrogen bonds involved in the R$_2^2$(8) synthon to give an interconnected ring pattern R$_3^2$(10), which is classified as third level graph-set. Also, this motif could be described on a binary-level through hydrogen bonding chains C(4) and C$_2^1$(6) [**Fig**. 2.4, motif **IV**].

In the case of organo(bis-silanediols) **D1** and **D2**, the organic group acts as bridging moiety between two silicate centers, resulting in higher order structures than in the monosilicate analogs. Thus, in such compounds the self-association produces a zig-zag interconnected chains described as C$_2^2$(26)[R$_2^2$(8)] and C$_2^2$(34)[R$_2^2$(8)]; respectively [**Fig**. 2.7].

In **D1** and **D2**, the hydrogen bonded chain formed of alternated ring homodimers R$_2^2$(8) between silicate centers are propagated parallel to the crystallographic *a*-axis and *c*-axis, respectively; where the organic *spacer* acts as pillar between those hydrogen bonded chains which gives rise to the formation of 2D extended networks constituted by supramolecular macrocycles, without the inclusion of solvent molecules [**Fig**. 2.4, motif **V**].
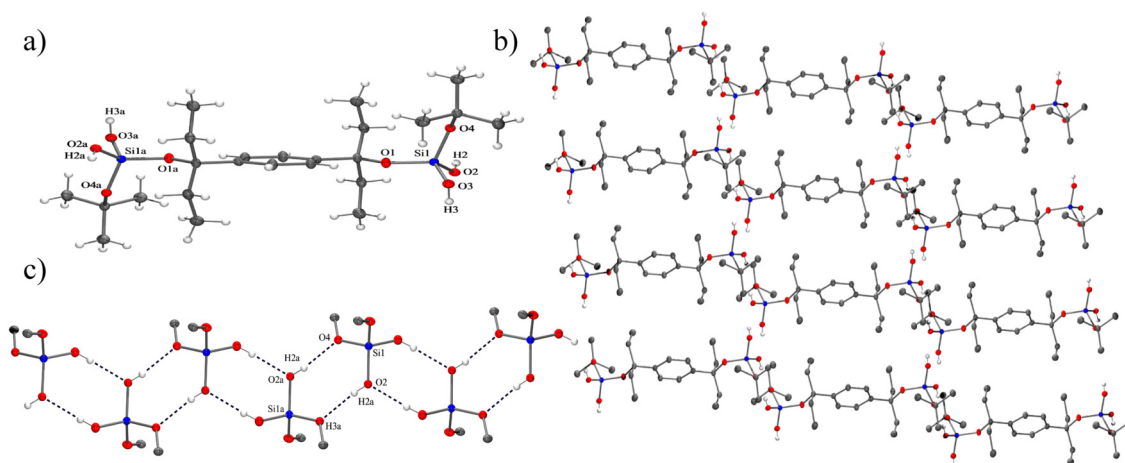
Figure 2.7. Supramolecular arrangement in the crystal of **D1**. (a) molecular structure of **D1**, (b) two-dimensional extended network, and (c) supramolecular chain formed by the self-association of the silanol moieties.

2.1.3 Catalytic studies

The synergic effect between onium salts such as phosphonium and ammonium halides and Si–OH groups in the catalytic cycloaddition of CO_2 to epoxides has been reported previously.[115–118] However, most of them operate as a heterogeneous catalyst where silica is used as silanol source acting as a support to immobilize the onium salts. Although this approach facilitates the separation and recycling of the catalyst due to its heterogeneous nature, this approach regularly requires harsh reaction conditions, such as high pressure and temperature.

As an alternative, the use of molecular bis(1-naphthyl)silanediol and tetrabutylammonium halides as co-catalysts has been reported.[12] This is an homogeneous system, that under mild reaction conditions, affords excellent yield in the CO_2 coupling with styrene oxide. Unfortunately, the major drawback for the industrial application of bis(1-naphthyl)silanediol for the catalytic upgrading of CO_2 is its the high cost of production, and that this compound can not be easily recovered and recycled.

In this context, our synthetic approach offers a simple and cost-efficient alternative to achieve an eco-friendly production of organosilanols, where the steric and/or electronic effects around the silicon atom can be easily modulated, and consequently, the number and strength of hydrogen bonds are also fine-tunable. This fact should have a direct effect on the activity of Si–OH groups in the hydrogen-bond donor (HBD) organocatalysis. To evaluate this hypothesis, the

organocatalytic cycloaddition of CO_2 with styrene oxide (SO) to yield styrene carbonate (SC) was tested using selected alkoxysilanols in the presence of tetrabutylammonium iodide (TBAI, 10 mol%) as a Lewis base catalyst. Thus, the binary systems (10 mol% organosilanol/TBAI) were used under solvent free and mild reaction conditions (60 °C, 15 h, using a balloon of CO_2) [**Scheme** 2.3].

Entry	Catalyst	Yield $(\%)^{a,b}$	Entry	Catalyst	Yield $(\%)^{a,b}$
1	–	31	4	**T5**	>99(96)^c, 85^d
2	**T1**	93	5	**D5**	>99
3	**D1**	99	6	**D6**	98
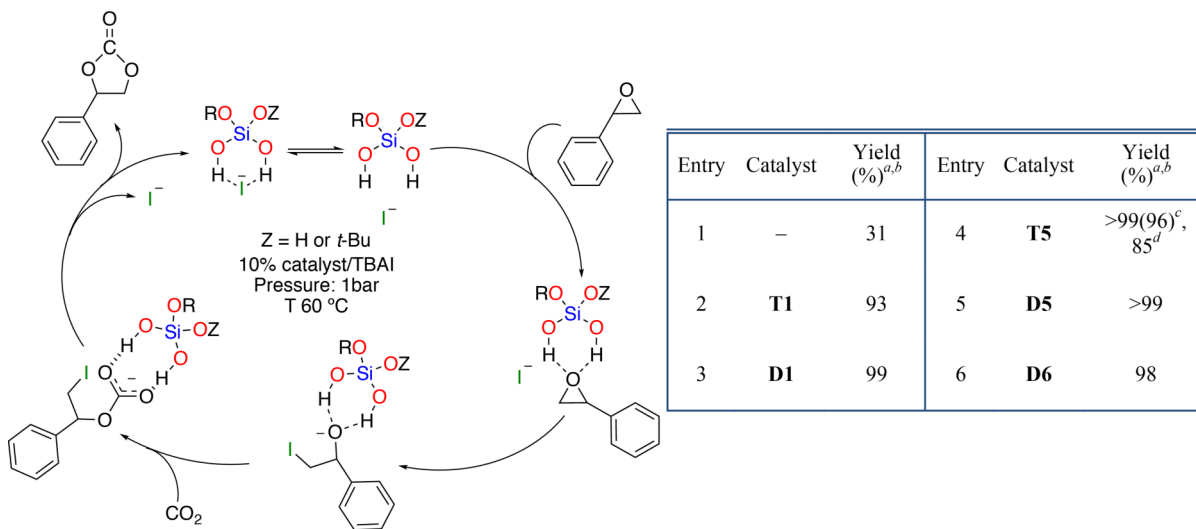
Scheme 2.3. Conversion of styrene oxide (SO) and CO_2 into styrene carbonate (SC). (^{a} each experiment was repeated 3 times and the average yield is reported; ^{b} reported yields are based on ^{1}H NMR using toluene as internal standard (selectivity > 99%), ^{c} yield obtained after 12 h, ^{d} yield obtained with 5 mol% cat).

However, the results obtained seem to be counterintuitive since it is generally assumed that the most acidic silanols are the best catalysts. Nevertheless, **T1** showed the lowest conversion, even when it is one of the most acidic alkoxysilanols in this study, and it contains, in principle, six active hydroxyl groups per molecule. By contrast, **D1** showed better catalytic performance, even though the substitution of two OH groups by two t-BuO moieties lowers its acidity. This behaviour can be rationalized in terms of the relative strength of their self-association, because **T1** is much more prone to form aggregates due to the lower steric hindrance around the silicon atom and due to its higher acidity; this compound. This fact is also supported by its low solubility in the media. Nonetheless, in **D1** the substitution of two OH groups by two t-BuO moieties not only reduces its acidity, but also increases the steric protection around the silicon atom and its solubility in the reaction media.

Consequently, this reduces its self-association and increases the availability of the OH groups in the catalytic process. Therefore, a balance between solubility and acidity is essential for an optimum catalytic performance [**Fig**. 2.8].
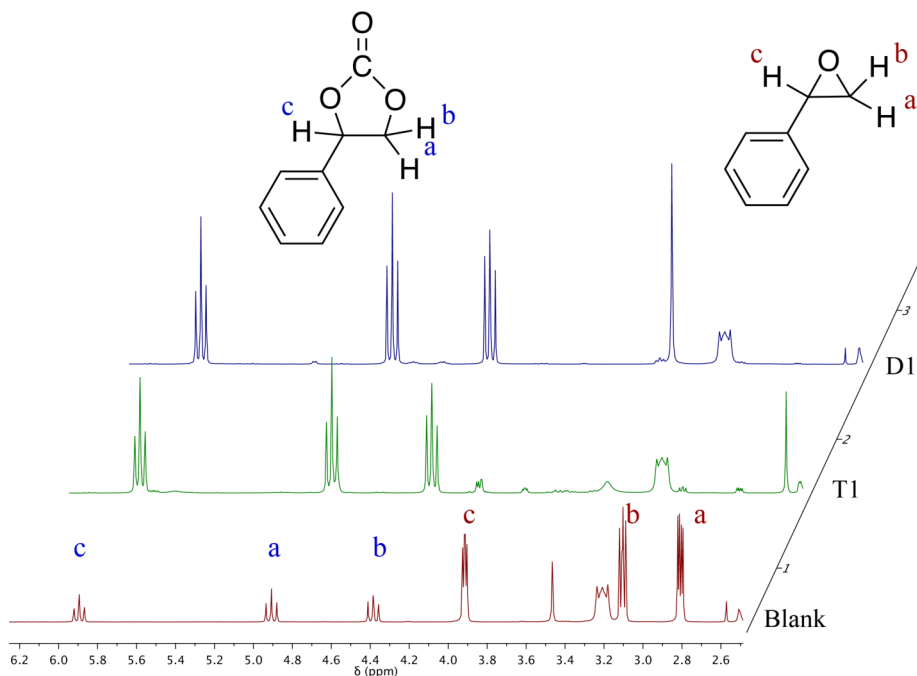
Figure 2.8. Relative differences in the organocatalytic performance of **T1** and **D1** for the CO_2 conversion, ^{1}H NMR in DMSO-d_6.

Finally, **T5** showed practically quantitative conversion after 12 h. We chose this system to test the sustainability and economical process where the recycling of the catalysts plays an important role. Therefore, the mixture of **T5** and TBAI was recycled by filtration through the addition of diethyl ether/hexane (1:2) mixture, which dissolves the SC preferentially. Moreover, **T5** can be used in three consecutive runs with only 13% activity loss in the third cycle. However, slight catalyst leaching effects were observed [**Fig**. 2.9]. Furthermore, the binary catalytic system **T5**/TBAI can be easily recycled through filtration as heterogeneous catalysts and its catalytic performance in the cycloaddition of CO_2 with SO to SC is comparable with that reported for bis(1-naphthyl)silanediol and others homogeneous HB organocatalysts reported in the literature.

40

Although **T1** shows only 93% of conversion, it is insoluble in diethyl ether and thus easily recyclable. Nonetheless, after the second run, we observed a significant loss of activity. This fact could be explained by the higher tendency of **T1** to undergo self-condensation under the reaction conditions.
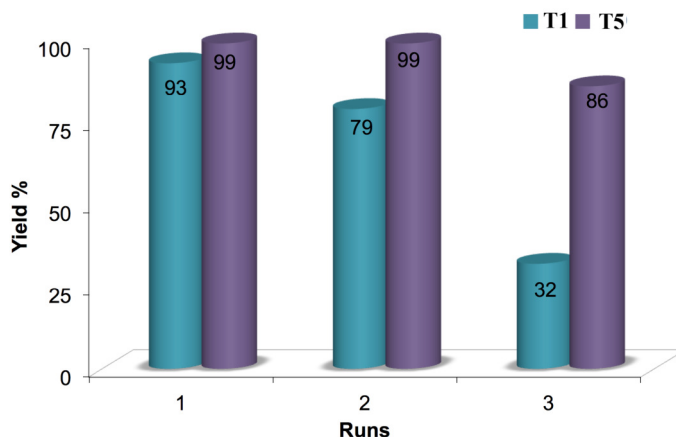
Figure 2.9. Comparative yields of SC obtained after three consecutive runs using recycled catalysts **T1** and **T5**.

2.2   Conclusions

Acetylsilylalkoxides (ASA) offer a straightforward scalable and cost-efficient synthetic pathway towards molecular hybrid organosilanoles. Such pathway eliminates the main disadvantages of the current synthetic methods, such as: large quantities of organic solvent, the use of a base, and long reaction times. Additionally, it allows a stepwise tuning of the steric and electronic environment of the silicon atom; the precise control of the number of OH groups attached to each silicon atom, as well as their Brønsted acidity and consequently their hydrogen bonding capabilities. Therefore, their organocatalytic properties can be easily tailored, as observed in the cycloaddition of CO_2 with styrene oxide, to form styrene carbonate in the presence of TBAI.

2.3 Experimental section

2.3.1 General methods

The syntheses of the ASA compounds (**BTAn**; n = 1–4, **MTA5**, **BDA1**, **BDA2**, **MDA5**, and **MDA6**) were performed under a dried dinitrogen atmosphere using Schlenk and glove-box techniques, using a general method developed in our research group for the synthesis of compounds **BTA1** and **BTA4**.[109] The solvents were purchased from Sigma-Aldrich and dried prior use with an MBraun SPS solvent purification system using Grubs' columns. *tert*-Butyl alcohol was dried with Na and distilled before use; tetrabutylammonium iodide (TBAI) was purchased from Sigma-Aldrich and recrystallized from a CH_2Cl_2/hexane mixture. The triphenylmethanol (**5**) and styrene oxide, were purchased from Sigma-Aldrich and used without further purification, whereas $Si(OAc)_4$, 1,4-bis(diethylhydroxymethyl)benzene (**1**), 4,4'-bis(diphenylhydroxymethyl) biphenyl (**2**), 1,4-bis(diphenylhydroxymethyl)benzene (**3**), 3,6-diethyl-4-octyne-3,6-diol (**4**), and (4R,5R)-2,2-dimethyl-$\alpha, \alpha, \alpha', \alpha'$-tetraphenyldioxolane-4,5-dimethanol (**6**) were prepared according to the literature procedures.[119–124] C_6D_6 was distilled from a Na/K alloy and $CDCl_3$ was dried with P_4O_{10}, both solvents were degassed before use. DMSO-d_6 was purchased from ABCR and used as received. Industrial grade CO_2 was purchased from INFRA S.A. de C.V. and used as received. NMR spectroscopic data were recorded on a Bruker Avance III 300 MHz spectrometer and referenced to residual signals of the deuterated solvent for ^{1}H and ^{13}C nuclei, or TMS as an external standard for the ^{29}Si spectra. The integral values of bridged organosilyl compounds were reported taking into account just one-half of the molecule. Electron impact mass spectrometry (EI-MS) and chemical ionization mass spectrometry were carried out on a Shimadzu GCMS-QP2010 Plus using direct injection in the detection range of m/z 20–1090. Elemental analyses (C, H, N) were determined on an Elementar MicroVario Cube analyzer. FT-IR spectra were recorded on a Bruker ALPHA FTIR spectrometer placed inside a glove-box using the ATR technique with a diamond window in the range of $\tilde{\nu}$ 500–4000 cm^{-1}. Melting points were measured in sealed capillaries on a Büchi B-540 melting point apparatus.

2.3.2 Preparation of ASA compounds

1,4-[(AcO)$_3$SiOCEt$_2$]$_2$C$_6$H$_4$ (BTA1): A solution of **1** (0.50 g, 2.00 mmol) in toluene (5 mL) was added dropwise to a suspension of silicon tetraacetate (1.06 g, 4.01 mmol) in toluene (10 mL). The reaction mixture was stirred for 4 h. Afterwards, all volatiles were removed under reduced pressure to afford the product as a white solid. **Yield**: 1.19 g, 1.81 mmol, 90%. **M.p.** 115–115 °C. Single crystals of compound **BTA1** were grown from a saturated toluene solution at –24 °C. **Elemental analysis** (%) Calcd for C$_{28}$H$_{42}$O$_{14}$Si$_2$ (658.80 g·mol^{-1}): C 51.05, H 6.43; Found: C 50.67, H 6.26. **FT-IR (ATR) (cm^{-1})** $\tilde{\nu}$ 2980, 2941 (w, C–H, CH$_3$, CH$_2$), 1739 (s, C=O), 951 (s, Si–O). **^{1}H NMR** (300.53 MHz, C$_6$D$_6$): δ (ppm) 0.85 (t, 6H, $^3J_{H-H}$ = 7.3 Hz, CH$_2$C*H*$_3$), 1.73 (s, 9H, OCC*H*$_3$), 1.93 (dq, 2H, $^2J_{H-H}$ = 14.5 Hz, $^3J_{H-H}$ = 7.3 Hz, C*H*$_2$), 2.13 (dq, 2H, $^2J_{H-H}$ = 14.5 Hz, $^3J_{H-H}$ = 7.3 Hz, C*H*$_2$), 7.47 (s, 2H, Ar*H*). **^{13}C{^{1}H} NMR** (75.57 MHz, C$_6$D$_6$): δ (ppm) 8.3 (CH$_2$*C*H$_3$), 22.0 (OC*C*H$_3$), 35.7 (*C*H$_2$CH$_3$), 87.2 (*C*Et$_2$), 125.9, 141.9 (*o*, *i*, *C* of Ar), 168.0 (*C*=O). **^{29}Si NMR** (59.63 MHz, C$_6$D$_6$): δ (ppm) –101.4. **EI-MS**: m/z (%) 629 (9) [M–Et]$^+$, 407 (100) [M–Et–Si(OAc)$_3$–OH]$^+$.

1,4-[{(AcO)$_2$(*t*-BuO)Si}OCEt$_2$]$_2$C$_6$H$_4$ (BDA1): *t*-BuOH (3 mL) was added to **BTA1** (1.00 g, 1.52 mmol) and the reaction mixture was stirred for 12 h. All volatiles were removed under reduced pressure and the product was isolated as a colorless oil. **Yield**: 0.91 g, 1.32 mmol, 87%. **Elemental analysis** (%) Calcd for C$_{32}$H$_{54}$O$_{12}$Si$_2$ (686.93 g·mol^{-1}): C 55.65, H 7.92; Found: C 55.65, H 7.88. **FT-IR (ATR) (cm^{-1})** $\tilde{\nu}$ 2975, 2937 (w, C–H, CH$_3$, CH$_2$), 1743 (s, C=O), 984 (s, Si–O). **^{1}H NMR** (300.53 MHz, CDCl$_3$): δ (ppm) 0.69 (t, 6H, $^3J_{H-H}$ = 7.2 Hz, CH$_2$C*H*$_3$), 1.37 (s, 9H, C(C*H*$_3$)$_3$), 1.84–2.05 (m, 4H, C*H*$_2$CH$_3$), 2.10 (s, 6H, OC*C*H$_3$), 7.28 (s, 2H, Ar*H*). **^{13}C{^{1}H} NMR** (75.57 MHz, CDCl$_3$): δ (ppm) 8.2 (CH$_2$*C*H$_3$), 23.0 (OC*C*H$_3$), 31.3 (C(*C*H$_3$)$_3$), 35.0 (*C*H$_2$CH$_3$), 76.2 (*C*(CH$_3$)$_3$), 85.3 (*C*Et$_2$), 125.4, 142.0 (*o*, *i*, *C* of Ar), 168.6 (*C*=O). **^{29}Si NMR** (59.63 MHz, CDCl$_3$): δ (ppm) –101.8. **EI-MS**: m/z (%) 657 (55) [M–Et]$^+$, 627 (10) [M–OAc]$^+$, 613 (30) [M–^{t}BuO]$^+$.

[1,1'-Biphenyl]-4,4'-[(AcO)$_3$SiOCEt$_2$]$_2$ (BTA2): A solution of **2** (1.00 g, 3.06 mmol) in toluene (10 mL) was added to a solution of silicon tetraacetate (1.62 g, 6.13 mmol) in dichlorome-thane (15 mL) at 0 °C. The reaction was allowed to warm to ambient temperature and stirred for 4 h. Afterwards, all volatiles were removed under reduced pressure to afford the corresponding bis(triacetoxylsilyl)alcoxide **BTA2** as a white solid. **Yield**: 2.02 g, 2.75 mmol, 90%. **M.p.** > 345 °C. **Elemental analysis** (%) Calcd for C$_{34}$H$_{46}$O$_{14}$Si$_2$ (784.89 g·mol^{-1}): C 55.57, H 6.31; Found: C 54.99, H 6.21. **FT-IR (ATR) (cm^{-1})** $\tilde{\nu}$ 2980, 2942 (w, C–H, CH$_3$, CH$_2$), 1740 (s, C=O), 950 (s, Si–O). **^{1}H NMR** (300.53 MHz, CDCl$_3$): δ (ppm) 0.77 (t, 6H, $^3J_{H-H}$ = 7.3 Hz, CH$_2$CH_3), 2.14 (s, 9H, OCCH_3), 2.01 (m, 4H, CH_2), 7.39 (d, 2H, $^3J_{H-H}$ = 8.3 Hz, ArH), 7.57 (d, 2H, $^3J_{H-H}$ = 8.3 Hz, ArH). **^{13}C{^{1}H} NMR** (75.57 MHz, C$_6$D$_6$): δ (ppm) 8.3 (CH$_2$$CH_3$), 22.0 (OC$CH_3$), 35.7 ($CH_2CH_3$), 87.2 ($CEt_2$), 125.9, 126.4 141.9, 144.9(C of Ar), 168.0 (C=O). **^{29}Si NMR** (59.63 MHz, C$_6$D$_6$): δ (ppm) –102.3. **EI-MS**: m/z (%) 766 (9) [M–Et]$^+$.

[1,1'-Biphenyl]-4,4'-[(AcO)$_2$(t-BuO)SiOCEt$_2$]$_2$ (BDA2): t-BuOH (3 mL) was added to **BTA1** (1.00 g, 1.27 mmol) and the reaction mixture was stirred for 12 h. All volatiles were removed under reduced pressure and the product was isolated as a colorless oil. **Yield**: 0.80 g, 1.05 mmol, 83%. **Elemental analysis** (%) Calcd for C$_{38}$H$_{58}$O$_{12}$Si$_2$ (763.04 g·mol^{-1}): C 59.82, H 7.66; Found: C 58.65, H 7.63. **FT-IR (ATR) (cm^{-1})** $\tilde{\nu}$ 2965, 2927 (w, C–H, CH$_3$, CH$_2$), 1744 (s, C=O), 970 (s, Si–O). **^{1}H NMR** (300.53 MHz, CDCl$_3$): δ (ppm) 0.69 (t, 6H, $^3J_{H-H}$ = 7.2 Hz, CH$_2$CH_3), 1.37 (s, 9H, C(CH_3)$_3$), 1.84–2.05 (m, 4H, CH_2CH$_3$), 2.10 (s, 6H, OCCH_3), 7.40, 7.60 (d, 4H, ArH). **^{13}C{^{1}H} NMR** (75.57 MHz, CDCl$_3$): δ (ppm) 8.2 (CH$_2$$CH_3$), 23.0 (OC$CH_3$), 31.3 (C($CH_3$)$_3$), 35.0 ($CH_2CH_3$), 76.2 ($C$(CH$_3$)$_3$), 85.3 ($CEt_2$), 125.4, 126.8, 142.0,145.0 (C of Ar), 168.6 (C=O). **^{29}Si NMR** (59.63 MHz, CDCl$_3$): δ (ppm) –102.0. **EI-MS**: m/z (%) 734 (55) [M–Et]$^+$.

1,4-[(AcO)$_3$SiOCPh$_2$]$_2$C$_6$H$_4$ (BTA3): To a mixture of **3** (0.50 g, 1.13 mmol) and silicon tetraacetate (0.6 g, 2.26 mmol) was added toluene (20 mL). The reaction mixture was heated under reflux for 3 h. Afterwards, all volatiles were removed under reduced pressure, to afford the product as a white solid. **Yield**: 0.77 g, 0.90 mmol, 80%. **M.p.** > 350 °C. **Elemental analysis** (%) Calcd for C$_{44}$H$_{42}$O$_{14}$Si$_2$ (850.97 g·mol^{-1}): C 62.10, H 4.97; Found: C 61.60, H 5.01. **FT-IR (ATR) (cm^{-1})** $\tilde{\nu}$ 1750 (s, C=O), 955 (s, Si–O). **^{1}H NMR** (300.53 MHz,

CDCl$_3$): δ (ppm) 1.83 (s, 9H, OCCH_3), 7.20–7.39 (m, 24H, ArH). ^{13}C$\{^1$H$\}$ NMR (75.57 MHz, C$_6$D$_6$): δ (ppm) 21.9 (OCCH$_3$), 88.5 (CPh$_3$), 127.9, 128.2, 128.4, 128.9, 144.8, 145.3(C of Ar), 167.7 (C=O). ^{29}Si NMR (59.63 MHz, CDCl$_3$): δ (ppm) –101.9. **EI-MS**: m/z (%) 365 (2) [M–Ph–2(Si(OAc)$_3$)]$^+$.

1,2-[(AcO)$_3$SiOCEt$_2$]$_2$C$_2$ (BTA4): A solution of **4** (0.50 g, 2.50 mmol) in toluene (5 mL) was added dropwise to a suspension of silicon tetraacetate (1.33 g, 5.05 mmol) in toluene (10 mL). The reaction was stirred for 4 h. Afterwards, all volatiles were removed under reduced pressure to afford the product as a white solid. **Yield**: 1.36 g, 2.24 mmol, 90%. **M.p.** 49–51 °C. Single crystals of compound **BTA4** were grown from a saturated toluene solution at –24 °C. **Yield**: 1.36 g, 2.24 mmol, 90%. **M.p.** 49–51 °C. **Elemental analysis** (%) Calcd for C$_{24}$H$_{38}$O$_{14}$Si$_2$ (606.72 g·mol^{-1}): C 47.51, H 6.31; Found: C 47.31, H 6.31 **FT-IR (ATR) (cm^{-1})** $\tilde{\nu}$ 2983, 2946 (w, C–H, CH$_3$, CH$_2$), 1744 (s, C=O), 947 (s, Si–O). ^{1}H NMR (300.53 MHz, C$_6$D$_6$): δ (ppm) 1.12 (t, 6H, $^3J_{H-H}$ = 7.4 Hz, CH$_2$CH_3), 1.78 (s, 9H, OCCH_3), 1.82–1.97 (m, 4H, CH_2CH$_3$). ^{13}C$\{^1$H$\}$ NMR (75.57 MHz, C$_6$D$_6$): δ (ppm) 8.8 (CH$_2$$CH_3$), 22.1 (OC$CH_3$), 35.0 ($CH_2CH_3$), 78.4 ($C\equiv C$), 86.6 ($CEt_2$), 167.9 ($C$=O). ^{29}Si NMR (59.63 MHz, CDCl$_3$): δ (ppm) –99.2. **EI-MS**: m/z (%) 577 (1) [M–Et]$^+$.

Ph$_3$COSi(OAc)$_3$ (MTA5): To a mixture of **5** (1.00 g, 3.84 mmol) and silicon tetraacetate (1.01 g, 3.84 mmol) was added toluene (20 mL). The reaction mixture was heated under reflux for 3 h. Afterwards, all volatiles were removed under reduced pressure, to afford the product as a white solid. Single crystals of compound **MTA5** were grown from a saturated THF solution at –35 °C. **Yield**: 1.52 g, 3.27 mmol, 85%. **M.p.** > 350 °C. **Elemental analysis** (%) Calcd for C$_{25}$H$_{24}$O$_7$Si (464.55 g·mol^{-1}): C 64.64, H 5.21; Found: C 64.30, H 5.26. **FT-IR (ATR) (cm^{-1})** $\tilde{\nu}$ 3059, 3023 (w, C–H, Ph), 1749 (s, C=O), 955 (s, Si–O). ^{1}H NMR (300.53 MHz, CDCl$_3$): δ (ppm) 1.52 (s, 9H, OCCH_3), 7.11–6.99 (m, 3H, CH of Ph), 7.26–7.12 (m, 6H, CH of Ph), 7.70 (d, 6H, $^3J_{H-H}$ = 8.0 Hz, CH of Ph). ^{13}C$\{^1$H$\}$ NMR (75.57 MHz, C$_6$D$_6$): δ (ppm) 21.8 (OCCH$_3$), 88.7 (CPh$_3$), 127.8, 128.2, 129.0, 145.5 (C of Ph) 167.7 (C=O) ^{29}Si NMR (59.63 MHz, CDCl$_3$): δ (ppm) –101.8. **EI-MS**: m/z (%) 464 (21) [M]$^+$.

Ph$_3$COSi(Ot-Bu)(OAc)$_2$ (MDA5): t-BuOH (3 mL) was added to **MTA5** (1.00 g, 2.15 mmol) and the reaction mixture was stirred for 12 h. Afterwards, all volatiles were removed under reduced pressure and the product was isolated as a white solid. **Yield**: 0.70 g, 1.46 mmol,

68%. **M.p.** 87–89 °C. **Elemental analysis** (%) Calcd for $C_{27}H_{30}O_6Si$ (478.61 g·mol^{-1}): C 67.76, H 6.32; Found: C 67.58, H 6.50 **FT-IR (ATR) (cm^{-1})** $\tilde{\nu}$ 3057 (w, C–H, Ph), 2982, 2937, (w, C–H, CH_3), 1740 (s, C=O), 951 (s, Si–O). **^{1}H NMR** (300.53 MHz, CDCl$_3$): δ (ppm) 1.17 (s, 9H, C(CH_3)$_3$), 1.88 (s, 6H, OCCH_3), 7.22–7.32 (m, 9H, CH of Ph), 7.38–7.42 (m, 6H, CH of Ph). **^{13}C{^{1}H} NMR** (75.57 MHz, C$_6$D$_6$): δ (ppm) 22.7 (OCCH$_3$), 31.0 (C(CH$_3$)$_3$), 76.2 (C(CH$_3$)$_3$), 87.2 (CPh$_3$), 127.3, 127.7, 128.8, 145.5 (C of Ph), 168.3 (C=O). **^{29}Si NMR** (59.63 MHz, CDCl$_3$): δ (ppm) –105.1. **EI-MS**: m/z (%) 478 (5) [M]$^+$.

O,O'-TADDOL-Si(OAc)$_2$ (MDA6): A solution of **6** (0.40 g, 0.86 mmol) in toluene (10 mL) was added to a suspension of silicon tetraacetate (0.23 g, 0.86 mmol) in toluene (5 mL) and the reaction mixture was heated under reflux for 3 h. Afterwards, all volatiles were removed under reduced pressure and the product was isolated as a white solid. **Yield**: 0.41 g, 0.67 mmol, 78%. **M.p.** 263 °C. **Elemental analysis** (%) Calcd for $C_{35}H_{34}O_8Si$ (610.73 g·mol^{-1}): C 68.83, H 5.61; Found: C 68.36, H 5.90. **FT-IR (ATR) (cm^{-1})** $\tilde{\nu}$ 1752 (m, C=O), 937 (m, Si–O). **^{1}H NMR** (300.53 MHz, CDCl$_3$): δ (ppm) 0.52 (s, 6H, C(CH_3)$_2$), 1.78 (s, 6H, OCCH_3), 5.24 (s, 2H, Ph$_2$CCHO), 7.13–7.38 (m, 16H, CH of Ph), 7.58 (d, 4H, $^3J_{H-H}$ = 7.9 Hz, CH of Ph). **^{13}C{^{1}H} NMR** (75.57 MHz, CDCl$_3$): δ (ppm) 22.1 (OCCH$_3$), 27.0 (C(CH$_3$)$_2$), 80.9 (Ph$_2$CCHO), 84.3 (CPh$_2$), 114.3 (C(CH$_3$)$_2$), 127.1, 127.1, 127.3, 127.7, 128.1, 129.1, 141.3, 146.0 (C of Ph), 168.2 (C=O). **^{29}Si NMR** (59.63 MHz, CDCl$_3$): δ (ppm) –94.3. **EI-MS**: m/z (%) 610 (16) [M]$^+$.

2.3.3 Synthesis of organosilanols

1,4-[(HO)$_3$SiOCEt$_2$]$_2$C$_6$H$_4$ (T1): BTA1 (0.35 g, 0.53 mmol) was suspended in cold distilled water (5 mL). The reaction mixture was vigorously stirred at 0 °C for 10 min. Afterwards, the white powder was collected via filtration and washed with cold water (2 x 2 mL) in order to remove the remanent acetic acid. **Yield**: 0.20 g, 0.50 mmol, 93%. **M.p.** > 350 °C. **Elemental analysis** (%) Calcd for C$_{16}$H$_{30}$O$_8$Si$_2$ (406.58 g·mol^{-1}): C 47.27, H 7.44; Found: C 46.90, H 7.30. **FT-IR (ATR) (cm^{-1})** $\tilde{\nu}$ 3143 (s, SiO–H), 2972, 2937 (w, C–H, CH$_3$, CH$_2$), 918 (s, Si–O). **^{1}H NMR** (300.53 MHz, DMSO-d_6): δ (ppm) 0.59 (t, 6H, $^3J_{H-H}$ = 7.3 Hz, CH$_2$CH_3), 1.76–2.04 (m, 4H, CH_2), 6.04 (s, 3H, Si(OH)$_3$), 7.26 (s, 2H, ArH). **^{13}C{^{1}H} NMR** (75.57 MHz, DMSO-d_6): δ (ppm) 8.4 (CH$_2$$CH_3$), 34.7 ($CH_2CH_3$), 80.6 ($CEt_2$), 124.9, 143.0 ($C$ of Ar), **^{29}Si NMR** (59.63 MHz, DMSO-d_6): δ (ppm) –79.4. **EI-MS**: m/z (%) 377 (6) [M–Et]$^+$.

1,4-[{(HO)$_2$(t-BuO)Si}OCEt$_2$]$_2$C$_6$H$_4$ (D1): BDA1 (0.20 g, 0.29 mmol) was added to a mixture of water (5 mL) and ethyl acetate (10 drops, 0 °C) and stirred for 15 min. The solvents were decanted and the product was isolated as a white solid. Single crystals were obtained by slow evaporation of THF solution at ambient temperature. **Yield**: 0.09 g, 0.17 mmol, 87%. **M.p.** 160–161 °C. **Elemental analysis** (%) Calcd for C$_{24}$H$_{46}$O$_8$Si$_2$ (518.79 g·mol^{-1}): C 55.51, H 8.86; Found: C 55.09, H 8.72. **FT-IR (ATR) (cm^{-1})** $\tilde{\nu}$ 3373 (s, SiO–H), 2975, 2935 (w, CH$_3$, CH$_2$), 961 (s, Si–O). **^{1}H NMR** (300.53 MHz, DMSO-d_6): δ (ppm) 0.59 (t, 6H, $^3J_{H-H}$ = 7.2 Hz, CH$_2$CH_3), 1.29 (s, 9H, C(CH_3)$_3$), 1.70–2.08 (m, 4H, CH_2CH$_3$), 6.19 (s, 2H, Si(OH)$_2$), 7.26 (s, 2H, ArH). **^{13}C{^{1}H} NMR** (75.57 MHz, DMSO-d_6): δ (ppm) 8.3 (CH$_2$$CH_3$), 31.3 (C($CH_3$)$_3$), 34.5 ($CH_2CH_3$), 71.2 ($C$(CH$_3$)$_3$), 81.0 ($CEt_2$), 124.8, 142.9 ($C$ of Ar). **^{29}Si NMR** (59.63 MHz, DMSO-d_6): δ (ppm) –85.5. **EI-MS**: m/z (%) 489 (100) [M–Et]$^+$.

[1,1'-Biphenyl]-4,4'-[(HO)$_3$SiOCEt$_2$]$_2$ (T2): BTA2 (0.5 g, 0.68 mmol) was suspended in cold distilled water (10 mL). The reaction mixture was vigorously stirred at 0 °C for 10 min. Afterwards, the white powder was collected via filtration and washed with cold water (2 x 2 mL) in order to remove the remanent acetic acid. **Yield**: 0.3 g, 0.62 mmol, 91%. **M.p.** > 350 °C. **Elemental analysis** (%) Calcd for C$_{22}$H$_{34}$O$_8$Si$_2$ (482.67 g·mol^{-1}): C 54.74, H 7.10; Found: C 53.22, H 6.86. **FT-IR (ATR) (cm^{-1})** $\tilde{\nu}$ 3300 (s, SiO–H), 2974, 2936 (w, C–H, CH$_3$, CH$_2$), 924 (s, Si–O). **^{1}H NMR** (300.53 MHz, DMSO-d_6): δ (ppm) 0.64 (t, 6H, $^3J_{H-H}$ = 7.3 Hz, CH$_2$CH_3), 1.79–2.11 (m, 4H, CH_2), 6.11 (s, 3H, Si(OH)$_3$), 7.45 (d, 2H, $^3J_{H-H}$ = 8.0 Hz,

ArH), 7.61 (d, 2H, $^3J_{H-H}$ = 8.0 Hz, ArH). ^{13}C{^{1}H} NMR (75.57 MHz, DMSO-d_6): δ (ppm) 8.4 (CH$_2$CH$_3$), 34.7 (CH$_2$CH$_3$), 80.6 (CEt$_2$), 125.5, 126.5, 137.3, 145.0 (C of Ar). ^{29}Si NMR (59.63 MHz, DMSO-d_6): δ (ppm) –79.3. EI-MS: m/z (%) 453.61 (6) [M–Et]$^+$.

[1,1'-Biphenyl]-4,4'-[{(HO)$_2$(t-BuO)Si}OCEt$_2$]$_2$ (D2): BDA2 (1.0 g, 1.31 mmol) was added to a mixture of water (5 mL) and ethyl acetate (10 drops, 0 °C) and stirred for 15 min. The solvents were decanted and the product was isolated as white solid. Single crystals were obtained by slow evaporation of THF solution at ambient temperature. Yield: 0.51 g, 0.85 mmol, 65%. M.p. 159–161 °C. Elemental analysis (%) Calcd for C$_{30}$H$_{50}$O$_8$Si$_2$ (594.89 g·mol^{-1}): C 60.57, H 8.47; Found: C 59.34, H 8.27. FT-IR (ATR) (cm^{-1}) $\tilde{\nu}$ 3331 (s, SiO–H), 2968, 2938 (w, C–H, CH$_3$, CH$_2$), 918 (s, Si–O). ^{1}H NMR (300.53 MHz, DMSO-d_6): δ (ppm) 0.65 (t, 6H, $^3J_{H-H}$ = 7.3 Hz, CH$_2$CH$_3$), 1.31 (s, 9H, C(CH$_3$)$_3$), 1.85–2.08 (m, 4H, CH$_2$CH$_3$), 6.26 (s, 2H, Si(OH)$_2$), 7.45, 7.62 (d, 4H, ArH). ^{13}C{^{1}H} NMR (75.57 MHz, DMSO-d_6): δ (ppm) 8.3 (CH$_2$CH$_3$), 31.4 (C(CH$_3$)$_3$), 34.6 (CH$_2$CH$_3$), 71.3 (C(CH$_3$)$_3$), 81.1 (CEt$_2$), 125.5, 126.4, 137.2, 144.9 (C of Ar). ^{29}Si NMR (59.63 MHz, DMSO-d_6): δ (ppm) –91.2. EI-MS: m/z (%) 453.61 (6) [M–Et]$^+$.

1,4-[(HO)$_3$SiOCPh$_2$]$_2$C$_6$H$_4$ (T3): BTA3 (0.5 g, 0.59 mmol) was suspended in cold distilled water (15 mL). The reaction mixture was vigorously stirred at 0 °C for 10 min. Then, the white powder was collected via filtration and washed with cold water (2 x 2 mL) in order to remove the remanent acetic acid. Yield: 0.28 g, 0.47 mmol, 81%. M.p. > 350 °C. Elemental analysis (%) Calcd for C$_{32}$H$_{30}$O$_8$Si$_2$ (598.75 g·mol^{-1}):): C 64.19, H 5.053; Found: C 66.39, H 5.12. FT-IR (ATR) (cm^{-1}) $\tilde{\nu}$ 3312 (s, SiO–H), 3057 (w, C–H, Ar), 907, 942 (s, Si–O). ^{1}H NMR (300.53 MHz, DMSO-d_6): δ (ppm) 5.92 (s, 3H, Si(OH)$_3$), 7.21–7.36 (m, 12H, ArH). ^{13}C{^{1}H} NMR (75.57 MHz, DMSO-d_6): δ (ppm) 84.0 (C of Ar), 126.5, 127.3, 127.4, 127.8, 128.1, 128.2, 145.0, 147.2 (C of Ar). ^{29}Si NMR (59.63 MHz, DMSO-d_6): δ (ppm) –81.0. EI-MS: m/z (%) 598 (1) [M]$^+$.

1,2-[(HO)$_3$SiOCEt$_2$]$_2$C$_2$ (T4): BTA4 (0.33 g, 0.54 mmol) was suspended in cold distilled water (1.5 mL). The reaction mixture was vigorously stirred at 0 °C for 2 min. Afterwards, the white powder filtered and washed with cold water (2 x 1 mL) in order to remove the remanent acetic acid. Yield: 0.14 g, 0.40 mmol, 75%. M.p. > 350 °C. Elemental analysis (%) Calcd for C$_{12}$H$_{26}$O$_8$Si$_2$ (354.50 g·mol^{-1}): C 40.66, H 7.39; Found: C 39.42, H 7.23. FT-IR

(ATR) (cm^{-1}) $\tilde{\nu}$ 3145 (s, SiO–H), 2972, 2940 (w, C–H, CH$_3$, CH$_2$), 928 (s, Si–O). **^{1}H NMR** (300.53 MHz, DMSO-d_6): δ (ppm) 0.94 (t, 6H, $^3J_{H-H}$ = 7.3 Hz, CH$_2$CH_3), 1.59–1.74 (m, 4H, CH_2CH$_3$), 6.18 (s, 3H, Si(OH)$_3$). **^{13}C{^{1}H} NMR** (75.57 MHz, DMSO-d_6): δ (ppm) 8.9 (CH$_2$$CH_3$), 34.3 ($CH_2CH_3$), 73.3 ($C{\equiv}C$), 85.9 ($CEt_2$). **^{29}Si NMR** (59.63 MHz, DMSO-d_6): δ (ppm) –78.3. **EI-MS**: m/z (%) 525 (5) [M–Et]$^+$.

Ph$_3$COSi(OH)$_3$ (T5): **MTA5** (0.32 g, 0.69 mmol) was suspended in cold distilled water (10 mL). The reaction mixture was vigorously stirred at 0 °C for 10 min. Afterwards, the white powder was collected via filtration and washed with cold water (2 x 2 mL) in order to remove the remanent acetic acid. **Yield**: 0.20 g, 0.59 mmol, 85%. **M.p.** 95–97 °C. **Elemental analysis** (%) Calcd for C$_{19}$H$_{18}$O$_4$Si (338.43 g·mol^{-1}): C 67.43, H 5.36; Found: C 66.39, H 5.12. **FT-IR (ATR) (cm^{-1})** $\tilde{\nu}$ 3312 (s, SiO–H), 3057 (w, C–H, Ph), 928, 898 (s, Si–O). **^{1}H NMR** (300.53 MHz, DMSO-d_6): δ (ppm) 5.90 (s, 3H, Si(OH)$_3$), 7.18–7.32 (m, 15H, CH of Ph). **^{13}C{^{1}H} NMR** (75.57 MHz, DMSO-d_6): δ (ppm) 84.1 (CPh$_3$), 126.6, 127.3, 128.2, 147.1 (C of Ph). **^{29}Si NMR** (59.63 MHz, DMSO-d_6): δ (ppm) –80.9. **EI-MS**: m/z (%) 338 (1) [M]$^+$.

Ph$_3$COSi(Ot-Bu)(OH)$_2$ (D5): **Hydrolysis route 1**: **MDA5** (1.00 g, 2.08 mmol) was suspended in a mixture of cold distilled water (20 mL) and concentrated ammonia solution (1 mL) and stirred at room temperature for 15 min. Subsequently, the product was extracted with ethylacetate and isolated after removing all volatiles. **Yield**: 0.53 g, 0.13 mmol, 65%. **Hydrolysis route 2**: **MDA5** (1.00 g, 2.08 mmol) was suspended in cold distilled water (20 mL) and stirred at room temperature for 15 hours. Subsequently, the product was isolated as a white powder via filtration. **Yield**: 0.58 g, 0.14 mmol, 71%. Single crystals of compound **D5** were grown: a) from a DMSO solution by slow solvent evaporation at ambient temperature b) by slow evaporation of wet dichloromethane solution. **M.p.** 73–75 °C. **Elemental analysis** (%) Calcd for C$_{23}$H$_{26}$O$_4$Si (394.54 g·mol^{-1}): C 63.53, H 6.80; Found: C 61.91, H 6.67. **FT-IR (ATR) (cm^{-1})** $\tilde{\nu}$ 3381 (m, SiO–H), 2973 (w, C–H, CH$_3$), 928 (s, Si–O). **^{1}H NMR** (300.53 MHz, DMSO-d_6): δ (ppm) 1.03 (s, 9H, C(CH_3)$_3$), 6.12 (s, 2H, Si(OH)$_2$), 7.18–7.32 (m, 15H, CH of Ph). **^{13}C{^{1}H} NMR** (75.57 MHz, DMSO-d_6): δ (ppm) 31.1 (C(CH$_3$)$_3$), 71.2 (C(CH$_3$)$_3$), 84.4 (CPh$_3$), 126.6, 127.2, 128.4, 147.0 (C of Ph). **^{29}Si NMR** (59.63 MHz, DMSO-d_6): δ (ppm) –87.0. **EI-MS**: m/z (%) 394 (5) [M]$^+$.

O,O'-TADDOL-Si(OH)$_2$ (D6): **MDA6** (0.31 g, 0.51 mmol) was suspended in cold distilled water (10 mL) and stirred for 10 min. Then the white solid was filtered off and washed once with 5 mL of water. **Yield**: 0.26 g, 0.49 mmol, 96%. **M.p.** 204 °C. **Elemental analysis** (%) Calcd for $C_{31}H_{30}O_6Si_{0.66}(CH_2Cl_2)$ (583.25 g·mol^{-1}): C 65.21, H 5.41. Found: C 65.13, H 5.49. **FT-IR (ATR) (cm^{-1})** $\tilde{\nu}$ 3577 (s, SiO–H), 939 (m, Si–O). **^{1}H NMR** (300.53 MHz, DMSO-d_6): δ (ppm) 0.51 (s, 6H, C(CH_3)$_2$), 4.89 (s, 2H, Ph$_2$CCHO), 6.89 (s, 2H, Si(OH)$_2$) 7.22–7.51 (m, 20H, CH of Ph). **^{13}C{^{1}H} NMR** (75.57 MHz, DMSO-d_6): δ (ppm) 26.8 (C(CH_3)$_2$), 80.9 (Ph$_2$CC HO), 84.3 (CPh$_2$), 112.5 (C(CH$_3$)$_2$), 126.6, 126.8, 126.9, 127.1, 127.9, 128.9, 142.5, 147.0 (C of Ph). **^{29}Si NMR** (59.63 MHz, DMSO-d_6): δ (ppm) –83.8. **EI-MS**: m/z (%) 526 (8) [M]$^+$.

2.3.4 General procedure for the catalytic cycloaddition of CO$_2$ to styrene oxide

A 10 mL reaction vial was charged with styrene oxide (1 equiv SO, 0.11 g, 0.88 mmol), tetra-butylammonium iodide (0.1 equiv, 0.033 g, 0.088 mmol), and silanol catalyst (0.1 equiv, 0.088 mmol). The vial was purged once with CO$_2$ and subsequently it was put under a positive pressure with a balloon of CO$_2$. The reaction mixture was stirred for 15 h at 60 °C. The conversion degree was determined using ^{1}H NMR spectroscopy using DMSO-d_6 as the deuterated solvent. Thus, after 15 h of reaction, the vial was cooled to room temperature and toluene (1 equiv, 0.081 g, 0.88 mmol) was added to the reaction to be used as internal standard. Silanol catalyst and TBAI were precipitated in diethyl ether, the mixture was filtered and the volatiles were removed from the filtrate to yield the product. The NMR spectroscopic data for the styrene carbonate match those reported in the literature. **^{1}H NMR** (300.53 MHz, DMSO-d_6): δ (ppm) 4.42 (apparent t, 1H, $J_{H-H} = 8.3$ Hz), 4.89 (apparent t, 1H, $J_{H-H} = 8.3$ Hz), 5.86 (apparent t, 1H, $J_{H-H} = 8.0$ Hz), 7.30 –7.57 (m, 5H, CH of Ph). **^{13}C{^{1}H} NMR** (75.57 MHz, DMSO-d_6): δ (ppm) 70.9, 77.8, 126.7, 128.9, 129.4, 136.3, 154.8.

2.3.5 Single-crystal X-ray diffraction analysis

Single crystals were mounted on a Bruker APEX DUO diffractometer equipped with an Apex II CCD detector at 100 K. Frames were collected using omega scans and integrated with SAINT.[125] Multi-scan absorption correction (SADABS)[125] was applied. The structures were solved by direct methods either with SHELXS[126] or using SHELXT[127] and refined using full-matrix least-squares on F^2 with SHELXL[128] within the ShelXle GUI.[128] Weighted R factors, R_w and all goodness-of-fit indicators, are based on F^2. All non-hydrogen atoms were refined anisotropically. The hydrogen atoms of the C–H bonds were placed in idealized positions, whereas the hydrogen atoms from the OH moieties in **D1**, **D2**, **D5**·DMSO, **D5**·H_2O and **D6** were localized from the difference electron density map and their positions were refined with U_{iso} tied to the parent atoms with distance restraints (DFIX or SADI). The disordered groups and solvent molecules (**MTA5** 1 x $CH_3C(O)$; **T5**·THF 1 x THF; **D5**·DMSO 1 x DMSO; **D5**·H_2O 1 x t-Bu, 1 x OH; **D6** 1 x CH_2Cl_2) were refined using geometry (SADI, SAME) and U_{ij} restraints (SIMU, RIGU) implemented in SHELXL.[128] The Flack parameter for compound **BTA1** 0.487(4) suggests that an inversion center could be present, but the structure cannot be refined neither in the $C2/c$ or $C2/m$ space group. Thus this unusual value is caused by the presence of racemic twinning. The molecular graphics were prepared using GRETEP, POV-RAY and GIMP.[129–131]

Crystal data and structure refinement details of the obtained compounds

	BTA1[c]	BTA4	MDA6[d]	MTA5	MDA5
Empirical formula	$C_{28}H_{42}O_{14}Si_2$	$C_{24}H_{38}O_{14}Si_2$	$C_{35}H_{34}O_8Si$	$C_{25}H_{24}O_7Si$	$C_{27}H_{30}O_6Si$
Formula mass (g/mol)	658.79	606.72	610.71	464.53	478.60
Space group	$C2$	$P\bar{1}$	$P2_12_12$	$P\bar{1}$	$P\bar{1}$
T (K)	100(2)	100(2)	100(2)	100(2)	100(2)
λ (Å)	1.54178	1.54178	1.54178	0.71073	0.71073
a (Å)	20.3982(4)	9.0912(2)	13.4373(3)	9.9282(4)	8.6997(2)
b (Å)	13.8584(4)	9.1134(2)	9.5065(2)	10.7649(4)	9.0317(2)
c (Å)	24.3524(6)	9.3268(2)	11.8659(3)	13.0781(5)	17.0129(4)
α (°)	90	87.784(1)	90	110.8963(7)	99.2568(5)
β (°)	94.712(2)	83.045(1)	90	97.5728(8)	90.5947(5)
γ (°)	90	76.746(2)	90	110.4489(7)	109.8012(5)
V (Å³)	6860.8(3)	746.58(3)	1515.77(6)	1169.85(8)	1238.31(5)
Crystal size (mm)	0.207 x 0.200 x 0.178	0.165 x 0.141 x 0.124	0.123 x 0.118 x 0.097	0.373 x 0.350 x 0.251	0.300 x 0.280 x 0.219
Z	8	1	2	2	2
$\varrho_{calc.}$ (g·cm⁻³)	1.276	1.349	1.338	1.319	1.284
μ (mm⁻¹)	1.486	1.658	1.131	0.144	0.135
$F(000)$	2800	322	644	488	508
θ range for data collection (°)	1.820 to 67.747	4.777 to 67.711	3.725 to 69.967	1.743 to 26.369	2.432 to 26.371
No. of reflections	48551	8081	18442	19964	37746
No. of independent reflections (R_{int})	12124 (0.0195)	2608 (0.0198)	2885 (0.0228)	4801 (0.0243)	5062 (0.0191)
No. of data/restraints/parameters	12124 / 1 / 813	2608 / 0 / 186	2885 / 0 / 202	4801 / 130 / 330	5062 / 0 /312
Goodnes-on-fit (GOF) on F^2	1.055	1.066	1.059	1.029	1.028
R_1,[a] wR_2[b] ($I > 2\sigma(I)$)	0.0402, 0.1081	0.0412, 0.1231	0.0270	0.0309, 0.0784	0.0296, 0.0766
R_1,[a] wR_2[b] (all data)	0.0407, 0.1088	0.0468, 0.1286	0.0709	0.0341, 0.0807	0.0311, 0.0778
Largest diff. peak/hole (e·Å⁻³)	0.541 / −0.269	0.407 / −0.309	0.201 / −0.250	0.306 / −0.355	0.356 / −0.342
CCDC	1453225	1453226	1453230	1453228	1453229

[a] $R_1 = \Sigma||F_o| - |F_c||/\Sigma|F_o|$. [b] $wR_2 = [\Sigma w(F_o^2 - F_c^2)^2/\Sigma w(F_o^2)^2]^{1/2}$. [c] Flack parameter 0.487(4). [d] Flack parameter: −0.008(5).

Table 2-3. Crystal data and structure refinement details for compounds **BTA1**, **BTA4**, **MDA6**, **MTA5** and **MDA5**.

	D1	T5·THF	D5·DMSO	D5·H₂O	D6·CH₂Cl₂ᶜ
Empirical formula	$C_{24}H_{46}O_8Si_2$	$C_{23}H_{26}O_5Si$	$C_{25}H_{32}O_5SSi$	$C_{23}H_{27}O_{4.5}Si$	$C_{32}H_{32}Cl_2O_6Si$
Formula mass (g/mol)	518.79	410.53	472.65	403.53	611.56
Space group	$P\bar{1}$	$P2_1/c$	$C2/c$	$P\bar{1}$	$P2_12_12_1$
T (K)	100(2)	100(2)	100(2)	100(2)	100(2)
λ (Å)	0.71073	0.71073	0.71073	0.71073	0.71073
a (Å)	7.1203(2)	12.3488(3)	30.6391(6)	8.8728(3)	9.2264(2)
b (Å)	10.0366(3)	8.9576(2)	8.7736(2)	10.2369(3)	13.6523(3)
c (Å)	10.5331(3)	19.5820(4)	20.1977(4)	12.7680(4)	23.0659(6)
α (°)	102.7633(5)	90	90	113.0905(6)	90
β (°)	95.1489(5)	107.9408(5)	113.6567(4)	95.8921(6)	90
γ (°)	103.8582(5)	90	90	91.7488(6)	90
V (Å³)	704.63(4)	2060.75(8)	4973.19(18)	1057.99(6)	2905.42(12)
Crystal size (mm)	0.417 x 0.301 x 0.206	0.286 x 0.218 x 0.184	0.296 x 0.261 x 0.239	0.289 x 0.207 x 0.163	0.251 x 0.248 x 0.226
Z	1	4	8	2	4
$\varrho_{calc.}$ (g·cm⁻³)	1.223	1.323	1.263	1.267	1.398
μ (mm⁻¹)	0.168	0.146	0.211	0.139	0.310
$F(000)$	282	872	2016	430	1280
θ range for data collection (°)	2.005 to 26.368	1.733 to 26.370	2.095 to 26.369	1.747 to 26.372	1.733 to 27.483
No. of reflections	13531	20204	22388	17675	64011
No. of independent reflections (R_{int})	2872 (0.0159)	4200 (0.0250)	5078 (0.0240)	4316 (0.0210)	6660 (0.0192)
No. of data/restraints/parameters	2872 / 0 / 165	4200 / 251 / 317	5078 / 107 / 330	4316 / 73 / 311	6660 / 93 / 406
Goodnes-on-fit (GOF) on F^2	1.025	1.025	1.033	1.033	1.049
R_1,ᵃ wR_2ᵇ ($I > 2\sigma(I)$)	0.0292, 0.0748	0.0346, 0.0892	0.0310, 0.0800	0.0414, 0.1083	0.0210, 0.0561
R_1,ᵃ wR_2ᵇ (all data)	0.0303, 0.0756	0.0378, 0.0916	0.0346, 0.0828	0.0446, 0.1109	0.0213, 0.0563
Largest diff. peak/hole (e·Å⁻³)	0.371, –0.310	0.379, –0.372	0.383 / –0.321	0.488 / –0.522	0.295 / –0.197
CCDC	1453233	1453232	1453234	1453235	1453236

ᵃ $R_1 = \Sigma||F_o| - |F_c||/\Sigma|F_o|$. ᵇ $wR_2 = [\Sigma w(F_o^2 - F_c^2)^2/\Sigma w(F_o^2)^2]^{1/2}$. ᶜ Flack parameter: 0.008(6)

Table 2-4. Crystal data and structure refinement details for compounds **D1**, **T5**·THF, **D5**·DMSO, **D5**·H₂O and **D6**·CH₂Cl₂.

Chapter 3

Synthesis of Hydrogen-bonded organic frameworks based on organo-bis(silanols)

As it was discussed earlier, the synthesis of ordered hybrid materials, where silanetriol and silanediol moieties act as nodes interconnecting the molecular building blocks through hydrogen bonding interactions is one of the possible applications of molecular organo-bis(silanols).[132]

In this context, herein, the principles of crystal engineering were used to form higher order supramolecular assemblies directed by hydrogen-bonding interactions, *via* the co-crystallization of selected organo-bis(silanols) (**T1**, **D1**, **T2**, and **T3**) and organic diamines with different basicity, such as 1,4-diazabicyclo[2.2.2]octane (DABCO) (**a**) and trans-1,2-bis(4-pyridyl)ethylene (4,4'-bpe) (**b**). Additionally, it is intended to gain a deeper understanding of the factors that determine the structural arrangement, stability, and porosity of the silanol-based HOFs. Accordingly, the organo-bis(silanols) were chosen based on certain structural variations such as (1) the size of the organic spacer (**T1** and **T2**), (2) the number of OH groups attached to the same silicon center (**T1** and **D1**), and (3) the steric hindrance around the silicon center (**T1** and **T3**).

3.1 Results and discussion

3.1.1 Synthesis and characterization

The HOFs **HT1a**, **HT1b**, **HD1a**, **HD1b**, **HT2a**, **HT2b**, and **HT3b** were prepared by dissolving, separately, the selected alkoxysilanol (**T1**, **D1**, **T2**, and **T3**) and two equivalents of the corresponding diamine (DABCO or 4,4'-bpe) in THF. Subsequently, such solutions were mixed and stirred for 15 min at room temperature.

Afterwards, each mixture was concentrated under vacuum, and it was stored at –24 °C to yield the corresponding hydrogen-bonded organic frameworks (HOFs) as white crystalline powder, which was isolated by filtration and washed with hexane. It is noteworthy that it was not possible to obtain a co-crystalline arrangement from **T3** and DABCO, as all attempts to grow crystals derived in the formation of polycondensation by-products [**Scheme** 3.1].
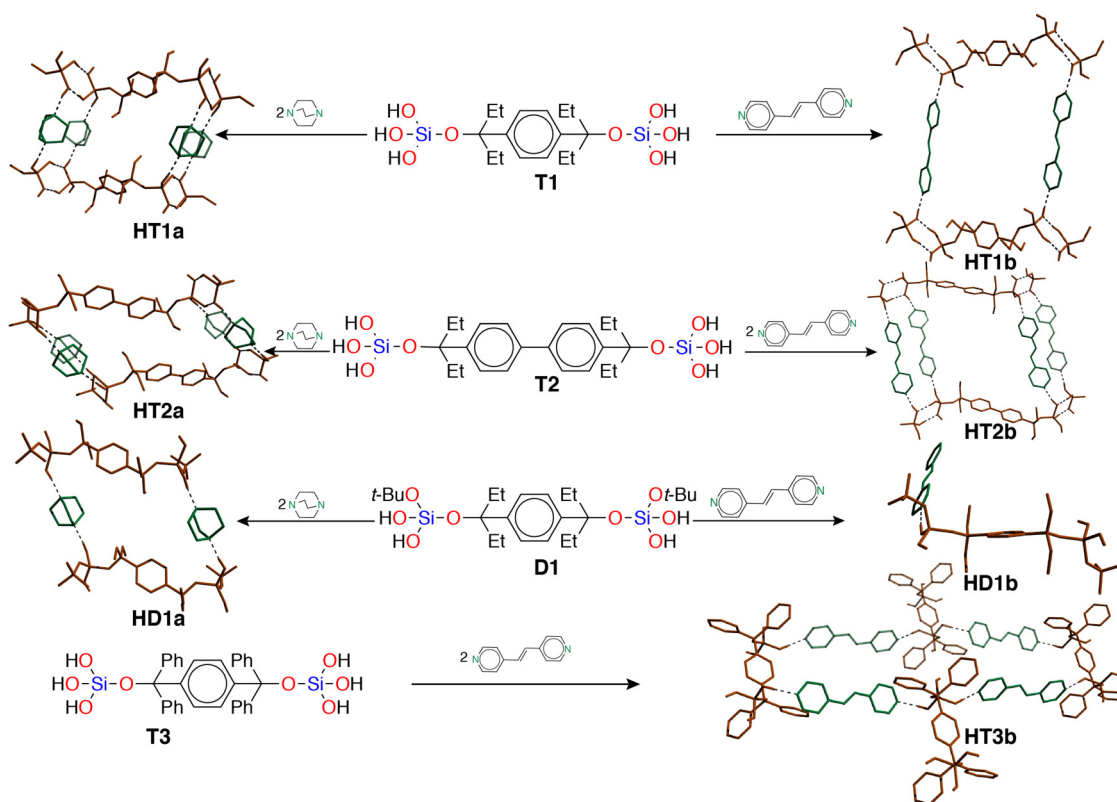
Scheme 3.1. Synthesis of HOFs based on organosilicate building blocks

The obtained HOFs were characterized by elemental analysis, IR and, single crystal X-ray diffraction (SCXRD) technique. Additionally, their thermal stability was determined by TGA analysis under N_2 atmosphere.

3.1.2   X-ray structural analysis

General Structural Remarks

It is observed that those HOFs obtained from organo-bis(silanetriols) (**HT1a**, **HT1b**, **HT2a**, **HT2b**, and **HT3b**) crystallized in the triclinic $P\bar{1}$ space group, whereas those derived from organo-bis(silanediols) (**HD1a** and **HD1b**) were refined in monoclinic $P2_1/n$ and $P2_1/c$ space groups, respectively. The HOFs **HT1a**, **HT2a**, **HT2b**, **HT3b**, and **HD1a** have a 2:1 diamine-alkoxysilanol ratio. Therefore, their asymmetric units comprise one-half of organo-bis(silanol) molecule, one diamine and one THF molecule (except for **HT1a**, which crystallized without solvent molecules).

In contrast, **HT1b** and **HD1b** crystallized with 1:1 diamine-alkoxysilanol stoichiometric ratio and their asymmetric units include only one-half of the diamine and organo-bis(silanol) molecules and in the case of the **HT1b** solvate its asymmetric unit contains also two THF molecules.

The crystalline structures of the HOFs show that the coordination geometry around the silicon atom corresponds to a distorted tetrahedron with angles ranging from $104.6(1)°$ to $114.0(1)°$. Additionally, the Si–O bond lengths lie between $1.593(2)$Å and $1.633(1)$Å (*see* Table 3-1).

	Bond lengths					Bond angles	
	Si–O$_{spacer}$	Si–O$_{tBu}$	Si–OH	Si–OH	Si–OH	<O–Si–O	<O–Si–O
HT1a	1.632(1)	—	1.624(1)	1.626(1)	1.617(1)	105.0(1)	113.2(1)
HT1b	1.626(1)	—	1.630(1)	1.618(2)	1.614(1)	105.2(1)	113.4(1)
HT2a	1.633(1)	—	1.614(1)	1.623(1)	1.620(1)	107.6(1)	112.6(1)
HT2b	1.626(1)	—	1.625(1)	1.623(1)	1.610(1)	104.6(1)	114.0(1)
HT3b	1.630(2)	—	1.613(2)	1.593(2)	1.630(2)	106.5(1)	113.3(3)
HD1a	1.632(2)	1.631(1)	1.604(2)	1.601(2)	—	112.2(1)	103.9(3)
HD1b	1.631(1)	1.628(1)	1.620(1)	1.626(1)	—	106.5(3)	113.0(1)

Table 3-1. Si–O distances (Å) and Si–O–Si angles (°) in **HT1a**, **HT1b**, **HT2a**, **HT2b**, **HT3b**, **HD1a** and **HD1b**.

Structural description of HT1a and HT1b

The X-ray crystallographic analysis of the supramolecular arrangements in **HT1a** and **HT1b** reveals that the molecules of the silanetriol **T1** are linked end-to-end through the formation of highly directional hydrogen-bonding interactions between adjacent $Si(OH)_3$ moieties. Such interaction can be described as the $R_2^2(8)$ eight-membered ring motif, according to the graph set theory [**Fig**. 3.1 (d) and **Fig**. 3.2 (d)]. The self-association between the consecutive **T1** molecules leads to the formation of infinite 1D supramolecular chains that propagate along the crystallographic c-axis and can be described by the $C_2^2(26)$ motif [**Fig**. 3.1 (c) and **Fig**. 3.2 (c)].
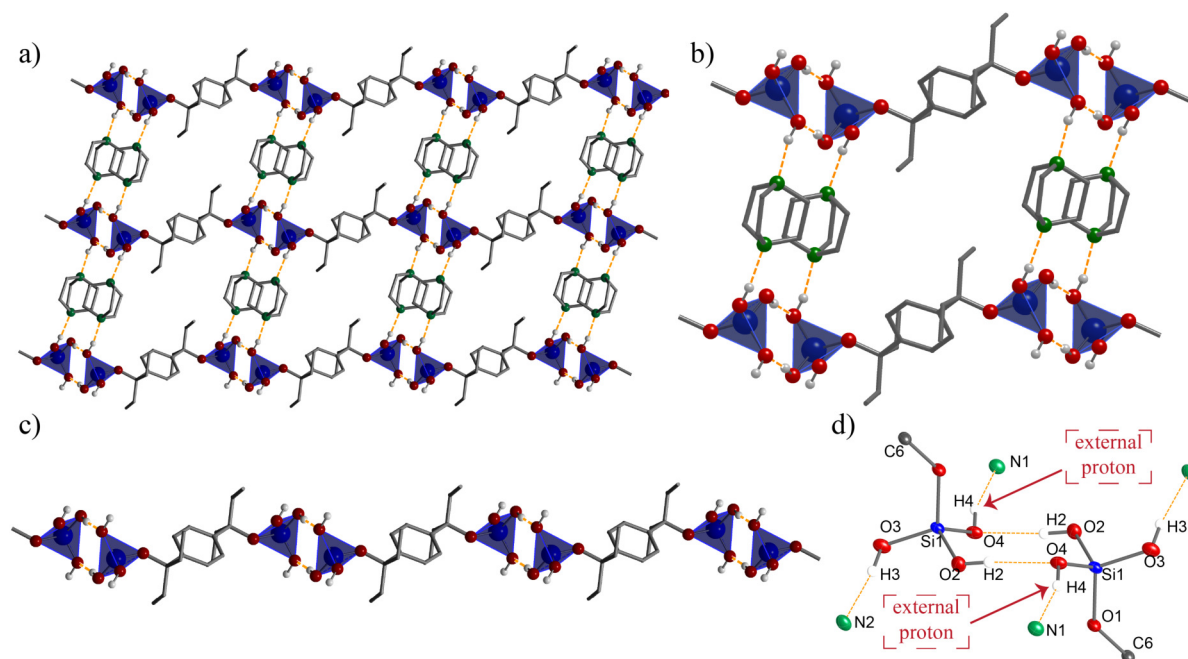
Figure 3.1. Supramolecular arrangement of **HT1a** HOF. (a) 2D supramolecular network constructed by the multiplication of the diamine-silanol macrocycles, (b) $R_4^4(36)$ macrocycle in **HT1a**, (c) $C_2^2(26)$ motif, (d) $R_2^2(8)$ chair-shaped ring motif.
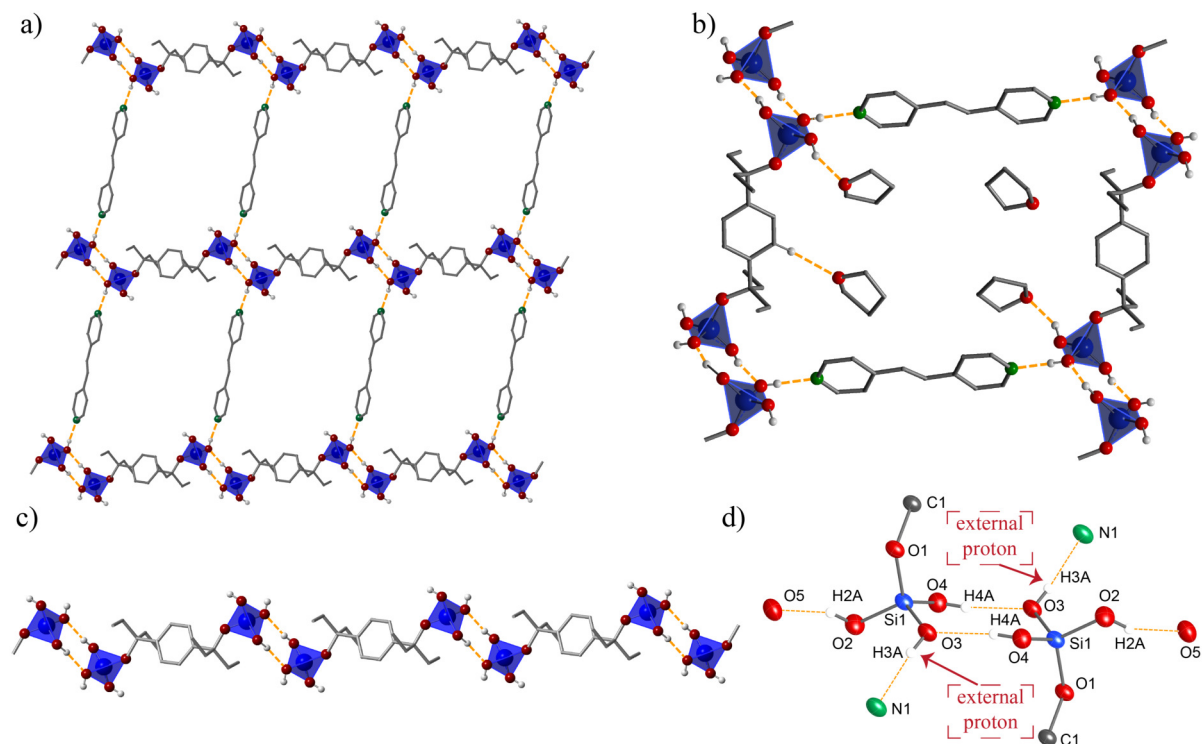
Figure 3.2. Supramolecular arrangement of HOF **HT1b**. (a) 2D supramolecular network constructed by the multiplication of the diamine-silanol macrocycles, (b) $R_6^6(52)$ macrocycle in **HT1b**, (c) $C_2^2(26)$ motif, (d) $R_2^2(8)$ chair-shaped ring motif.

It should be pointed out that this $R_2^2(8)$ ring motif is also commonly observed in other supramolecular arrangements formed by carboxylic and boronic acid derivatives.[85,133–136] However, due to the trigonal planar geometry of the carbon and boron atoms, the formed $R_2^2(8)$ eight-membered rings are planar.

In contrast, the $R_2^2(8)$ synthon observed in **HT1a** and **HT1b** has a chair-shaped conformation [**Fig**. 3.1 (d) and **Fig**. 3.2 (d)]. This geometry can be also observed for other tetrahedral tectons, such as sulfonic (–SO$_3$H) and phosphonic (–PO$_3$H$_2$) acids.[137,138] Nonetheless, in the case of the –Si(OH)$_3$ tecton, the presence of three terminal OH groups attached to the same tetrahedral silicon atom, widens the capacity of these molecular building blocks in terms of the possible supramolecular arrangements. Additionally, the cooperative hydrogen-bonding between neighbor Si(OH)$_3$ moieties increases the acidic character of the external protons, which are not involved in the formation of the $R_2^2(8)$ synthon, resulting in a stronger hydrogen-bonding with additional Lewis base molecules [**Fig**. 3.2 (d)].

Consequently, these external protons bind to the first equivalent of DABCO and 4,4'-bpe in **HT1a** and **HT1b**, respectively. As expected, these SiO–H···N interactions are stronger in **HT1a** than in **HT1b** due to the fact that DABCO is a stronger Lewis base than 4,4'-bpe. This is evidenced by the shorter $D···A$ distance in **HT1a** O(4)–H(4)···N(1) 2.658(2) Å, than in **HT1b** O(3)–H(3A)···N(1) 2.716(2) Å. Additionally, this observation is also in accordance with the IR spectrum of **HT1a**, where the band of the νO–H stretching vibration associated to Si–OH groups is almost negligible, while in the spectrum of **HT1b** this band appears at lower frequency ($\tilde{\nu}$ 3087 cm^{-1}) compared to that of free organo-bis(silanetriol) **T1** ($\tilde{\nu}$ 3143 cm^{-1}).

Therefore, the first equivalent of the amine makes a link between the 1D bis(silanol) supramolecular chains present in the **HT1a** and **HT1b** arrangements leading to the formation of ladder-like macrocyclic systems. These macrocycles can be described according to the graph set theory as a second order $R_4^4(36)$ and $R_6^6(52)$ ring motifs, respectively. Additionally, the relative size of such macrocycles (**HT1a** $d_{Si···Si}$= 10.5 x 9.8 Å and **HT1b** $d_{Si···Si}$= 10.5 x 17.9 Å) is governed by the length of the organic amine as in both cases, the size of the organic *spacer* between the silicate moieties is identical [**Fig.** 3.1 (b) and **Fig.** 3.2 (b)].

The third OH group attached to the silicon center in **HT1a** binds to a second DABCO molecule, to afford a double-pillared macrocyclic arrangement, through the formation of additional SiO–H···N interaction, with a $D···A$ distance of 2.742(2) Å, that is 0.08 Å longer than that observed in the SiO–H···N interaction with the external protons. This fact may be understood taking into account the relative acidic character of the protons involved in such interactions. The $D···A$ distances and D–H···A angles are listed in Table 3-2.

In contrast, in the crystalline structure of **HT1b**, the third OH group, acts as a hydrogen-bond donor for a THF molecule, with $D···A$ bond distance of 2.67(2) Å and a DHA angle of 157.0(3)° (*see* Table 3-2). Consequently, **HT1b** keeps a single-pillared ladder-like macrocycle arrangement, where, in order to achieve a close-packed structure, a second molecule of THF fills the empty space within the $R_6^6(52)$ macrocycle. Only weak C–H···O (C···O 3.593(1) Å) van der Waals interactions can be observed between this THF molecule and the neighbouring fragments.

HOF	D–H···A	d(D···A) (Å)	<DHA (º)	Symmetry Code
HT1a	O(2)–H(2)···O(4)#2	2.780(2)	173.2(2)	#2–x+1,–y+1,–z
	O(3)–H(3)···N(2)#3	2.742(2)	171.7(2)	#3 x,y+1,z
	O(4)–H(4)···N(1)	2.658(2)	162.6(2)	
HT1b	O(2)–H(2A)···O(5)$_{THF}$	2.67(2)	157.0(3)	
	O(3)–H(3A)···N(1)	2.716(2)	174.0(3)	#3–x+2,–y+1,–z+2
	O(4)–H(4A)···O(3)#3	2.703(2)	172.0(3)	
HT2a	O(2)–H(2A)···N(1)	2.653(2)	161.0(2)	#2x,y+1,z
	O(3)–H(3A)···N(2)#2	2.700(2)	177.0(2)	#3–x+1,–y+1,–z
	O(4)–H(4A)...O(2)#3	2.735(2)	177.0(2)	
HT2b	O(2)–H(2)···N(1)	2.705(2)	165.0(2)	#2–x,–y+2,–z+2
	O(3)–H(3)···O(2)#2	2.736(1)	171.0(2)	#3–x+2,–y+1,–z+2
	O(4)–H(4)···N(2)#3	2.736(2)	168.0(2)	
HT3b	O(2)–H(2A)···N(1)	2.688(3)	169.0(4)	#1–x+2,–y+1,–z+1
	O(3)–H(3A)···N(2)	2.791(3)	177.0(4)	#2–x,–y,–z+1
	O(4)–H(4A)···O(5)	2.732(1)	162.0(3)	#3–x+3,–y+1,–z+2
HD1a	O(3)–H(3A)···N(1)	2.655(2)	167.0(3)	#2x,y–1,z
	O(4)–H(4A)···N(2)#2	2.672(2)	168.0(4)	
HD1b	O(3)–H(3A)···N(1)	2.745(7)	167.0(2)	#3–x+1,y+1/2,–z+1/2
	O(4)–H(4A)···O(3)#3	2.846(1)	163.0(2)	

Table 3-2. Selected bond distances (Å), angles (°) and geometric parameters for the hydrogen-bonds in **HT1a**, **HT1b**, **HT2a**, **HT2b**, **HT3b**, **HD1a** and **HD1b**.

Subsequently, the complete 2D supramolecular network in **HT1a** and **HT1b** is constructed by the multiplication of these macrocycles. Finally, an ABABAB stacking of these layers along the *a* and *b* crystallographic axes, respectively, affords the final 3D structure. These 3D arrangements are held together by weak intermolecular interactions between the adjacent 2D layers. Hence, in **HT1a**, there are C–H···π interactions between DABCO molecules within one 2D layer and the aryl- group of the organic *linker* in the adjacent layer; whereas in **HT1b**, C–H···O interactions between the hydrogen atoms of the pyridine rings in 4,4'-bpe and the oxygen atoms (O(2) and O(4)) of the silanetriol moieties are observed [**Fig**. 3.3 and **Fig**. 3.4].
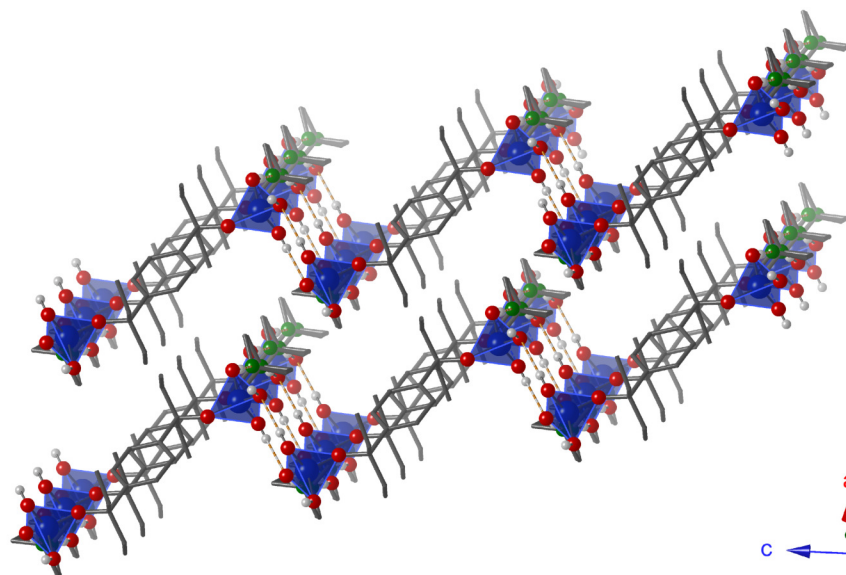
Figure 3.3. 3D supramolecular arrangement of **HT1a** formed by the ABABAB stacking of the 2D layers along the crystallographic *a*-axis.
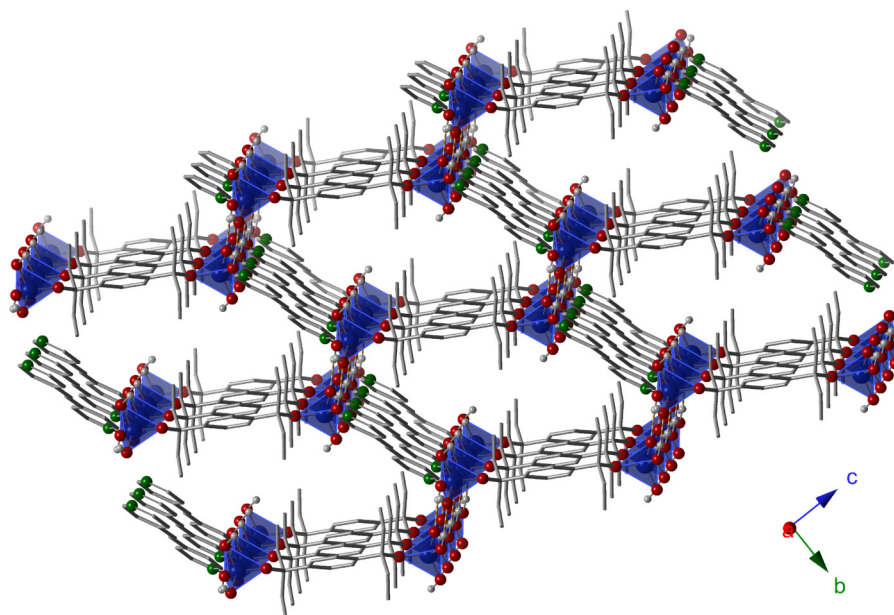
Figure 3.4. 3D supramolecular arrangement of **HT1b** formed by the ABABAB stacking of the 2D layers along the crystallographic *b*-axis; the solvent molecules were omitted for clarity.

It is noteworthy that the almost parallel stacking of the 2D layers in **HT1b**, results in the formation of uniform 1D THF-filled channels running parallel to the crystallographic *b*-axis. The contact surface of the channels was calculated with a probe radius of 1.2 Å, and grid spacing of 0.2 Å within Mercury[139] to be 44% of the whole crystal volume [**Fig**. 3.5].
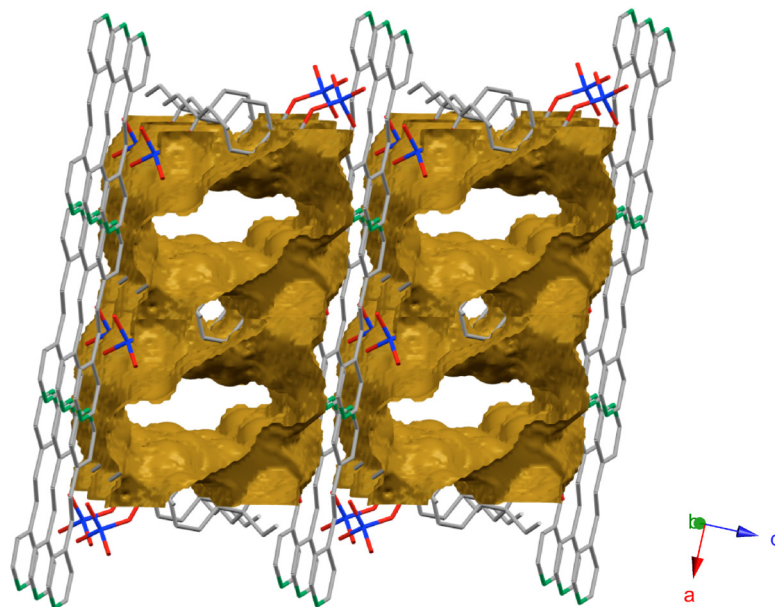
Figure 3.5. Porous structure of HOF **HT1b**. Formation of uniform 1D channels running parallel to the crystallographic *b*-axis.

Structural description of HT2a and HT2b

To investigate how the size of the organic *spacer* between the silicate moieties in the organo-bis(silanetriol) affects the porosity of the supramolecular arrangement, the precursor **T2** was tested as a molecular tecton for the construction of multicomponent HOFs, as the size of the organic *spacer* in **T2** is longer than in the analogous **T1**. Therefore, following the procedure used for the synthesis of **HT1a** and **HT1b**, the compound **T2** was co-crystallized with two equivalents of DABCO and 4,4'-bpe to yield the **HT2a** and **HT2b** HOFs, respectively. In both cases the $R_2^2(8)$ synthon, formed through the self-association of adjacent silicate moieties and observed also in **HT1a** and **HT1b**, is present leading to the formation of 1D infinite chains that can be described by a $C_2^2(34)$ graph set motif [**Fig**. 3.6 and **Fig**. 3.7].
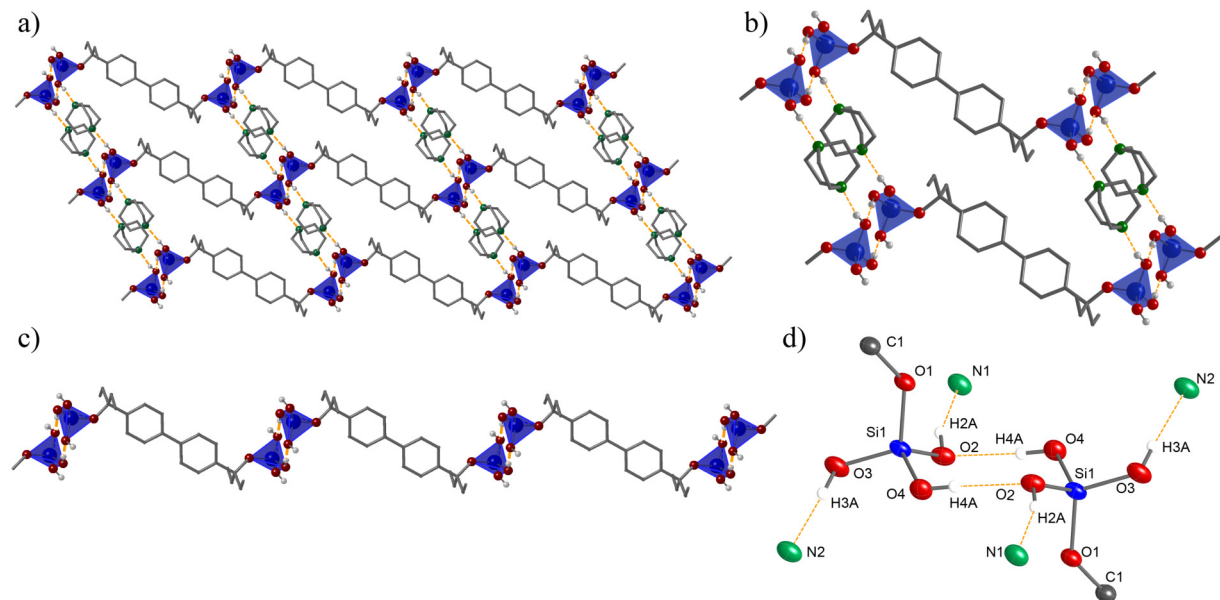
Figure 3.6. Supramolecular arrangement of HOF **HT2a**. (a) 2D supramolecular network constructed by the multiplication of diamine-silanol macrocycles, (b) $R_4^4(44)$ macrocycle of **HT2a**, (c) $C_2^2(34)$ motif, (d) $R_2^2(8)$ chair-shaped ring motif.

In analogy to the HOFs obtained from the organo-bis(silanetriol) **T1**, in **HT2a** and **HT2b** the first equivalent of the diamine interconnects the aforementioned 1D chains through the formation of SiO–H⋯N interactions between the amine molecule and the external protons of the $R_2^2(8)$ eight-membered ring motif. Again, these SiO–H⋯N interactions are stronger in **HT2a** ($D\cdots A$, O(2)–H(2A)⋯N(1) 2.653(2) Å), than those observed in its **HT2b** analogue ($D\cdots A$, O(2)–H(2)⋯N(1) 2.705(2) Å), because DABCO is a stronger base than 4,4'-bpe.

The presence of the amine molecules in **HT2a** and **HT2b** leads to the formation of macrocyclic systems described by $R_4^4(44)$ and $R_4^4(56)$ ring motifs, respectively. Therefore, the presence of a longer *spacer* did not affect the self-assembly process, and the formation of the diamine-silanol macrocycles, but it modifies the size of the latter in comparison with those in the **HT1a** and **HT2b** analogues. Thus, in the case of the supramolecular arrangements derived from DABCO the $d_{Si\cdots Si}$ distances within the diamine-silanol macrocycle change from 10.5 x 9.8 Å in **HT1a** to 9.6 x 14.6 Å in **HT2a**. Similar change was detected also in the arrangements obtained from 4,4'-bpe: 10.5 x 17.9 Å in **HT1b** and 14.5 x 17.1 Å in **HT2b** [**Fig**. 3.6b and **Fig**. 3.7b].

63
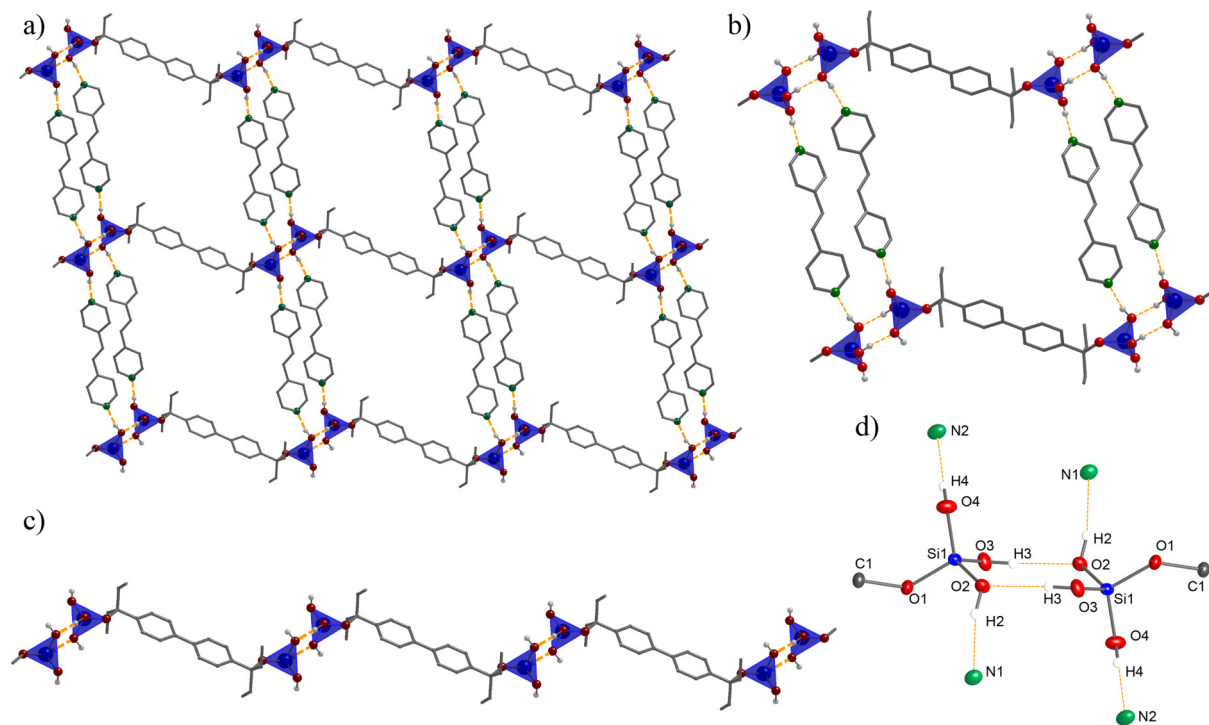
Figure 3.7. Supramolecular arrangement of HOF **HT2b**. (a) 2D supramolecular network constructed by the multiplication of diamine-silanol macrocycles, (b) $R_4^4(56)$ macrocycle of **HT2b**, (c) $C_2^2(34)$ motif, (d) $R_2^2(8)$ chair-shaped ring motif.

In both HOFs derived from the organo-bis(silanetriol) **T2**, the double-pillared 2D supramolecular network is generated by the SiO–H$\cdots$N hydrogen-bonding interaction with the third OH group of the $Si(OH)_3$ moieties, where these OH groups act as a single point donor towards amine molecules. It is noteworthy, that these SiO–H$\cdots$N hydrogen-bonding interactions are weaker than those in which the more acidic external protons are involved, as evidenced by longer $D\cdots A$ distances (**HT2a** O(3)–H(3A)$\cdots$N(2) 2.700(2) Å; **HT2b** O(3)–H(3)$\cdots$O(2) 2.736(1) Å) [**Fig**. 3.6d and **Fig**. 3.7d].

It should be pointed out, that the crystalline structure of **HT2b** does not contain solvent molecules interacting with the Si–OH moieties, as was observed in **HT1b** and instead, this position is occupied by a second equivalent of 4,4'-bpe. Consequently, these diamine molecules, in **HT2b**, are oriented in an almost parallel fashion with 4.37 Å between their centroids, and it is observed that the pyridine rings of each 4,4'-bpe molecule are slightly twisted forming a dihedral angle of 34°.

Finally, an ABABAB arrangement of the aforementioned 2D double-pillared layers is observed in **HT2a** and **HT2b**, affording the resulting 3D structures. The comparison between the supramolecular arrangements in **HT1a** and **HT2a** reveals the effect of the larger size of the organic *spacer* in the **T2** tecton, as while **HT1a** does not contain solvent molecules within the network, **HT2a** presents THF molecules enclosed in the 0D voids between the adjacent 2D supramolecular layers. These solvent molecules interact *via* C–H$\cdots\pi$ contacts with the organic *spacer* of the organosilanol tectons (2.900(1) Å, 129.1(1)°) [**Fig**. 3.8].
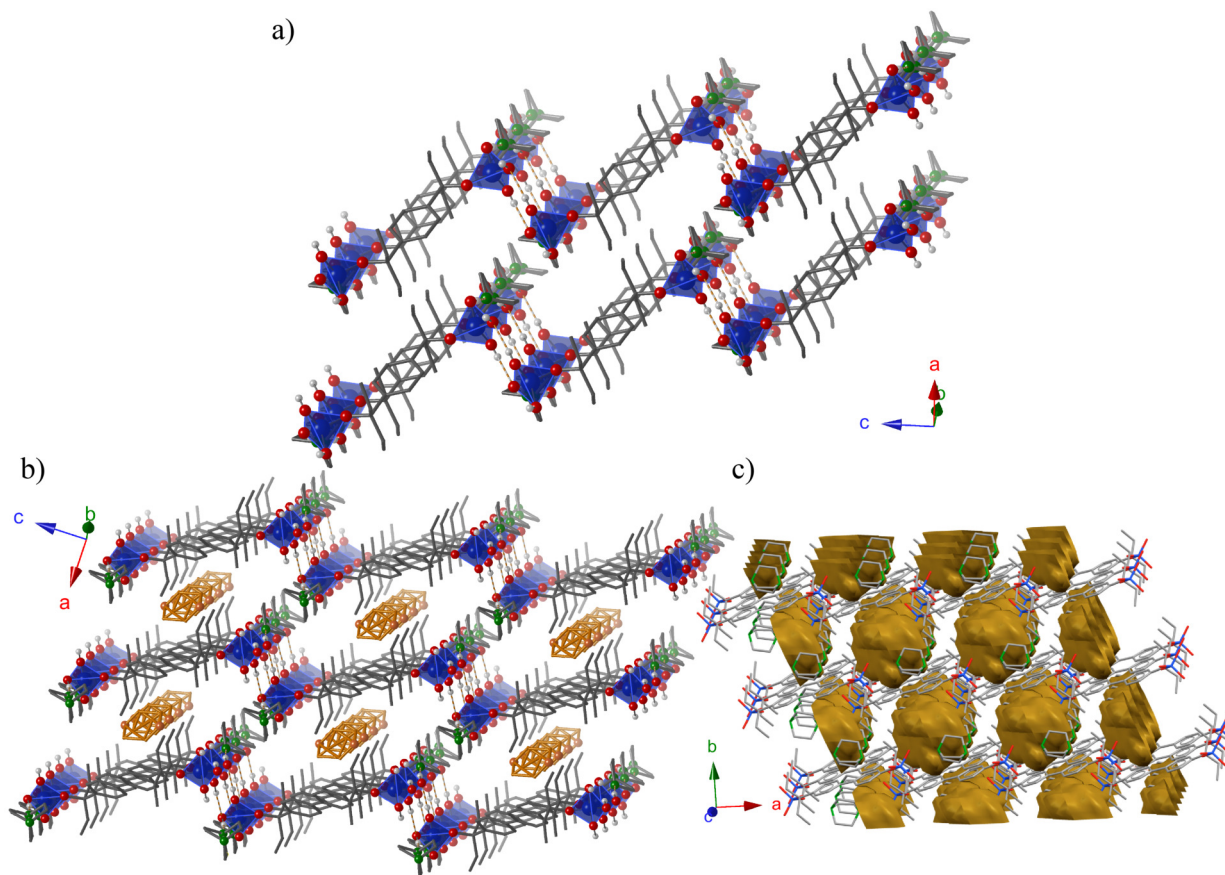
Figure 3.8. 3D supramolecular network in **HT1a** and **HT2a**. (a) ABABAB stacking of the supramolecular layers in **HT1a**, (b) ABABAB stacking of the supramolecular layers in **HT2a**, (c) Formation of 0D voids within the structure of **HT2a**.

Similarly, **HT2b** contains THF molecules between the adjacent 2D supramolecular layers affording the formation of 0D voids, where the solvent molecules participate in weak C–H$\cdots\pi$ (2.900(1) Å) and C–H$\cdots$O (2.542(1) Å) van der Waals interactions with the organic *spacer* of the organosilanol tecton [**Fig**. 3.9]. It should be noticed, that although both **HT1b** and

HT2b crystallize as solvates, in the second, the larger size of the organic *spacer* in the tecton **T2** has a clear effect on the resulting supramolecular structure, because this change allowed not only the insertion of the second equivalent of 4,4'-bpe but also reduced the dimensionality of the voids within the structure. Hence, while **HT1b** exhibits the formation of 1D channles, **HT2b** presents only 0D voids. Accordingly, it is evident that the subtle interplay between the geometrical and chemical factors during the formation of the multicomponent HOFs has a direct effect on the porosity of the resulting structure.
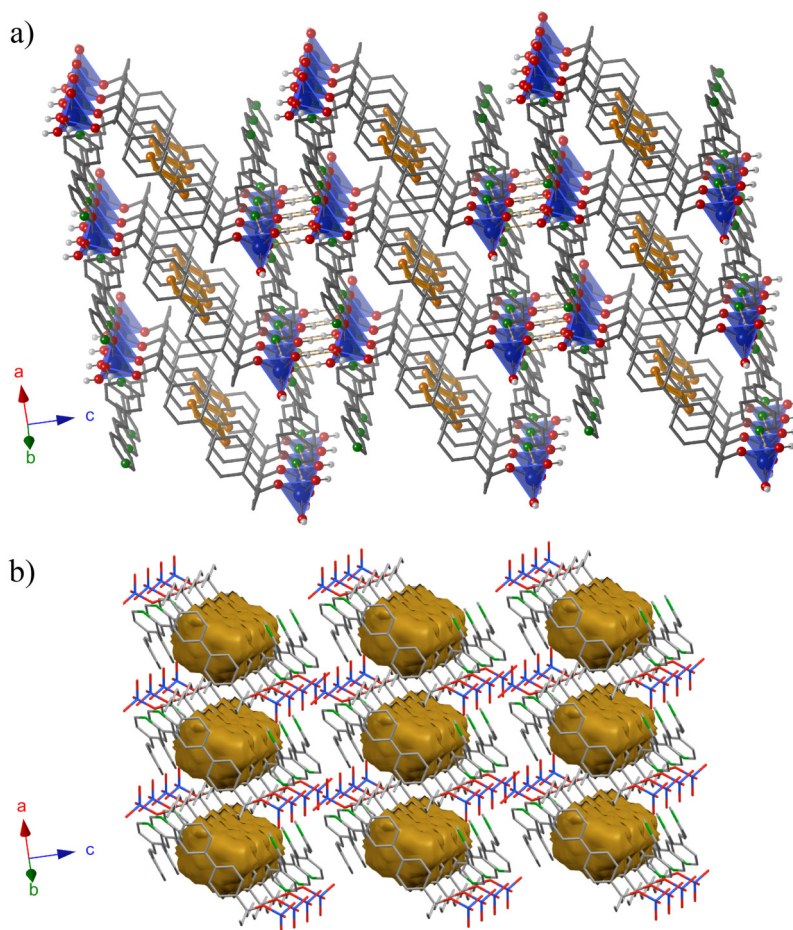
Figure 3.9. 3D supramolecular network of **HT2b**. (a) ABABAB stacking of the supramolecular layers in **HT2b**, (b) 0D voids within the structure of **HT2b**.

Structural description of HT3b

To gain a deeper understanding of how the steric effects around the silicate group in the organo-bis(silanetriol) tecton affect the supramolecular arrangement of the diamine-silanol based HOFs, the organo-bis(silanetriol) **T3** was tested as molecular tecton in the construction of multicomponent HOFs. Such tecton was selected because it has the same organic *spacer* between the silicate moieties as **T1**, but the ethyl groups, present in **T1**, have been replaced by bulkier phenyl groups in **T3**. Although the co-cristalization of the organo-bis(silanetriol) **T3** with two equivalents of DABCO was tested, the no formation of a co-crystalline network was observed. In contrast, using **T3** with two equivalents of 4,4'-bpe led to the formation of **HT3b**. Surprisingly, **HT3b** does not present the formation of the $R_2^2(8)$ homosynthon, instead, each OH group acts as a single point donor towards a Lewis base that can be either amine or a solvent molecule. Therefore, two of the OH groups of each $Si(OH)_3$ moiety are involved in SiO–H$\cdots$N interactions with 4,4'-bpe (O(2)–H(2A)$\cdots$N(1) 2.688(3) Å and O(3)–H(3A)$\cdots$N(2) 2.791(3) Å), whereas the third one binds to a THF molecule through a SiO–H$\cdots$O interaction (O(4)–H(4A)$\cdots$O(5) 2.732(1) Å) [**Fig**. 3.10].
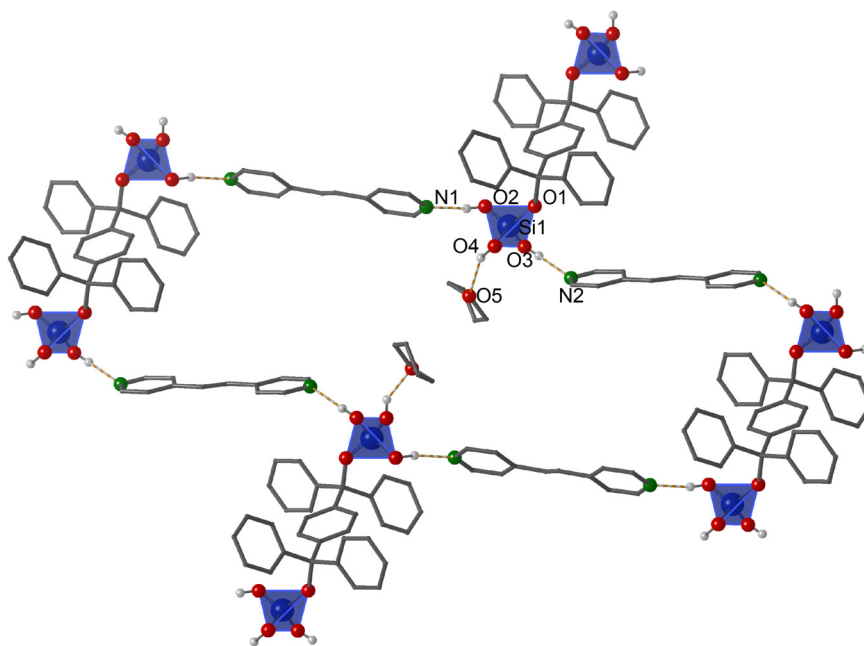
Figure 3.10. $R_8^8(78)$ supramolecular macrocycle in **HT3b**.
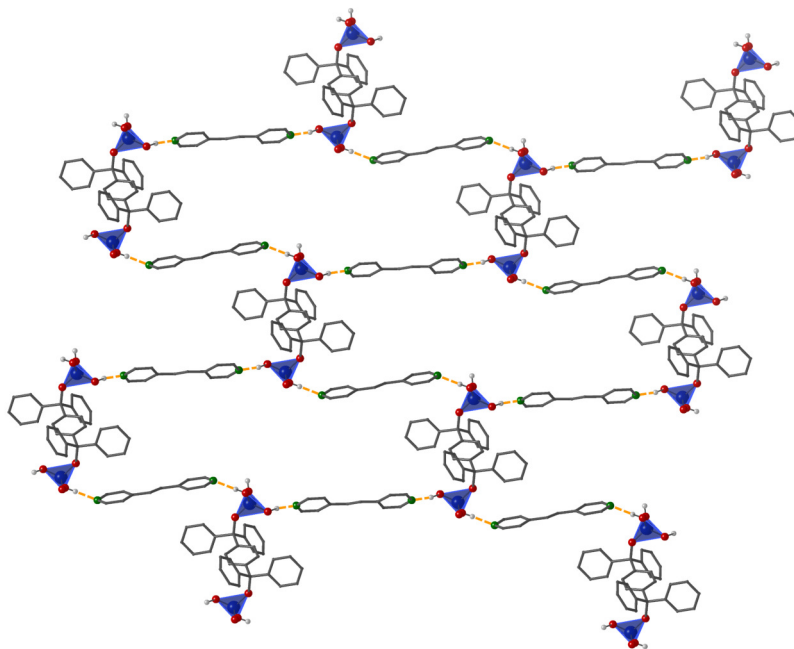
Figure 3.11. 2D supramolecular layers in **HT3b**. The solvent molecules were omitted for clarity.

This unusual behavior might be rationalized by considering both, the steric effects and the kinetic aspects during the crystallization process. It is well known that the interactions that are more probable to form first in the solution, will dominate the first stage of the assembly. In this context, it should be pointed out that the tertiary Ph_3C groups not only increased the steric hindrance around the silicate moieties, but they also enhanced significantly the solubility of **T3** in organic solvents including THF. Both facts affect the self-association between the $Si(OH)_3$ moieties and reduce the aggregation in solution. Therefore, the SiO–H$\cdots$N interactions will govern the self-assembly process during the formation of the supramolecular arrangement in this specific case. Consequently, the 4,4'-bpe molecules end up bridging two silicate moieties affording intercalated hydrogen-bonded chains parallel to the crystallographic *a*-axis, which can be described by the $C_4^4(30)$ graph set motif. It is noteworthy, that these supramolecular chains are further interconnected by the organic *spacer* of the organo-bis(silanetriol), acting as pillar resulting in 2D supramolecular layers formed by $R_8^8(78)$ macrocycles ($d_{Si\cdots Si}$= 32.57 x 9.12 Å) [**Fig**. 3.11].

These two-dimensional supramolecular layers are further packed *via* ABABAB stacking along the *b* crystallographic axis to a 3D framework. The network contains channels running along the crystallographic *a*-axis, that are filled by THF molecules held in place by hydrogen bonds to the remaining Si–OH groups. The contact surface of the channels was calculated with probe radius of 1.2 Å, and a grid spacing of 0.2 Å within Mercury[139] to be 19% of the whole crystal volume [**Fig**. 3.12].
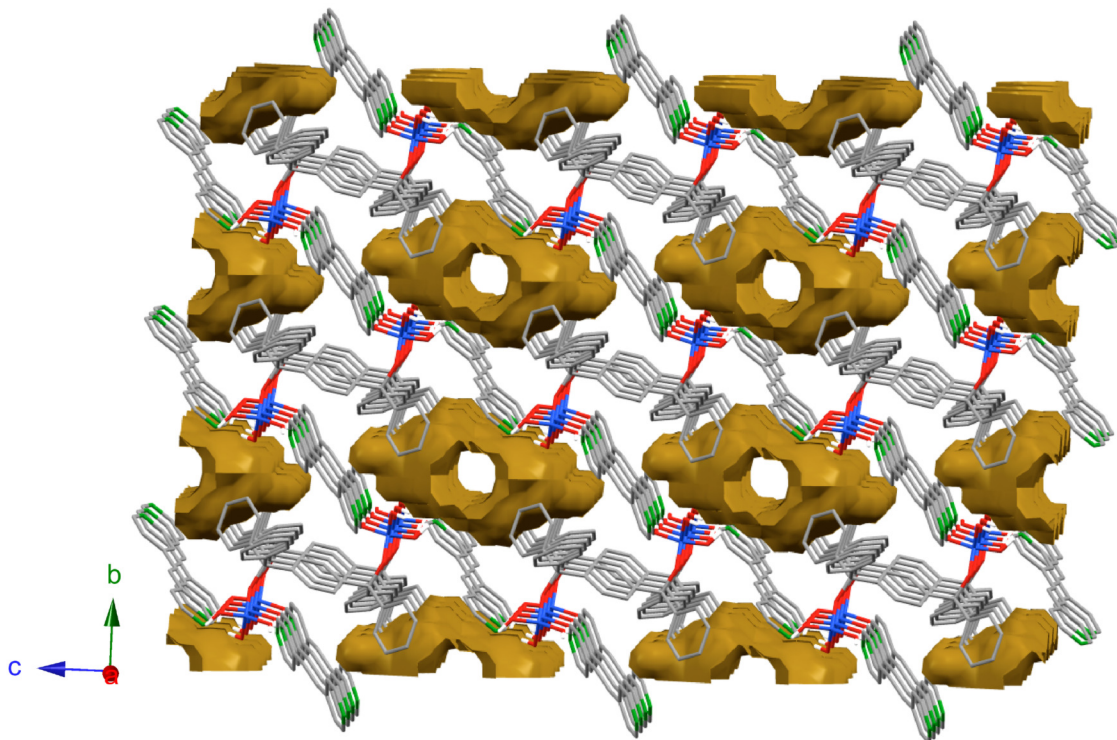
Figure 3.12. Surface of the channels present in **HT3b**. The channels are oriented along the crystallographic *a*-axis.

Structural description of the supramolecular assemblies HD1a and HD1b obtained from organo-bis(silanediols)

The next step in this study was to evaluate the role of the number of the Si–OH groups during the self-assembly process towards the formation of diamine-silanediol based HOFs. Therefore, the organo-bis(silanediol) $(HO)_2(t\text{-BuO})Si\text{–}O\text{–}R\text{–}O\text{–}Si(Ot\text{-Bu})(OH)_2$ (**D1**) was tested as a molecular tecton, as regarding to the size and rigidity of the organic liking group, **D1** is analogous to **T1**. However, one of the three OH groups of each $Si(OH)_3$ moiety has been blocked with

one *t*-BuO group. Therefore, the co-crystallization of **D1** in the presence of two equivalents of DABCO or 4,4'-bpe afforded the **HD1a** and **HD1b** HOFs, respectively.

In the case of **HD1a**, the formation of a HOF with a 2:1 diamine-silanol stoichiometric ratio was observed. The $R_2^2(8)$ synthon, that was recurrently observed in the previous HOFs, is absent. Instead, the diamine molecules are inserted between the silicate moieties through SiO–H$\cdots$N interactions, where the $D\cdots A$ distances are O(3)–H(3A)$\cdots$N(1) 2.655(2) Å, O(4)–H(4A)$\cdots$N(2) 2.672(2) Å. These interactions give rise to a supramolecular macrocycle that is comprised of intercalated amine-silanediol molecules and can be described by the $R_4^4(36)$ ring motif with $d_{Si\cdots Si}$ spacing of 10.5 x 10.1 Å.

Subsequently, these rings form 1D supramolecular strands running along the crystallographic *b*-axis. It should be pointed out, that the latter are surrounded by solvent molecules that form weak van der Waals contacts with the neighboring 1D strands, holding the whole crystal together in the other two dimensions [**Fig**. 3.13].
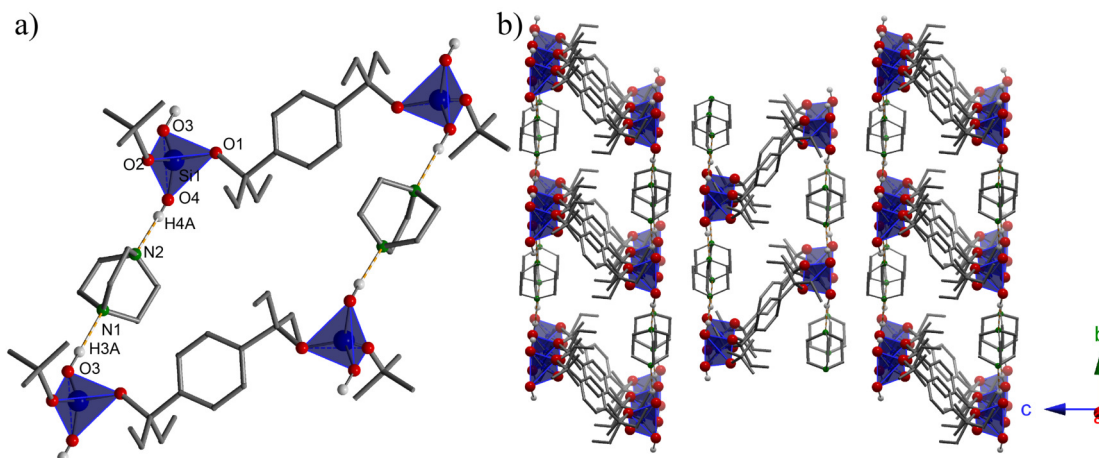
Figure 3.13. Supramolecular arrangement in the molecular structure of **HD1a**. (a) The $R_4^4(36)$ ring motif, (b) 1D supramolecular strands running along the crystallographic *b*-axis. The solvent molecules have been omitted for clarity.

In contrast to **HD1a**, the **HD1b** HOF crystallizes with a 1:1 diamine-silanol stoichiometric ratio. In addition, the supramolecular structure of the latter is completely different from that described for **HD1a**.
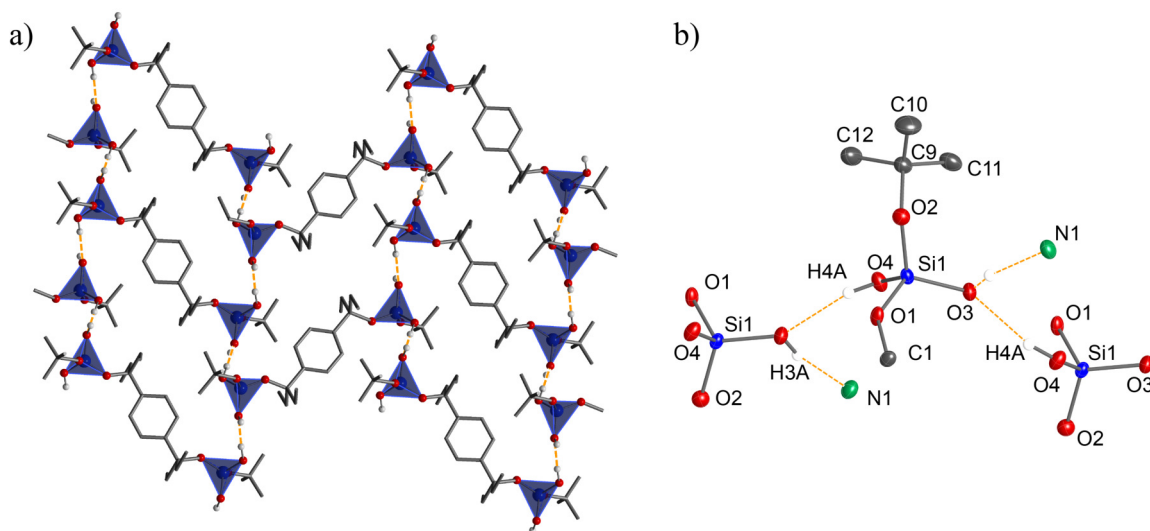
Figure 3.14. Supramolecular arrangement in the molecular structure of **HD1b**. (a) 2D supramolecular layers formed by the self-association between D1 molecules, (b) Principal hydrogen-bonding interactions.

First, despite that the eight-membered $R_2^2(8)$ synthon is not present, the OH groups of the silanediol moieties participate in SiO–H$\cdots$O hydrogen-bonding interactions with other two neighbouring molecules of **D1** (O(4)$\cdots$O(3) distance of 2.846(1) Å), affording the formation of supramolecular $C_1^1(4)$ chains running along the crystallographic b-axis. These chains are further interconnected by the organic linkers between the silicate moieties thereby creating a $R_4^4(34)$ ring motif, comprised of only organo-bis(silanediol) molecules. Such ring motif is extended parallel to crystallographic bc plane leading to the formation of 2D supramolecular layers [**Fig**. 3.14]. Second, one of the OH groups of the silanediol moiety presents an additional hydrogen-bonding interaction with 4,4'-bpe molecule ($D\cdots A$ distance of 2.745(7) Å). This permits the interconnection of the 2D layers, to yield a close-packed 3D supramolecular network [**Fig**. 3.15].

In **HD1a** and **HD1b**, the relative strength of the hydrogen bonds formed by the diamine-silanol interactions is in an accordance with their IR spectra. In **HD1a**, the band of the stretching vibration νO–H of the Si–OH groups, is shifted to a far lower frequency. In fact, this band is superimposed with the bands associated to the CH_3 stretching vibrations, whereas, in the IR spectra of **HD1b** the band for the νO–H stretching vibration is clearly identifiable at upper wave number ($\tilde{\nu}$ 3436 cm^{-1}) [**Fig**. 3.16].
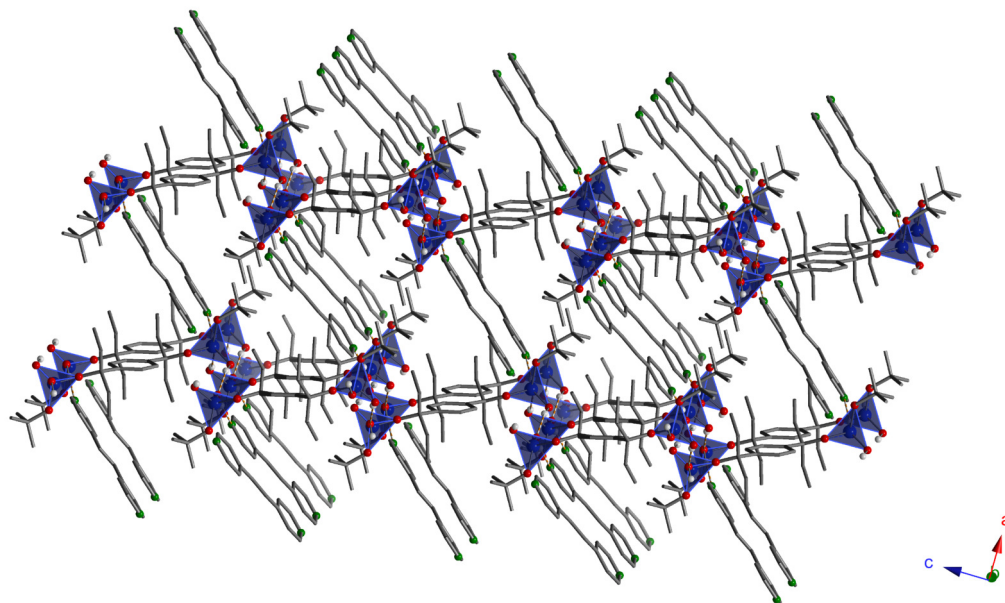
Figure 3.15. 3D close-packed network showing the 4,4'-bpe molecules acting as pillars interconnecting the 2D supramolecular layers.
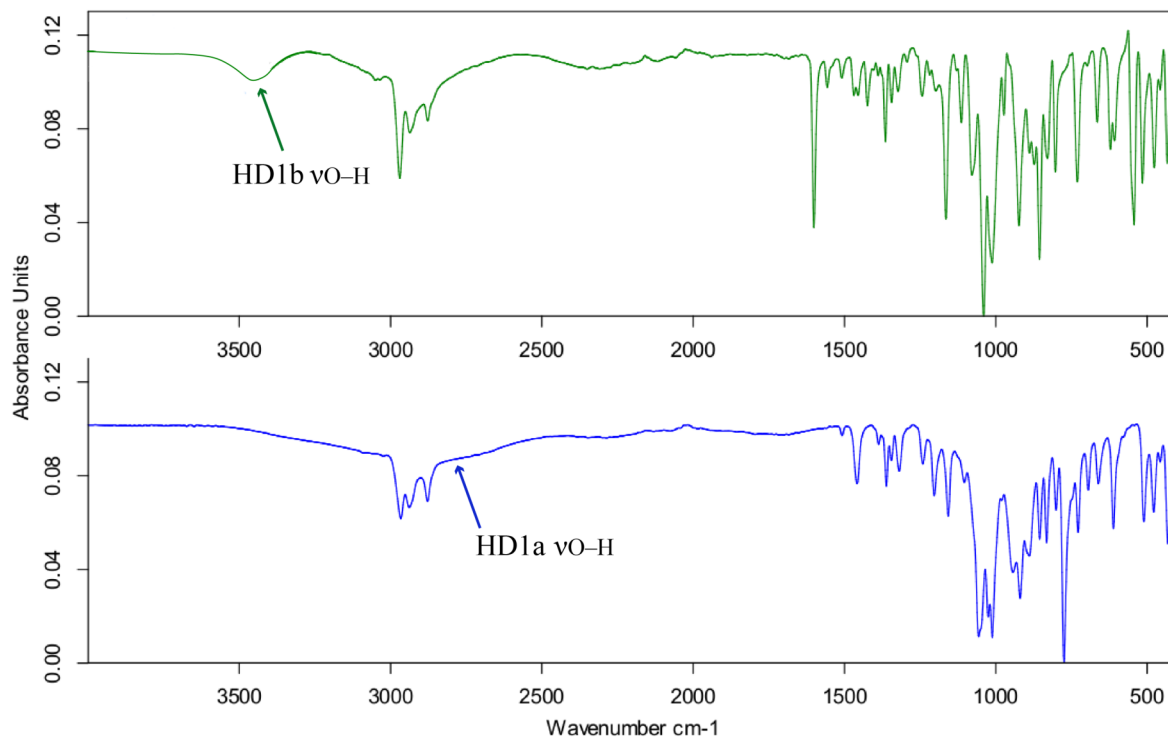
Figure 3.16. Comparison of the IR spectra of **HD1a** and **HD1b** HOFs.

Comparative view: $-Si(OH)_3$ versus $-Si(Ot\text{-}Bu)(OH)_2$ moieties

One of the most important goals in crystal engineering is the understanding of the final supramolecular arrangement in terms of the intermolecular interactions among the molecular building blocks that constitute the framework. In as much as we gain a wider understanding of the factors that govern such interactions, it will be possible to design more precisely new materials with the desired physical and chemical properties.

In this context, the foregoing description of the crystalline structures of **HT1a**, **HT1b**, **HT2a**, **HT2b**, and **HT3b**, **HD1a**, and **HD1b** HOFs provides an opportunity to examine how the Brønsted acidity of the Si–OH groups affects their hydrogen-bonding interactions either *via* self-association or with other polar organic molecules resulting in the formation of supramolecular structures with different porosity (1D channels, 0D voids, and non-porous arrangements).

It should be noted that the resulting structure is easily affected by subtle changes in the steric and electronic properties of the molecular building blocks. Thus, at first instance, the major difference between the HOFs derived from the organo-bis(silanetriols) **T1** and **T2** (**HT1a**, **HT1b**, **HT2a** and **HT2b**), and those derived from the organo-bis(silanediol) **D1** (**HD1a** and **HD1b**) is the degree of self-association between the silicate moieties. While the first group exhibits the formation of the eight-membered $R_2^2(8)$ ring synthon, the latter shows weaker or no interactions between the silicate moieties.

This behavior might be rationalized taking into account the importance of the kinetic aspects during the crystallization process. It is well known that those interactions that are more probable to form first in the solution, will dominate at the first stage of the building up process.[140] Accordingly, the formation of robust synthons, with strong and directional interactions, is a probabilistic process. Once they are formed, they do not break easily, and their existence is mediated by the variable interplay of chemical and geometrical recognition. Additionally, the critical role of the solvent in the formation of interactions in solution modulated by the solvation process has been studied previously.[140]

Given all these considerations, the presence of the aforementioned Si–OH$\cdots$O interaction based $R_2^2(8)$ synthon in **HT1a**, **HT1b**, **HT2a** and **HT2b**, rather than the more favorable SiO–H$\cdots$N interactions, may be explained by the strong tendency of the silanols groups to the

self-association even in solution, as demonstrated previously by Franz and co-workers.[141]

On the contrary, when one OH group of the silicate moiety is blocked by a bulky t-BuO group, not only the steric hindrance around the silicate moieties is enhanced, but also the Brønsted acidity of the Si–OH groups decreases. Therefore, the synergistic effect of the afore-mentioned two factors reduces the possibility of the –Si(Ot-Bu)(OH)$_2$ moieties to autoasso-ciate, in solution. This assumption is also supported by the lower solubility of the organo-bis(silanetriol) **T1**, when it is compared with the analog organo-bis(silanediol) **D1**. Thus, in the case of **D1**, the interaction hierarchy (strongest donor to strongest acceptor) between Si–OH groups and amines, gains more relevance during the first steps of the assembly process. On the other hand, in the case of organo-bis(silanetriols) **T1** and **T2**, the self-association between the Si(OH)$_3$ moieties into the R$_2^2$(8) synthons is kinetically preffered at the first stage of the assembly process. Additionally, it is important to take into account the role of the Lewis base during the construction of the molecular assembly. For instance in **HD1b**, the synthon R$_2^2$(8) is partially opened. Hence, one OH group of the adjacent silicate moiety participates in a weak SiO–H$\cdots$O interaction to afford a 2D layered structure, while the second OH group of the silicate moiety interacts with an amine molecule to interconnect these layers into a 3D supramolecular net-work. In case of **HD1a**, the increase in the basicity of the amine gives rise to the formation of only SiO–H$\cdots$N interactions, and consequently, the absence of the R$_2^2$(8) synthon. This results in the reduction of the overall dimensionality of the supramolecular arrangement from 3D to 1D, where the THF molecules are present between such 1D diamine-silanol ribbons to allow an efficient packing in the other two dimensions.

Similarly, when the molecular structures of **HT1a**, **HT1b**, **HT2a**, and **HT2b** are compared, the effect of the relative strength of the Lewis base and the size of the *spacer* on the porosity of the supramolecular arrangements can be observed.

As mentioned earlier, the cooperative hydrogen-bonding association between two Si(OH)$_3$ moieties enhances the acidic character of the two external protons that do not participate in the dimeric R$_2^2$(8) ring. Consequently, this lets us consider that at this point of the self-assembly process, the SiO–H$\cdots$N interactions are more relevant resulting in the incorporation of the first equivalent of the amine into the supramolecular arrangement. Nevertheless, the insertion of the second equivalent of the amine is determined by the interplay of geometrical and chemical

aspects. Accordingly, in the case of **HT1a**, **HT2a** and **HT2b**, the insertion of the second amine equivalent to yield a double-pillared 2D layered arrangement is favored.

Moreover, **HT1b** exhibits only 1:1 amine:silanol stoichiometric ratio resulting in a single-pillared arrangement of the amine molecules. This is probably due to the synergic effect of two factors. First, 4,4'-bpe is less basic than DABCO, while the second is the the size of the organic *linker*. This is based on the reasoning that when one of these two variables is modified using a stronger base, as in **HT1a**, or larger organic *linker* as in **HT3b**, the expected 2:1 stoichiometric ratio is maintained.

3.1.3   Thermal stability

The thermogravimetric analysis of the organo-bis(silanetriol) **T1** and its analogous organo-bis(silanediol) **D1**, under nitrogen atmosphere, revealed that the tecton **T1** present higher thermal stability than **D1**. This observation may be explained by the thermal lability of the t-BuO groups, which can suffer a β-elimination process to afford isobutene.

Thus, on the one hand, the thermal decomposition of **T1** takes place in a single-stage process that involves the condensation of the $Si(OH)_3$ moieties, accompanied by the loss of the organic bridging group (temperature range 175–325 °C), leaving a residual weight corresponding to hydrated silica $2\ SiO_2 \cdot H_2O$ (observed residual weight: 31.4%, calculated residual weight: 34.0%) *see* Table 3-3. On the other hand, the thermal decomposition of **D1** takes place in several steps. In the first stage, **D1** looses one water molecule in the temperature range 50–120 °C (observed weight loss: 3.6%, calculated weight loss: 3.5%). The second step of its decomposition (temperature range 120–180 °C) corresponds to the β-elimination of two equivalents of isobutene (observed weight loss: 18.7%, calculated weight loss: 21.0%). The last transformation corresponds to the loss of the organic bridging group to afford hydrated silica $2\ SiO_2 \cdot H_2O$ as residual mass at 450 °C (observed residual weight: 28.9%, calculated residual weight: 26.2%) [**Fig**. 3.17].

Sample	Temperature range (ºC)	Weight loss	% Calc.	% Found	Residual mass at 450ºC
T1	175–325	$-\{H_2O\},-\{1,4-[OCEt_2]_2C_6H_4\}$	65.5	68.6	31.4
HT1a	130–275	$-\{H_2O\},-2\{DABCO\}$	38.5	49.0	22.8
	275–400	$-\{1,4-[OCEt_2]_2C_6H_4\}$	39.4	28.2	
HT1b	125–175	$-2\{H_2O\}$	6.1	5.9	24.4
	200–450	$-\{4,4'-bpe\}, -\{1,4-[OCEt_2]_2C_6H_4\}$	73.1	69.7	
T2	100–225	$-2\{H_2O\}$	7.5	14.9	26.8
	225–450	$-\{1,1'-Biphenyl-4,4'-(COEt_2)_2\}$	67.2	58.3	
HT2a	75–250	$-\{H_2O\},-2\{DABCO\},-\{THF\}$	40.3	43.9	15.2
	250–375	$-\{1,1'-Biphenyl-4,4'-(COEt)_2\}$	41.6	41.0	
HT2b	75–200	$-2\{H_2O\},-\{THF\}$	11.8	13.1	18.8
	200–450	$-\{1,1'-Biphenyl-4,4'-(COEt)_2\} -2\{4,4'-bpe\}$	74.9	68.1	
HT3b	75–200	$-2\{THF\}$	13.0	18.3	56.9
	200–375	$-2\{4,4'-bpe\}$	33.0	38.6	
D1	50–120	$-2\{H_2O\}$	3.5	3.6	28.9
	120–180	-2 isobutene	21.0	18.7	
	180–450	$-\{1,4-[OCEt_2]_2C_6H_4\}$	47.9	48.8	
HD1a	100–450	Decomposition of the organic moieties	83.6	83.2	16.82
HD1b	125–450	Decomposition of the organic moieties	82.9	81.8	18.2

Table 3-3. Thermal decomposition of **HT1a**, **HT1b**, **HT2a**, **HT2b**, **HT3b**, **HD1a** and **HD1b**, **T1**, **T2** and **D1**.
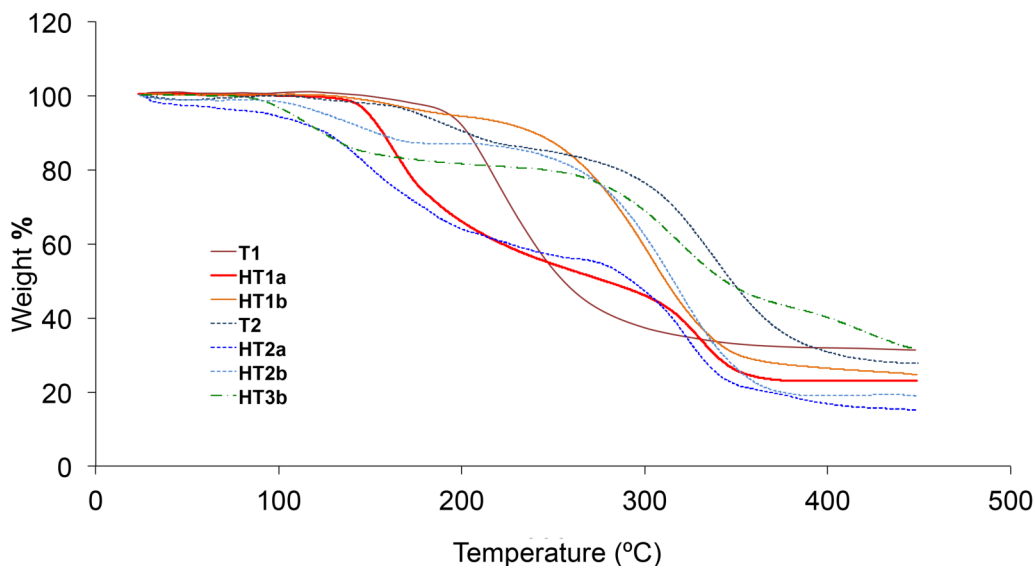
Figure 3.17. TGA trace for HOFs derived from organo-bis(silanetriols).

76

The thermal decomposition of **HT1a** occurs in two stages. The first stage (temperature range 130–275 °C) may be associated with the condensation of the $Si(OH)_3$ moieties accompanied by the release of the two equivalents of DABCO *see* Table 3-3. This assumption was made taking into account the reported thermal stability of pure DABCO that decomposes in the temperature range of 75–250 °C.[142] The second stage corresponds to the decomposition of the organic bridging group, which leads to the formation of hydrated silica 2 $SiO_2 \cdot H_2O$ as residual mass at 450 °C (observed residual weight: 22.8%, calculated residual weight: 21.9%).

On the contrary, **HT1b** presents higher thermal stability than **HT1a** and can be explained by the higher thermal stability of 4,4'-bpe when compared to DABCO. Thus, **HT1b** decomposes in two steps, where the first stage (temperature range 125–175 °C) is attributed to the thermal condensation of $Si(OH)_3$ moieties (observed weight loss: 5.9%, calculated weight loss: 6.1%). The second stage, in the temperature range 200–450 °C, corresponds to the decomposition of the organic bridging group and 4,4'-bpe (observed weight loss: 69.7%, calculated weight loss: 73.1%). This leads to the formation of silica 2 SiO_2 as residual mass at 450 °C (observed residual weight: 24.4%, calculated residual weight: 20.4%).

It is noteworthy, that the TG curve of **HT1b** does not show the elimination of the solvent, even though the network contains THF molecules filling the 1D channels. This fact is also in accordance with the elemental analysis of **HT1b** obtained after being dried under vacuum for 4 h (*see Experimental section*).

Conversely, the thermogravimetric curve of **HT2a** and **HT2b**, that also crystallized as solvates, exhibit the loss of the solvent molecules in the first stage of their thermal decomposition.

Therefore, **HT2a** shows in its first stage of decomposition (temperature range 75–250 °C) not only the condensation of $Si(OH)_3$ moieties and the thermal decomposition of DABCO molecules, but it also looses one THF molecule (observed weight loss: 40.3%, calculated weight loss: 43.9%). Subsequently, the next mass loss observed between 250 and 375 °C corresponds to the decomposition of the organic bridging group (observed weight loss: 41.6%, calculated weight loss: 41.0%). This leads to the formation of hydrated silica 2 $SiO_2 \cdot H_2O$ as residual mass at 450 °C (observed residual weight: 15.2%, calculated residual weight: 17.0%).

Similarly, **HT2b** exhibits a two stage decomposition, where the first step observed between 75 and 200 °C corresponds to the condensation of the $Si(OH)_3$ moieties and the release of

solvent molecules (observed weight loss: 13.1%, calculated weight loss: 11.8%). Then, the second stage (temperature range 200–450 °C) is associated with the thermal decomposition of the organic bridging group and the amine molecules (observed weight loss: 68.1%, calculated weight loss: 74.9%). This leads to the formation of silica 2 SiO_2 as residual mass at 450 °C (observed residual weight: 18.8%, calculated residual weight: 17.0%).

In the case of **HT3b** it is observed that the first weight loss is observed between 75 and 200 °C, and it is attributed to the loss of the two hydrogen-bonded THF molecules (observed weight loss: 18.3%, calculated weight loss: 13.0%). The subsequent weight loss corresponds to the decomposition of the 4,4'-bpe molecules. Nevertheless, it is noteworthy that this compound did not decompose completely in the range of temperatures applied during the thermogravimetric analysis. Consequently, the percentage associated with the residual mass at 450 °C (56.9 %) does not correspond to a pure silica, as in the case of the HOFs described earlier.

Finally, the thermal analysis curves of **HD1a** and **HD1b** demonstrate that their thermal decompositions are more complex and have several stages ending with silica as the residual mass at 450 °C [**Fig**. 3.18].
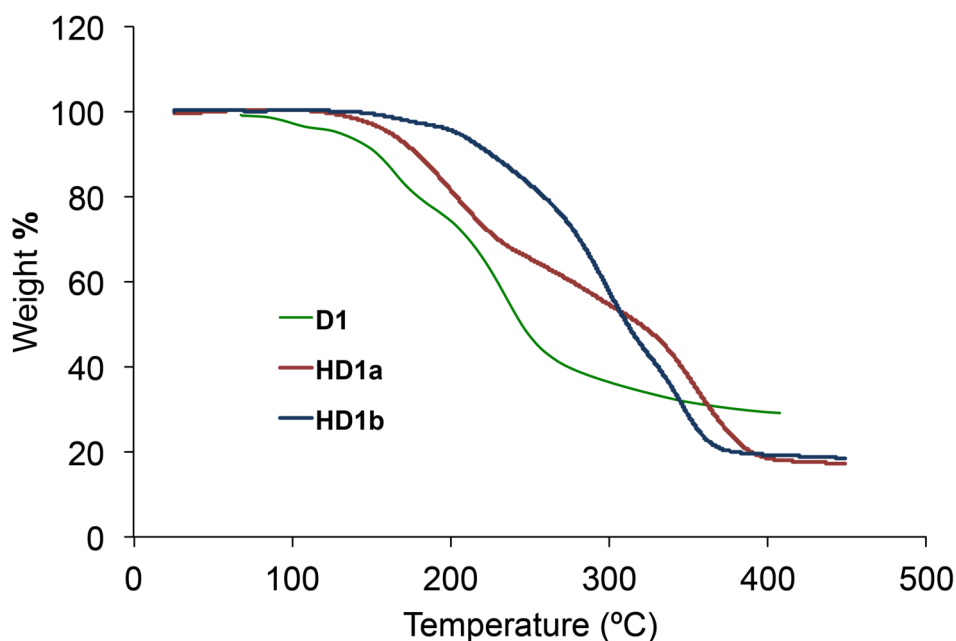
Figure 3.18. TGA trace for HOFs derived from the organo-bis(silanediol) **D1** .

3.2　Conclusions

In summary, the work described in this chapter demonstrates the use of bridged organo-bis(silanols) as molecular tectons in the synthesis of multicomponent HOFs based on organosilicates, which to the best of our knowledge, do not have any precedent in the literature. Additionally, applying subtle structural modifications to these molecular tectons, it was possible to modulate the porosity of the final material and the dimensionality of the resulting.

Finally, it is noteworthy that the diamine molecules traped between adjacent $Si–(OH)_n$ moieties, act as stabilizing agents reducing the kinetic tendency of the organo-bis(silanols) to self-condensation. Consequently, the HOFs exhibit higher stability towards condensation reactions in comparison to their corresponding free organo-bis(silanols). This was confirmed experimentally as the HOFs are stable under normal laboratory conditions for extended periods of time.

3.3 Experimental section

3.3.1 General methods

The solvents were purchased from Sigma-Aldrich and dried prior use with an MBraun SPS solvent purification system using Grubs' columns. Organic diamines 1,4-diazabicyclo[2.2.2]ocatne (DABCO) and 4,4'-vinylenedipyridine (4,4'-bpe) were purchased from Sigma-Aldrich and used without further purification. Elemental analyses (C, H, N) were determined on an Elementar MicroVario Cube analyzer. FT-IR spectra were recorded on a Bruker ALPHA FTIR spectrometer using the ATR technique with a diamond window in the range of $\tilde{\nu}$ 500–4000 cm^{-1}. Melting points were measured in sealed capillaries on Büchi B-540 melting point apparatus. TG measurements were carried on a Netzsch STA 449 F3 Jupiter with a heating rate of 10 °C/min from room temperature to 450 °C. The measurements were performed with a constant flow of dinitrogen gas (50 mL/min), using 5 mm aluminum crucible. Savitzky-Golay smoothing algorithm was employed for the TG curves.

3.3.2 Synthesis of HOFs

HT1a: A solution of DABCO (0.11 g, 0.98 mmol) in THF (2 mL) was added to a solution of **T1** (0.20 g, 0.49 mmol) in THF (10 mL) and the mixture was stirred for 15 min. The white precipitate was filtered off. Crystals of **HT1a** were grown from a saturated THF solution at –24 °C. **Yield**: 0.24 g, 0.37 mmol, 76%. **M.p.** > 350 °C. **Elemental analysis** (%) Calcd for $C_{28}H_{54}O_8Si_2N_4$ (630.52 g·mol^{-1}): C 53.34, N 8.88, H 8.56; Found: C 52.65, N 8.52, H 8.47. **FT-IR (ATR) (cm^{-1})** $\tilde{\nu}$ 2958, 2881 (w, C–H, CH$_3$, CH$_2$), 927 (s, Si–O).

HT1b: To a solution of **T1** (0.50 g, 1.23 mmol) in THF (15 mL) was added a solution of 4,4'-bpe (0.45 g, 2.46 mmol) in THF (3 mL) and the mixture was stirred for 15 min and saturated under vacuum. Afterwards this mixture was stored at –24 °C to afford the HOF **HT1b** as a white crystalline solid, which was isolated by filtration. **Yield**: 0.63 g, 1.10 mmol, 87%. **M.p.** 290 °C (dec). **Elemental analysis** (%) Calcd for $C_{28}H_{40}O_8Si_2N_2$ (588.80 g·mol^{-1}): C 57.12, H 6.85, N 4.76; Found: C 55.84, H 6.53, N 4.43. **FT-IR (ATR) (cm^{-1})** $\tilde{\nu}$ 3087 (s, SiO–H), 2960, 2880 (w, C–H, CH$_3$, CH$_2$), 927 (s, Si–O).

HT2a: To a solution of **T2** (0.50 g, 1.03 mmol) in THF (20 mL) was added a solution of DABCO (0.23 g, 2.10 mmol) in THF (5 mL), and the mixture was stirred for 15 min. The white precipitate was filtered off and crystals of **HT2a** were grown from a saturated THF solution at –24 °C. **Yield**: 0.55 g, 0.71 mmol, 69%. **M.p.** 250 °C (dec). **Elemental analysis** (%) Calcd for $C_{34}H_{58}O_8Si_2N_4$·THF (779.14 g·mol^{-1}): C 58.58, H 8.03, N 6.46; Found: C 57.55, H 8.03, N 6.46. **FT-IR (ATR) (cm^{-1})** $\tilde{\nu}$ 3291 (s, SiO–H), 2934, 2876 (w, C–H, CH$_3$, CH$_2$), 916 (s, Si–O).

HT2b: To a solution of **T2** (0.50 g, 1.03 mmol) in THF (20 mL) was added a solution of 4,4'-bpe (0.38 g, 2.10 mmol) in THF (5 mL)) and the mixture was stirred for 15 min and saturated under vacuum. Afterwards this mixture was stored at –24 °C to afford the HOF **HT2b** as a white crystalline solid, which is isolated by filtration. **Yield**: 0.74 g, 0.80 mmol, 78%. **M.p.** 270 °C (dec). **Elemental analysis** (%) Calcd for $C_{46}H_{54}O_8Si_2N_4$·THF (919.24 g·mol^{-1}): C 65.33, H 6.80, N 6.10; Found: C 64.85, H 7.02, N 5.84. **FT-IR (ATR) (cm^{-1})** $\tilde{\nu}$ 3294 (s, SiO–H), 2961, 2932, 2876 (w, C–H, CH$_3$, CH$_2$), 919 (s, Si–O).

HT3b: To a solution of **T3** (1.00 g, 1.67 mmol) in THF (20 mL) was added a solution of 4,4'-bpe (0.61 g, 3.34 mmol) in THF (5 mL). The mixture was stirred over a period of 15 min. Single crystals of **HT3b** were grown from a saturated solution of THF at –24 °C and the HOF **HT3b** was isolated by filtration as white crystalline solid. **Yield**: 1.00 g, 0.92 mmol, 54%. **M.p.** > 470 °C. **Elemental analysis** (%) Calcd for $C_{56}H_{50}O_8Si_2N_4$·2THF (1107.42 g·mol^{-1}): C 69.41, H 6.01, N 5.06; Found: C 68.98, H 6.07, N 4.94. **FT-IR (ATR) (cm^{-1})** $\tilde{\nu}$ 3210 (s, SiO–H), 2978, 2932, 2875 (w, C–H, CH$_3$, CH$_2$), 907 (s, Si–O).

HD1a: A solution of DABCO (0.13 g, 1.16 mmol) in THF (2 mL) was added to a solution of **D1** (0.30 g, 0.60 mmol) in THF (5 mL) and the mixture was stirred for 15 min and saturated under vacuum. Afterwards this mixture was stored at –24 °C to afford the HOF **HD1a** as a white crystalline solid, which was isolated by filtration. **Yield**: 0.47 g, 0.53 mmol, 88%. **M.p.** 170 °C. **Elemental analysis** (%) Calcd for $C_{36}H_{70}O_8Si_2N_4$·0.44 THF (774.87 g·mol^{-1}): C 58.53, H 9.56, N 7.23; Found: C 57.75, H 9.68, N 7.23. **FT-IR (ATR) (cm^{-1})** $\tilde{\nu}$ 2966, 2938, 2878 (w, C–H, CH$_3$, CH$_2$), 919 (s, Si–O).

HD1b: To a solution of **D1** (0.50 g, 1.0 mmol) in THF (7 mL) was added a solution of 4,4'-bpe (0.34 g, 2.0 mmol) in THF (5 mL) and the mixture was stirred for 15 min and saturated under vacuum. Afterwards this mixture is stored at –24 °C to afford the HOF **HD1b** as a white crystalline solid, which was isolated by filtration. **Yield**: 0.51 g, 0.73 mmol, 73%. **M.p.** 165–168 °C (dec). **Elemental analysis** (%) Calcd for $C_{36}H_{56}O_8Si_2N_2$ (701.02 g·mol^{-1}): C 61.68, H 8.05, N 4.00; Found: C 61.38, H 8.31, N 3.86. **FT-IR (ATR) (cm^{-1})** $\tilde{\nu}$ 3436 (s, SiO–H), 2969, 2936, 2877 (w, C–H, CH$_3$, CH$_2$), 924 (s, Si–O).

3.3.3   Single-crystal X-ray diffraction analysis

Crystal data and structure refinement details of the obtained compounds

Single crystals were mounted on a Bruker APEX DUO diffractometer equipped with an Apex II CCD detector at 100 K. Frames were collected using omega scans and integrated with SAINT.[125] Multi-scan absorption correction (SADABS) was applied.[125] The structures were solved by direct methods (SHELXT)[127] and refined using full-matrix least-squares on F^2 with SHELXL[128] using the ShelXle GUI.[128] Weighted R factors, R_w and all goodness-of-fit indicators, are based on F^2. All non-hydrogen atoms were refined anisotropically. The hydrogen atoms of the C–H bonds were placed in idealized positions, whereas the hydrogen atoms from the OH moieties in HOFs were localized from the difference electron density map and their position was refined with U_{iso} tied to the parent atom with distance restraints (DFIX or SADI). The disordered groups and solvent molecules (**HT1b** : 2 x THF; **HT2a**: 1 x THF; **HT2b**: 1 x THF, 1 x OH; **HD1a**: 1 x *t*-BuO, 1 x THF, 2 x Et; **HD1b**: 1 x 4,4'-bpe, 2 x Et) were refined using geometry (SADI, SAME) and U_{ij} restraints (SIMU, RIGU) implemented in SHELXL.[128]

	HT1a	HT1b	HT2a	HT2b	HT3b	HD1a	HD1b
Empirical formula	$C_{28}H_{54}N_4O_8Si_2$	$C_{44}H_{27}N_2O_{12}Si_2$	$C_{38}H_{66}N_4O_9Si_2$	$C_{50}H_{62}N_4O_9Si_2$	$C_{64}H_{66}N_4O_{10}Si_2$	$C_{44}H_{86}N_4O_{10}Si_2$	$C_{44}H_{86}N_4O_{10}Si_2$
Formula mass (g/mol)	630.93	877.21	779.12	919.21	1107.38	887.34	701.00
Space group	$P\bar{1}$	$P\bar{1}$	$P\bar{1}$	$P\bar{1}$	$P\bar{1}$	$P2_1/n$	$P2_1/c$
T (K)	100(2)	100(2)	100(2)	100(2)	100(2)	100(2)	100(2)
λ (Å)	0.71073	1.54178	1.54178	1.54178	1.54178	1.54178	0.71073
a (Å)	8.5208(4)	10.0113(4)	9.2526(2)	9.45190(10)	9.3585(2)	10.5432(4)	11.1858(3)
b (Å)	9.8696(5)	10.5786(4)	9.6010(2)	9.56110(10)	10.1254(3)	10.0965(4)	9.2167(2)
c (Å)	11.7679(6)	12.8998(4)	13.5651(2)	15.3911(2)	14.9494(4)	24.1212(9)	18.6477(5)
α (°)	103.7594(11)	74.9757(19)	81.2971(11)	75.3208(8)	92.3766(19)	90	90
β (°)	97.5810(11)	88.026(2)	75.9465(11)	85.8506(7)	92.1012(19)	90.0303(19)	98.6109(5)
γ (°)	113.1915(11)	63.2189(19)	66.2153(12)	62.9820(7)	90.993(2)	90	90
V (Å³)	854.90(7)	1172.54(8)	1067.76(4)	1197.18(2)	1414.16(6)	2567.69(17)	1900.84(8)
Crystal size (mm)	0.189 x 0.052 x 0.040	0.247 x 0.202 x 0.104	0.432 x 0.14 x 0.032	0.151 x 0.105 x 0.098	0.143 x 0.072 x 0.034	0.238 x 0.210 x 0.177	0.285 x 0.206 x 0.118
Z	1	1	1	1	1	2	2
$\varrho_{calc.}$ (g·cm⁻³)	1.226	1.242	1.212	1.275	1.300	1.148	1.225
μ (mm⁻¹)	0.154	1.189	1.201	1.161	1.094	1.066	0.144
$F(000)$	342	474	422	490	586	972	756
θ range for data collection (°)	1.841 to 26.371	3.564 to 67.734	3.365 to 67.727	2.972 to 70.056	2.960 to 68.243	3.665 to 68.240	2.209 to 27.499
No. of reflections	16864	4133	22314	21340	23641	21510	18657
No. of independent reflections (R_{int})	3500 (0.0390)	4133	3788 (0.0346)	4438 (0.0246)	5035 (0.0404)	4685 (0.0262)	4334 (0.0240)
No. of data/restraints/ parameters	3500/3/201	4133/526/374	3788/71/273	4438/75/327	5035/550/475	4685/1086/523	4334/577/333
Goodnes-on-fit (GOF) on F^2	1.018	1.061	1.043	1.039	1.046	1.058	1.075
R_1,[a] wR_2[b] ($I > 2\sigma(I)$)	0.0335, 0.0786	0.0514, 0.1424	0.0403, 0.1042	0.0340, 0.0907	0.0548, 0.1464	0.0649, 0.1845	0.0368, 0.0996
R_1,[a] wR_2[b] (all data)	0.0436, 0.0844	0.0581, 0.1486	0.0490, 0.1111	0.0384, 0.0942	0.0682, 0.1562	0.0673, 0.1870	0.0407, 0.1024
Largest diff. peak/hole (e·Å⁻³)	0.341, −0.252	0.610, −0.481	0.508, −0.216	0.294, −0.349	0.479, −0.538	0.454, −0.389	0.391, −0.318

[a] $R_1 = \Sigma||F_o| - |F_c||/\Sigma|F_o|$. [b] $wR_2 = [\Sigma w(F_o^2 - F_c^2)^2/\Sigma w(F_o^2)^2]^{1/2}$.

Table 3-4. Crystal data and structure refinement details for **HT1a**, **HT1b**, **HT2a**, **HT2b**, **HT3b**, **HD1a** and **HD1b**.

Chapter 4

Synthesis of cyclic and cage borosilicates

As we demonstrated earlier, due to the intrinsic features of the hydrogen bonding interactions between the molecular building blocks, that constitute a bulk material. It is possible to build long range ordered supramolecular networks that can be fully characterized using the SCXRD technique. This fact facilitates the control over the design, topology and ultimately over the functionality of the outcome material.

Notwithstanding, the wide range of practical applications of HOFs and MOFs, the development of more robust hybrid materials, formed linking molecular building blocks by stronger covalent bonds has also taken particular attention, especially for those applications that require high thermal stability.

However, the major drawback in the rational design of such covalent organic frameworks (COFs) is their poor crystallinity compared with their analogous HOFs and MOFs, which in turns complicate their structural characterization. Therefore, to overcome this characterization problem Yaghi *et al.* showed that using preconceived molecular clusters, as models and applying the reticular chemistry principles, it is possible to achieve the structural characterization of porous materials with a poor cystallinity. Thus, to assure an accurate prediction of the resultant structure under certain conditions, it is mandatory to have a deeper knowledge about the kinetic and thermodynamic aspects that determine the formation of certain morphologies in

the molecular clusters used as models.

In this realm, this chapter describes a facile synthesis of molecular borosilicates containing either eight-membered $B_2Si_2O_4$ rings, cage-like inorganic $B_4Si_4O_{10}$ cores or hitherto unknown six-membered B_2SiO_3 cycle, through the condensation reaction between the phenylboronic or 3-hydroxyphenylboronic acid derivatives with the corresponding monodiacetoxy- and monotri-acetoxysilylalkoxides **MDA5** and **MTA5**, respectively.

These molecules represent to the best of our knowledge the firsts examples of cyclic molecular borosilicates containing SiO_4 units. Finally, due to the competition observed in the formation of six- and eight-membered rings, theoretical calculations were carried out to determine the probable routes of synthesis for each ring as well as their thermochemistry. All compounds were obtained in high yields and were characterized by analytical methods and single crystal X-Ray diffraction. Finally, the thermal stability of all compounds was investigated by TG analysis.

4.1 Results and discussion

4.1.1 Synthesis and characterization

For this study, we proposed three starting ratios between the phenylboronic acid and diace-toxysilylalkoxide (t-BuO)(Ph$_3$CO)Si(OAc)$_2$ **MDA5** in order to obtain compounds with six-membered B_2SiO_3 (2:1) or BSi_2O_3 (1:2) rings. Besides, the ratio 1:1 was chosen for the synthesis of the eight-membered $B_2Si_2O_4$ ring containing species.

The reaction in a 2:1 ratio was carried out in anhydrous toluene and resulted in the formation of (t-BuO)(Ph$_3$CO)Si{(μ-O)BPh}$_2$(μ-O) (**BS1**) borosilicate with the desired cyclic six-membered B_2SiO_3 inorganic core (*vide infra*). This compound was isolated as a white solid, which is highly soluble in polar solvents [**Scheme** 4.1]. The progress of the reaction was monitored by a complete disappearance of the signals of the acetate ($\delta = 1.88$ ppm) and B–OH ($\delta = 7.99$ ppm, DMSO-d_6) groups of the starting materials in the ^{1}H NMR spectrum. The ^{1}H and ^{13}C NMR spectra of **BS1** contain peaks at $\delta = 1.40$, 31.6 and 75.2 ppm, respectively, belonging to the t-Bu moieties. Furthermore, the ^{11}B and ^{29}Si NMR spectra contain only one peak at $\delta = 28.9$ and –93.5 ppm, respectively, confirming the presence of the heteroatoms in the molecule

and purity of the compound [**Fig**. 4.1].
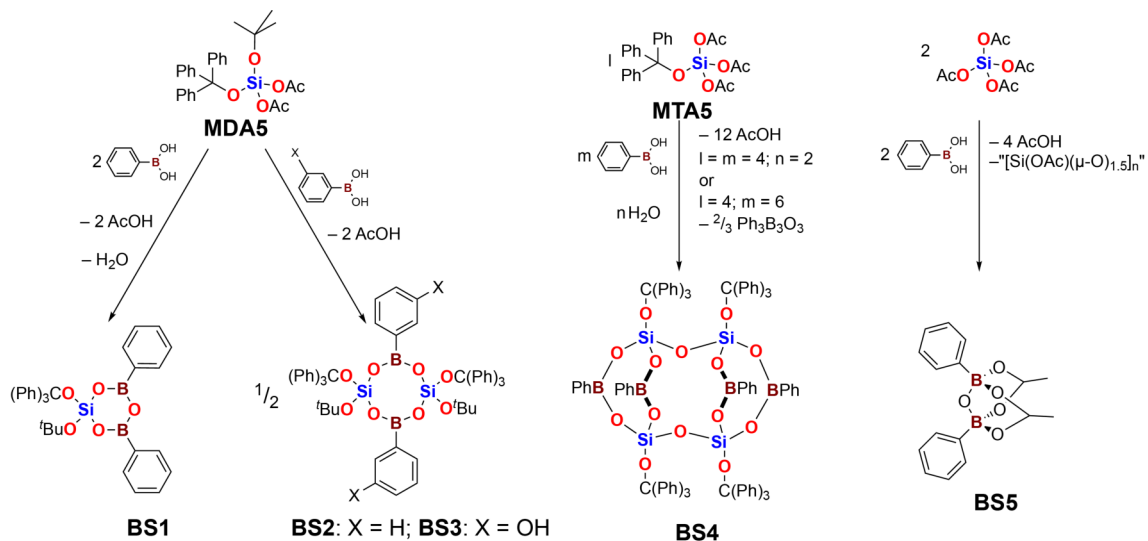
Scheme 4.1. Synthesis of compounds **BS1**–**BS5**.
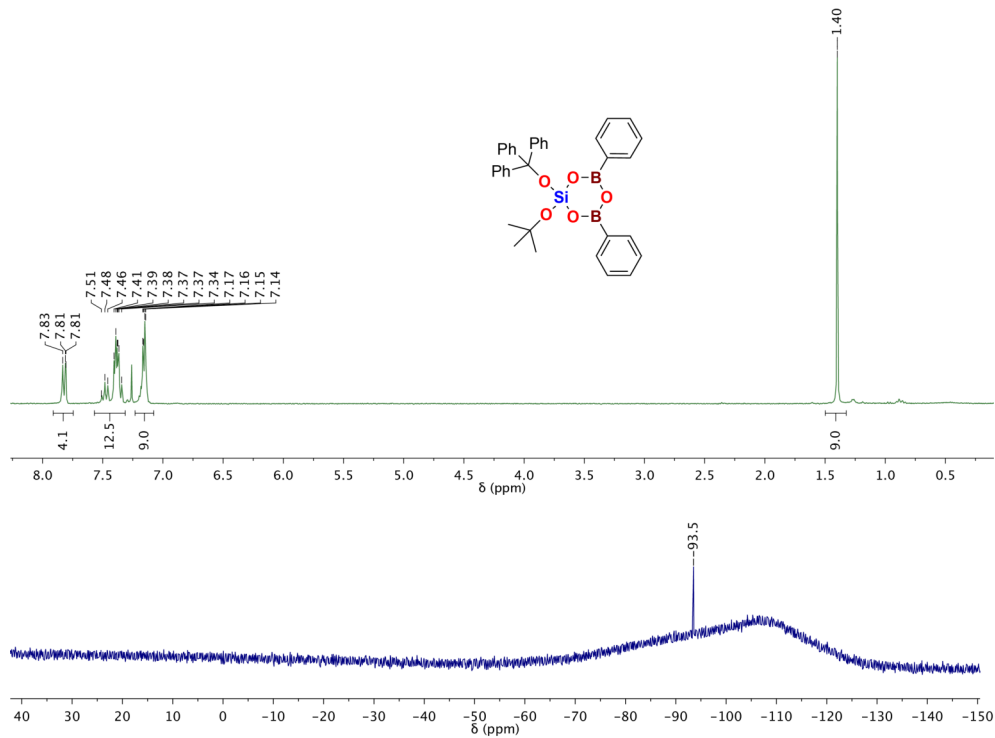
Figure 4.1. ^{1}H and ^{29}Si NMR spectra of **BS1**.

86

When the reaction ratio between **MDA5** and phenylboronic acid was changed to 1:1, another product was obtained as a highly crystalline white powder and was identified by X-Ray diffraction studies as [{(t-BuO)(Ph$_3$CO)Si(μ-O)BPh(μ-O)}$_2$] (**BS2**) with an eight-membered B$_2$Si$_2$O$_4$ ring. However, as revealed by ^{1}H, ^{13}C, and ^{29}Si NMR analysis, compound **BS2** is even after recrystallization contaminated by compound **BS1**, although repeated recrystallizations led to approximately 95% purity of **BS2** [**Fig**. 4.2].
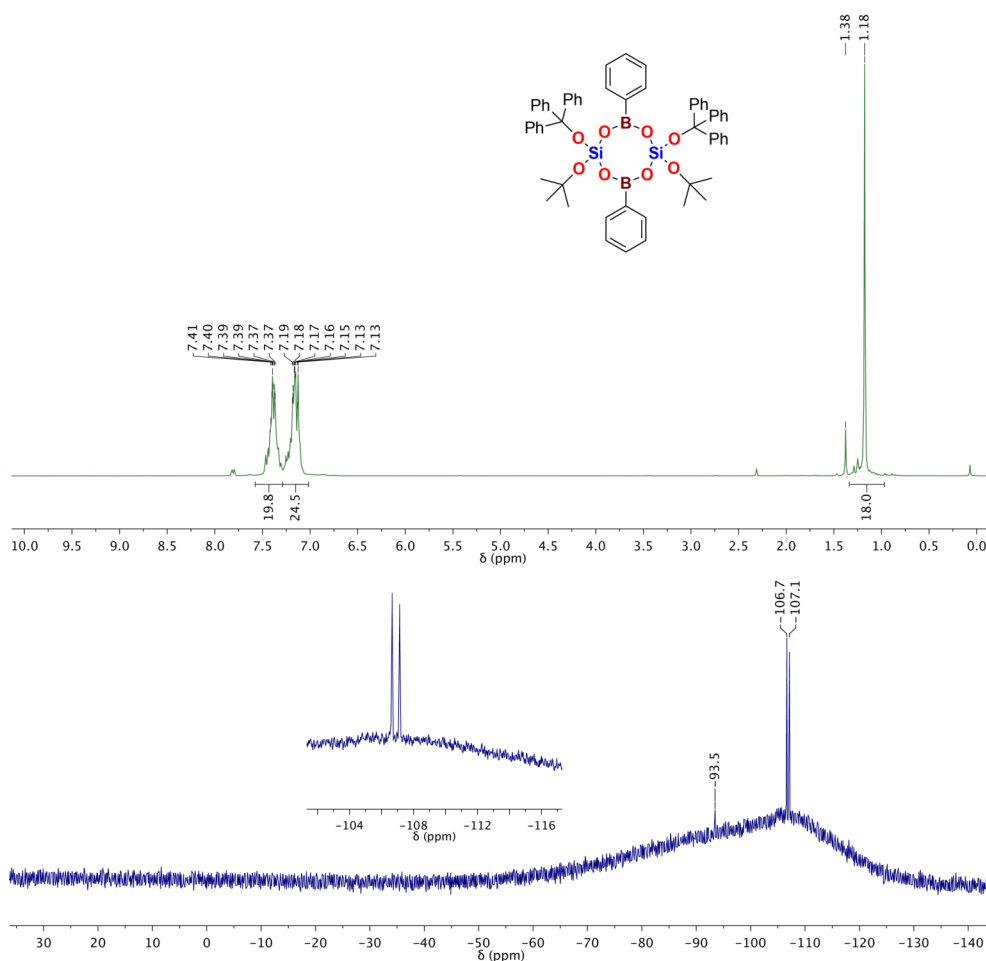
Figure 4.2. ^{1}H and ^{29}Si NMR spectra of **BS2** with residues of **BS1**.

Compared to **BS1**, the signal of the t-Bu group in **BS2** in the ^{1}H NMR spectrum exhibits an upfield shift to $\delta = 1.18$ ppm, while a 3 ppm difference was observed for the ^{11}B NMR chemical shifts of **BS1** and **BS2** (**BS1**: $\delta = 28.9$ ppm, **BS2**: $\delta = 26.1$ ppm). Surprisingly, the ^{29}Si NMR spectrum of **BS2** contains three signals. On the one hand, there are two signals with a 1:1

intensity at $\delta = -106.7$ and -107.1 ppm caused probably by the mutual orientation of the two different t-Bu groups present in the molecule with respect to the plane of the borosilicate ring. On the other hand, the third signal belongs to compound **BS1**. A more exhaustive study about the formation of compounds **BS1** and **BS2** with six- and eight-membered rings, respectively, is presented further ahead.

With the intent to incorporate functional groups to the borosilicate molecule, 3-hydroxyphenyl-boronic acid was used instead of PhB(OH)$_2$ in the reactions with **MDA5**. Independently of the reaction conditions or the ratio of the 3-hydroxyphenylboronic acid and **MDA5**, only the 1:1 product [{(t-BuO)(Ph$_3$CO)Si(μ-O)B(3-HOPh)(μ-O)}$_2$] (**BS3**) with the eight-membered B$_2$Si$_2$O$_4$ ring was obtained. The signals for the t-Bu group in ^{1}H and ^{13}C NMR spectra of **BS3** can be found at $\delta = 1.19$, 31.4 and 74.0 ppm, respectively, while the signal for the Ph–OH group in the ^{1}H NMR spectrum is at $\delta = 4.32$ ppm [**Fig**. 4.3].
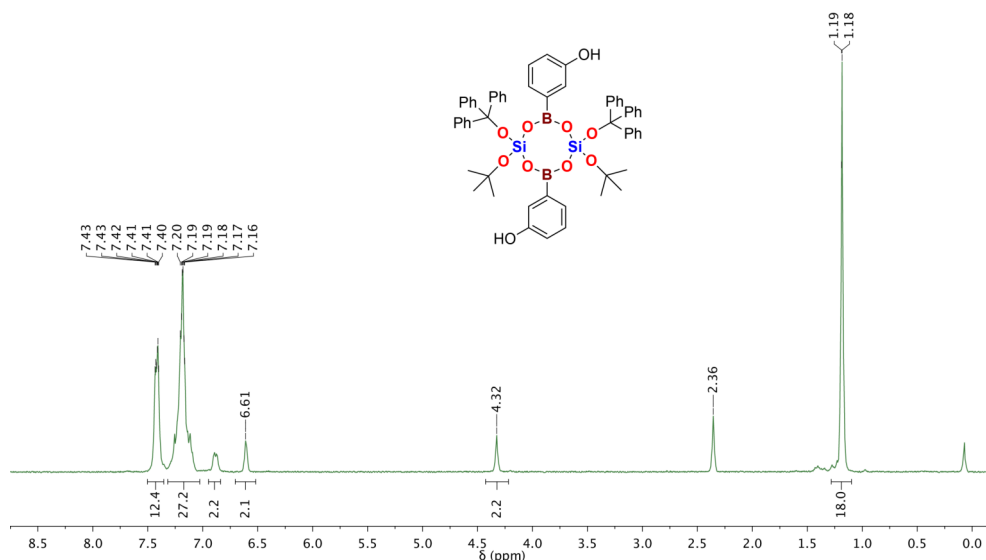
Figure 4.3. ^{1}H NMR spectrum of **BS3**.

Next, to investigate the effect of the number of the acetate groups on the resulting borosilicate core, we used the triacetate (Ph$_3$CO)Si(OAc)$_3$ **MTA5** instead of the diacetate **MDA5** in the reaction with phenylboronic acid in a 2:3 ratio to assess the formation of bicyclic RSi(O–BPh–O)$_3$SiR (R = Ph$_3$CO) species [**Fig**. 4.4]. However, the presence of three acetate groups per silicon atom resulted in a higher reactivity and in the formation of a cage-type borosilicate [{(Ph$_3$CO)Si(μ-O)BPh(μ-O)}$_2$(μ-O)]$_2$ (**BS4**) with an inorganic B$_4$Si$_4$O$_{10}$ core formed by

two $B_2Si_2O_4$ rings connected together by two Si–O–Si bridges, as determined by an X-Ray diffraction analysis (*vide infra*).
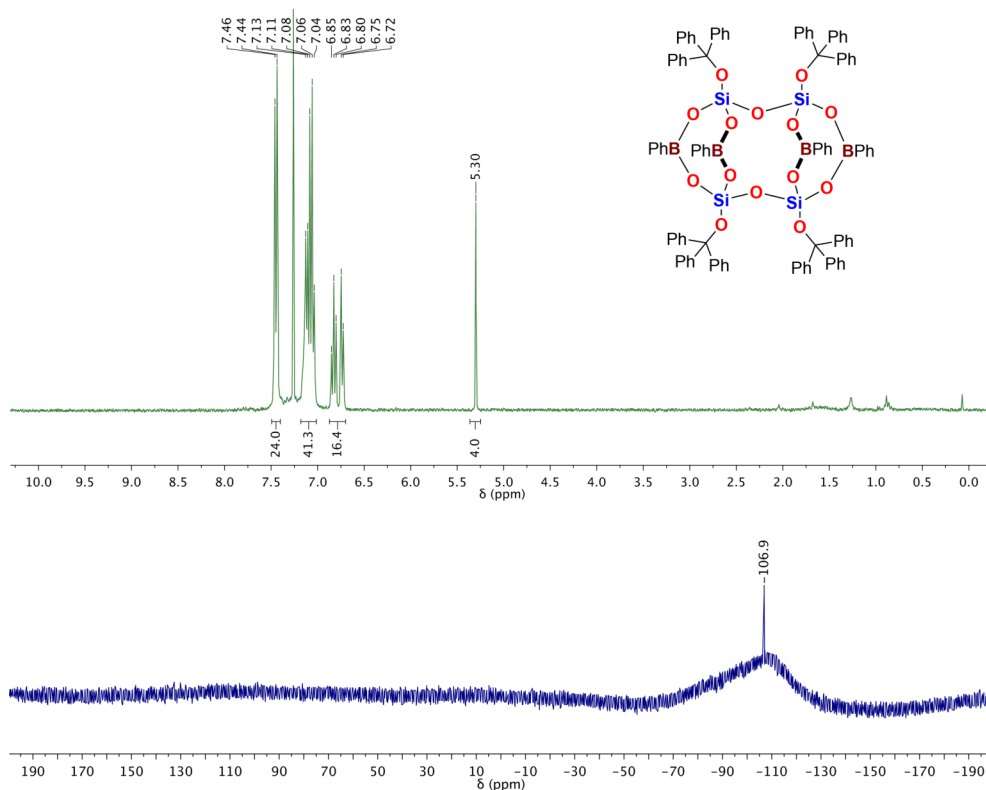
Figure 4.4. ^{1}H and ^{29}Si spectra of NMR of **BS4**.

Nevertheless, it is noteworthy that the formation of siloxane type Si–O–Si bonds requires the presence of water in the reaction media. Thus, we assume that this comes from the condensation of the extra equivalent of the phenylboronic acid to the corresponding boroxine; which was identified in the reaction media. Moreover, to prove this hypothesis we tested the synthesis of compound **BS4** using an adequate stoichiometry of the reactants 1:1:1 (PhB(OH)$_2$:**MTA5**:H$_2$O). Consequently, using these conditions, we also observed the formation of **BS4**, albeit in a low yield (45% instead of 83%). Thus, we conclude that the concentration of water in the reaction media plays an important role, and its generation through the slow condensation of boronic acid is preferred, as a higher amount of water leads to the hydrolysis of **MTA5**. The ^{11}B and ^{29}Si NMR spectra of **BS4** contain peaks at $\delta = 29.6$ and -106.9 ppm, respectively, pointing on only one coordination environment of both elements in the solution. The observed ^{11}B NMR

chemical shifts for compounds **BS1**, **BS2** and **BS4** are in the range for a trivalent boron atoms, while an upfield chemical shift ($\delta = $ –95.3 to –116.9 ppm) in the ^{29}Si NMR spectra was observed for the SiO$_4$ unit when compared with similar borosilicates reported in the literature ($\delta = $ –3.3 to –45.0 ppm) (*see Experimental section*).[143,144]

Finally, the reactivity of the boronic acid with silicon tetraacetate was explored, to assess the possibility to form products with higher dimensionality. However, the NMR studies revealed that the obtained compound contained at least one remaining acetate group (^{1}H NMR $\delta = $ 2.35 ppm), only one type of boron atoms (^{11}B NMR $\delta = $ 5.9 ppm) and suggested that no silicon atoms are present as no silicon signal was observed in the ^{29}Si NMR spectrum. This was confirmed by a single crystal X-Ray diffraction (*vide infra*), and the product was identified as 1,3-bis(acetate)-1,3-diphenyldiboraxane (μ-O)(PhB)$_2$(μ-O,O'-OAc)$_2$ (**BS5**).

Although several compounds with the RB(μ-O)(μ-O,O'-OAc)$_n$BR (n = 1, R = F, C$_6$F$_5$; n = 2, R = F, C$_6$F$_5$, C$_2$H$_5$, C$_8$H$_{15}$, OCOCH$_3$) unit are known, their synthesis requires predesigned compounds with B–O–B units and large quantities of acetic anhydride.[145–147] Furthermore, all such reactions proceed at high temperatures, and none starts from a boronic acid. These facts clearly show the advantages of the present synthetic route. In EI-MS spectra, the molecular ions were observed for all compounds (m/z = 584 (**BS1**), 945 (**BS2**), 992 (**BS3**) and 312 (**BS5**)) except for compound **BS4**, whose molecular mass (1693 g·mol^{-1}) is out of the range of our equipment (max. m/z 1090).

The FT-IR spectra of compounds **BS1**–**BS4** contain strong bands corresponding to the stretching vibrations of the Si–O and B–O bonds in the range of $\tilde{\nu}$ 1014–1074 and 1258–1311 cm^{-1}, respectively. Additionally, the progress of the reaction can be monitored by the absence of the characteristic C=O vibrations of the acetate group at $\tilde{\nu} \sim$ 1740 cm^{-1}, or of the OH groups of the boronic acid at $\tilde{\nu} \sim$ 3230 cm^{-1}.

4.1.2 X-ray diffraction structural analysis

The molecular structures of the borosilicates **BS1**, **BS2**, **BS4** and the 1,3-bis(acetyloxy)-1,3-diphenyldiboraxane **BS5** were determined by single crystal X-Ray diffraction experiments. In the case of **BS3** only very small and weakly diffracting crystals were obtained. Thus, although the measured data had sufficient quality to corroborate the connectivity of **BS3**, they were not

sufficient for full structure refinement. Consequently, only X-ray data based connectivity model for **BS3** is presented.

Compounds **BS1** and **BS5** were recrystallized from saturated hexane or THF solutions, respectively, and crystallize in orthorhombic $P2_12_12_1$ and $Pca2_1$ space groups with one molecule in the asymmetric unit. Slow recrystallization of compounds **BS2** and **BS4** from hexane or CH_2Cl_2/hexane mixture, respectively, yielded triclinic $P\bar{1}$ crystals with half a molecule of the compound in the asymmetric unit accompanied in the case of **BS4** by a dichloromethane molecule.

The molecular structure of **BS1** confirmed the formation of a B_2SiO_3 ring, where the silicon atom has a tetrahedral geometry, while the boron atoms have a trigonal planar environment. Two different Si–O bonds (Si–O_C and Si–O_B) have been observed. The av. Si–O_C bond length is 1.603(2) Å while the av. Si–O_B distance is slightly longer with a value of 1.640(2) Å . On the other hand, the B–O bond lengths are nearly identical with the average value of 1.374(3) Å. The B_1O_2–Si_1–O_3B_2, Si_1–O_2–B_1, Si_1–O_3–B_2 and B_1–O–B_2 angles have values of 104.6(1)°, 124.1(2)°, 124.0(2)° and 124.6(2)°, respectively, and are similar to the angles observed in related compounds with the six-membered BSi_2O_3 ring (105.3° to 129.4°).[144,148–150] The values for the O–B–O angles fall into a very narrow range of 119.1(2)° to 120.5(2)°. Although the silicon atom in the B_2SiO_3 ring in **BS1** has a tetrahedral geometry, the ring is nearly planar with a mean deviation of the atoms from the plane of 0.044 Å and the values of the internal Si–O–B–O torsion angles of –8.3(4)° and 13.2(3)°, respectively. Finally, the phenyl rings are involved in several C–H$\cdots\pi$ interactions and one is nearly coplanar with the B_2SiO_3 ring (dihedral angle 23.3°, centroid to centroid distance = 3.55 Å). It is also noteworthy that this is to the best of our knowledge the first example of such six-membered B_2SiO_3 ring.

The molecular structure of compound **BS2** corresponds to a centrosymmetric molecule with an eight-membered $B_2Si_2O_4$ ring located on an inversion center. The ring is formed by alternating SiO_4 and BO_2 units and is nearly planar with a mean deviation of the atoms from the plane of 0.034 Å. Due to the crystallographic symmetry, the t-BuO groups are in a *trans*-orientation to each other. The Si–O_C (1.608(1)–1.629(1) Å) and Si–O_B (1.602(1)–1.608(1) Å) bond lengths are very similar and are comparable to those reported for compounds with the same eight-membered $B_2Si_2O_4$ ring ([ArB(μ-O)Sit-Bu$_2$(μ-O)$_2$]$_2$ (Ar = Ph, p-BrC$_6$H$_4$, p-CHOC$_6$H$_4$,

3,4-ethylendioxythiophene), $[p\text{-BrC}_6\text{H}_4\text{B}(\mu\text{-O})\text{SiPh}_2(\mu\text{-O})_2]_2$, and $[\text{PhB}(\mu\text{-O})\text{SiFc}_2(\mu\text{-O})_2]_2$ (Fc = ferrocenyl) (Si–O_B; 1.626(1)–1.635(1) Å). It is noteworthy that the Si–O_B bonds in **BS2** are shorter than those observed in **BS1** (av. 1.640(2) Å). The presence of an additional SiO_4 unit diminishes the ring strain, as demonstrated by the increased values of the $\text{O}_3\text{–Si}_1\text{–O}_4$, $\text{Si}_1\text{–O}_3\text{–B}_1$, $\text{Si}_1\text{–O}_4\text{–B}_1$ and $\text{O}_3\text{–B}_1\text{–O}_4$ angles (110.3(0)°, 138.1(1)°, 167.5(1)° and 121.4(1)°) in the inorganic ring, when compared to those in **BS1**. In this case, the bridging oxygen atoms act as tension releasing elements. These values are comparable to those found in the literature for similar compounds with the $\text{B}_2\text{Si}_2\text{O}_4$ rings (O–Si–O, 111.2°–112.0°; Si–O–B, 149.0°–166.7°; O–B–O, 120.7°–123.4°) [**Fig**. 4.5].[148,150–154]
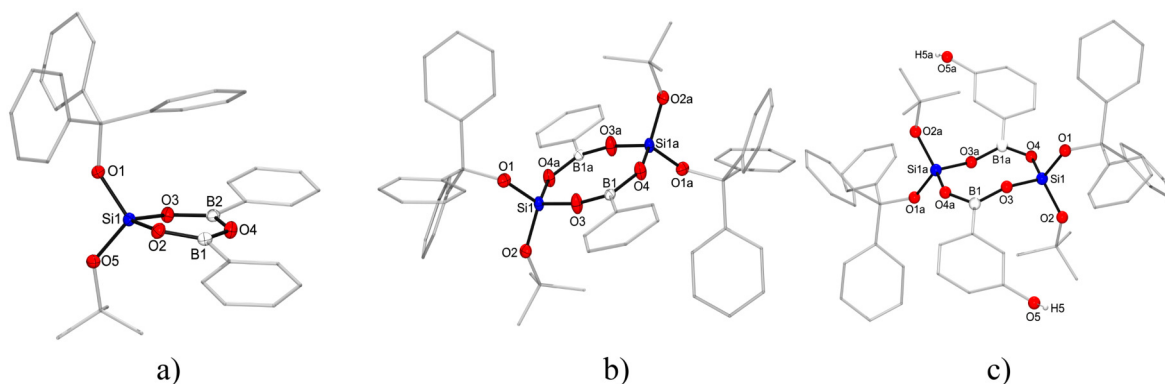
Figure 4.5. Perspective views of solid state structures of **BS1** (a), **BS2** (b) and the connectivity model of **BS3** (c) all of them with highlighted B_2SiO_3 and $\text{B}_2\text{Si}_2\text{O}_4$ core rings. The thermal ellipsoids in **BS1** and **BS2** are drawn at the 50 % probability level; carbon ellipsoids and carbon-bound hydrogen atoms were eliminated for the sake of clarity.

As mentioned earlier, compound **BS4** contains a centrosymmetric cage-like $\text{B}_4\text{Si}_4\text{O}_{10}$ inorganic core, composed of two $\text{B}_2\text{Si}_2\text{O}_4$ rings connected via two Si–O–Si bridges. To the best of our knowledge, only two compounds with such a core have been reported: $(t\text{-BuSi})_4(\text{ArB})_4\text{O}_{10}$ (Ar = $\text{CH}_2=\text{CHC}_6\text{H}_4$, BrC_6H_4) [**Fig**. 4.6].[155]

Although **BS4** contains three different Si–O bond types (Si–O_C, Si–O_{Si} and Si–O_B) their average bond lengths around the two crystallographically independent silicon atoms (Si1 y Si2) are in the range from 1.598(1) to 1.623(1) Å and are comparable to values previously reported for $\text{B}_4\text{Si}_4\text{O}_{10}$ systems (1.60–1.63 Å).[155,156]

The average values for the internal O–Si–O_B, $\text{Si}_1\text{–O–B}$, $\text{Si}_2\text{–O–B}$ and O–B–O_{Si} angles within the eight-membered ring are 111.5(1)°, 132.9(1)°, 149.7(1)°, 121.7(1)°, respectively, and are

similar to those in **BS2**. The Si–O–Si angle is with $167.1(1)°$ very close to the ideal value for an *sp* hybridization $(180°)$ and is most probably caused by the steric bulk around the silicon atoms. It is more obtuse than Si–O–Si angles in $(t\text{-BuSi})_4(\text{ArB})_4\text{O}_{10}$ (Ar $=$ $\text{CH}_2{=}\text{CHC}_6\text{H}_4$, $(154.1(1)°$; Ar $=$ BrC_6H_4; $147.5(2)°),^{155}$ that have smaller steric protection around the silicon atom.
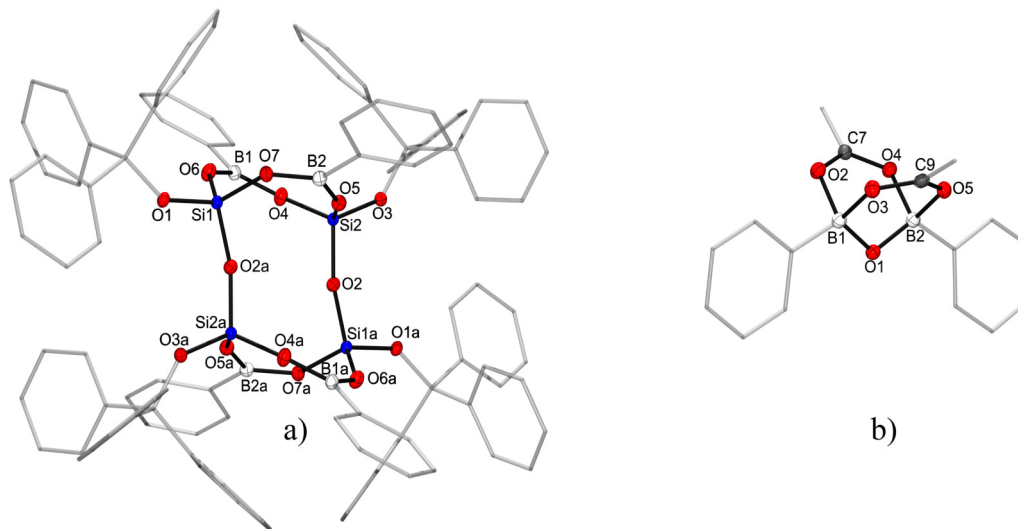
Figure 4.6. Perspective views of solid state structures of **BS4** (a) and **BS5** (b). The thermal ellipsoids are drawn at the 50 % probability level; carbon ellipsoids and carbon-bound hydrogen atoms were eliminated for the sake of clarity.

Compound **BS5**, has a bicyclic core with a B–O–B unit and tetracoordinated boron atoms with B–OB bond length of $1.402(2)$ Å and B–O–B angle of $111.7(2)°$. The acetate groups are bridging the B–O–B unit in an O,O'-isobidentate mode with average B–O_C bond lengths of $1.569(2)$ Å [**Fig**. 4.6].

The geometry around the boron atoms can be best described as distorted tetrahedral with angles between $101.1(1)°$ and $118.6(1)°$. The C–O bond lengths in the acetate units are identical within the esd's $(1.269(2)\text{--}1.275(2)$ Å) pointing to a complete delocalization of the electron density over the O–C–O unit. These parameters are similar to those observed for other systems with the RB(μ-O)(μ-O,O'-OOCCH$_3$)$_2$BR core where the values for the B–O_B, B–O_C bonds and B–O–B angle are in range of $1.38\text{--}1.40$ Å, $1.53\text{--}1.58$ Å and $108.1°\text{--}113.3°$, respectively.[145]

However, these values are different from those found in systems where only one acetate group is bridging the two boron atoms of the B–O–B unit as the values for the B–O, B–

O$_C$ bonds and B–O–B angle are in the range of 1.49–1.52 Å, 1.48–1.62 Å and 118.4°–128.9°, respectively.[146,147]Selected bond lengths and angles for compounds **BS1**–**BS4** are listed in **Table 4-1**.

	Bond lengths				Bond angles		
	BS1	**BS2**	**BS4**		**BS1**	**BS2**	**BS4**
Si–O$_C$	1.601(2)	1.602(1)	1.599(1)	$_CO$–Si–O$_C$	103.3(1)	109.6(0)	–
	1.606(2)	1.608(1)	1.602(1)	$_CO$–Si–O$_B$	112.2(1)	110.6(1)	110.5(1)
Si–O$_B$	1.640(2)	1.609(1)	1.601(1)		111.7(1)	104.0(0)	111.2(1)
	1.641(2)	1.629(1)	1.604(1)		113.2(1)	110.9(0)	109.7(1)
	–	–	1.611(1)		112.1(1)	111.2(1)	112.7(1)
	–	–	1.613(1)	$_BO$–Si–O$_B$	104.6(1)	110.3(0)	112.6(1)
B–O$_{Si}$	1.373(3)	1.345(1)	1.363(2)		–	–	110.4(1)
	1.372(3)	1.359(1)	1.362(2)	$_{Si}O$–B–O$_{Si}$	–	121.4(1)	121.6(1)
			1.365(2)		–	–	121.7(1)
	–	–	1.365(2)	B–O–B	124.6(2)	–	–
B–C	1.558(4)	1.594(5)	1.557(3)	Si–O–B	124.1(2)	167.5(1)	148.7(1)
	1.560(4)	–	1.554(3)		124.0(2)	138.1(1)	150.7(1)
Si–O$_{Si}$	–	–	1.588(2)		–	–	134.9(1)
B–O$_B$	1.377(3)	–	–		–	–	131.0(1)
	1.377(3)			Si–O–Si	–	–	167.0(1)

Table 4-1. Selected bond distances (Å), angles (°) for the compounds **BS1**, **BS2** and **BS4**.

4.1.3 Study of the formation of borosilicates BS1 and BS2 in solution

The fact that compound **BS2** is always contaminated by compound **BS1**, and the fact that from a thermodynamic standpoint, the eight-membered B$_2$Si$_2$O$_4$ ring is the most stable structure in borosilicates,[149] prompted us to follow the synthesis of compound **BS2** via periodic ^{1}H NMR measurements in toluene-d_8 [**Fig**. 4.7].

Surprisingly, this NMR study revealed, that compound **BS1** is formed immediately after adding the deuterated solvent to the mixture of **MDA5** and the phenylboronic acid, and that the compound **BS2** appears only after 30 minutes. Furthermore, when **BS2** starts to form, the quantity of **BS1** diminishes suggesting a transformation of **BS1** to **BS2**. However, after three hours, the proportion between **BS1** and **BS2** remains almost constant. Finally, after 24 hours, nearly all **MDA5** is consumed.
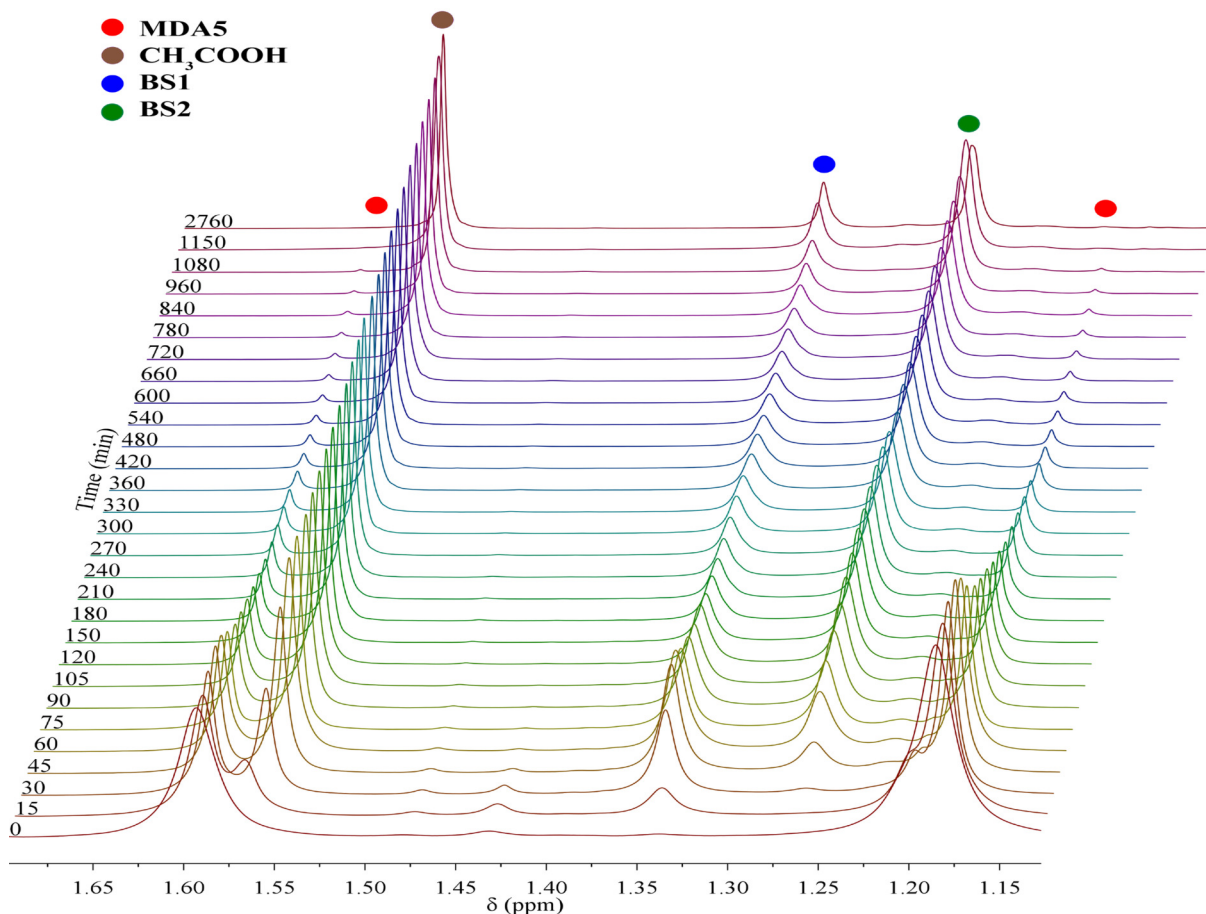
Figure 4.7. 300 MHz ^{1}H NMR spectra (toluene-d_8) showing the equimolar reaction between phenylboronic acid and diacetoxysilylalkoxide **MDA5**.

This is consistent with the isolation of a mixture of **BS1** and **BS2** from a 1:1 reaction (**MDA5**:phenylboronic acid) in toluene. To explain the transformation of **BS1** to **BS2**, we explored the stability of compound **BS1** in solution, but no changes were observed even after one week in a dry solvent excluding redistribution. Nonetheless, when **BS1** was mixed with (t-BuO)(Ph$_3$CO)Si(OH)$_2$ to encourage the splitting of the B–O–B unit in **BS1**, it was observed that approximately 80% of **BS1** was converted to **BS2** after 12 hours.

On the other hand, compound **BS**1 does not react with **MDA5**, therefore, this suggests that for the conversion of **BS1** to **BS2** the presence of a protic reagent is necessary. However, the addition of one equivalent of water into the equimolar reaction of the phenylboronic acid with **MDA5**, led to decomposition of **MDA5** to polysilicate derivatives and only small amount of **BS1** was formed while compound **BS2** was absent.

Independently, water is being generated in the reaction mixture in the condensation of the phenylboronic acid necessary to form the B–O–B unit present in **BS1**. This water molecule most probably reacts with **MDA5** to form the $(t\text{-BuO})(Ph_3CO)Si(OH)(OAc)$ intermediate. This is corroborated by the presence of a weak signal at ($\delta = 1.21$ ppm, visible between the 15th and 45th minute of the reaction) that is in-between the values for the parent compound **MDA5** $(t\text{-BuO})(Ph_3CO)Si(OAc)_2$ ($\delta = 1.19$ ppm) and the fully hydrolyzed silanodiol **D5** $(t\text{-BuO})(Ph_3CO)Si(OH)_2$ ($\delta = 1.23$ ppm) (*see Chapter 1*). However, this compound is consumed during the first hour of the reaction and is not detectable again later in the reaction mixture.

It is thus possible that its higher initial concentration is caused by traces of water originated from the recrystallization of the phenylboronic acid.

4.1.4   DFT calculations: Reaction mechanism

To shed more light on the reaction mechanism and the formed intermediates and to be able to explain why in the case of the 3-hydroxyphenylboronic acid, no compound homologous to **BS1** is observed, theoretical calculations were performed.

The thermochemistry of several reaction paths was investigated [**Fig**. 4.8]. The most logical step would be the condensation of **MDA5** with the phenylboronic acid to afford the formation of $(t\text{-BuO})(Ph_3CO)(AcO)\ Si(\mu\text{-O})BPh(OH)$ (**D**). However, the very low solubility of the boronic acid in toluene speaks against this reaction pathway, as the transformation of **D** into **BS1** would have to proceed via the $(t\text{-BuO})(Ph_3CO)Si(OBPhOH)_2$ (**C**) intermediate that would cyclize to **BS1**. Nonetheless, the dehydration of **C** to **BS1** is slightly endergonic ($+4.49$ kcal·mol^{-1}) and additionally the formation of **C** from **D** is highly unlikely because the high concentration of **MDA5** in the reaction media (and low solubility of the phenylboronic acid in toluene) would convert **D** to $PhB((\mu\text{-O})Si(OCPh_3)(Ot\text{-Bu})(OAc)_2$ (**E**) and **E** cannot be converted to **BS1**. Therefore, to obtain **BS1**, the B–O–B unit must be formed first. Taking into account that while the boronic acid is virtually insoluble in toluene, the corresponding trimeric anhydride $(PhBO)_3$ (**A**) is highly soluble in this solvent, therefore the solubility of the partial anhydride $(\mu\text{-O})(BPhOH)_2$ (**B**) should be higher than that of the boronic acid. Also, such condensation of phenylboronic acid is known to take place in solution, and the formation of **B** is slightly exergonic (-4.21 kcal·mol^{-1}).
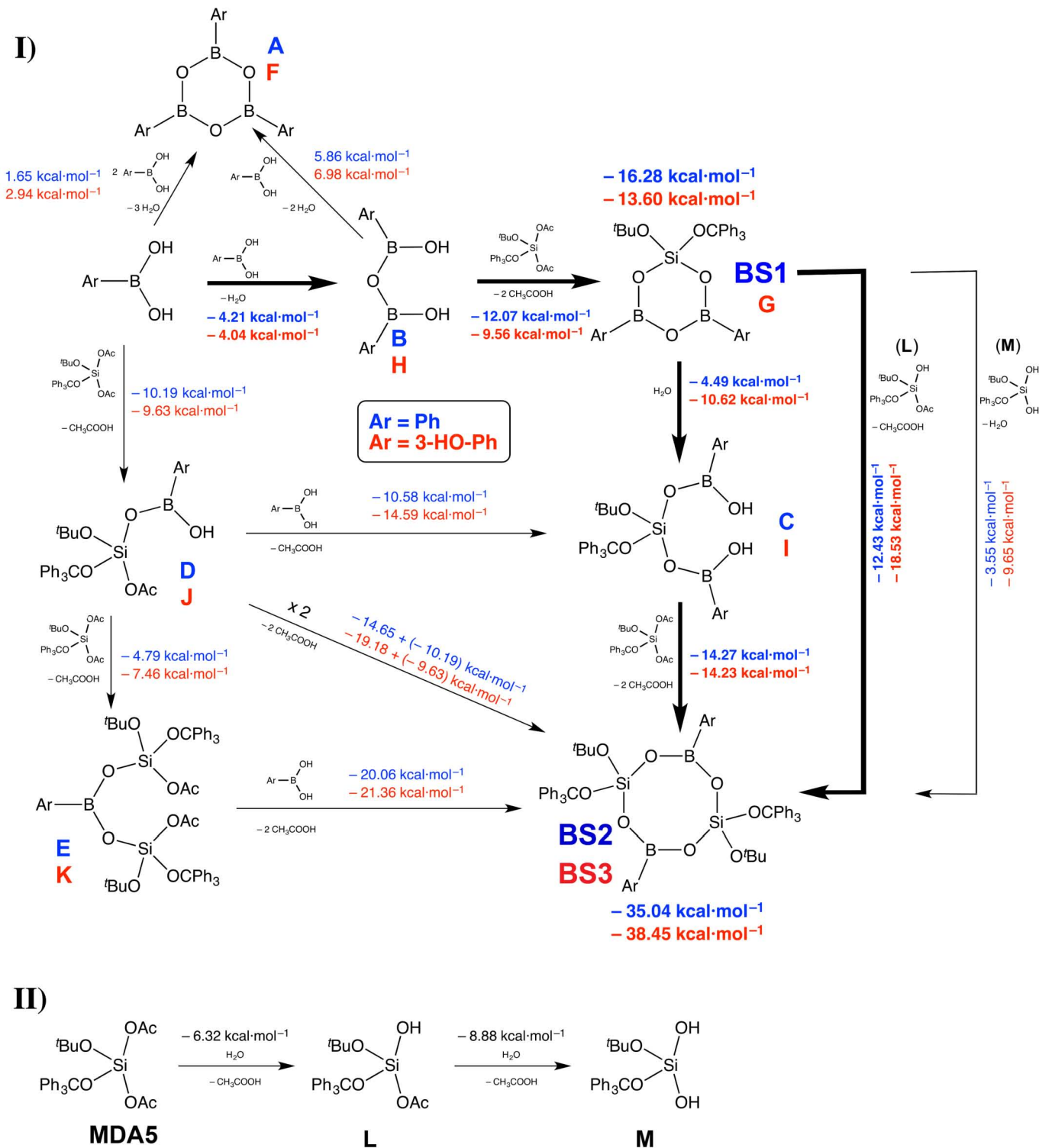
Figure 4.8. Possible reaction routes in the formation of **BS1**–**BS3** (I) and the stepwise hydrolysis of **MDA5** to the corresponding silanediol (II) with the free energies of formation. Blue text corresponds to derivatives based on phenylboronic acid, while red labels belong to species with 3-hydroxyphenylboronic acid.

97

Thus, we hypothesize, that this partial condensation to form **B** is the first step in the formation of **BS1**. This intermediate would react with a molecule of **MDA5** upon the elimination of two molecules of acetic acid resulting in the cyclic structure of **BS1**. **B** cannot be isolated, but the formation of the B–O–B unit is further supported by the formation of **BS5** in the reaction between the phenylboronic acid and silicon tetraacetate. It is noteworthy, that **BS5** was not observed in the reaction mixture at any time. Furthermore, compound **BS1** can react with the water molecule generated during the formation of **B** causing ring opening and formation of **C** (-4.49 kcal·mol^{-1}). Such hydrolysis of B–O–B units have been reported earlier.[157,158]

Due to the low steric bulk around the OH groups in **C** and their *syn* orientation, a reaction with **MDA5** would close the eight-membered ring in **BS2**. As mentioned earlier, **BS1** can be transformed in **BS2** in a reaction with (t-BuO)(Ph$_3$CO)Si(OH)$_2$, and from the thermodynamic point of view, the reaction between **BS1** and (t-BuO)(Ph$_3$CO)Si(OH)(OAc) (**L**, that was identified in the reaction mixture) would also lead to **BS2** and thus constitutes an alternative route from **BS1** to **BS2**.

Thus, we believe that initially, two equivalents of phenylboronic acid condense to form **B**, which reacts with an equivalent of **MDA5** giving **BS1**. In the presence of water, **BS1** transforms to **C** that is converted by another equivalent of **MDA5** to the thermodynamically more stable **BS2** or **BS1** reacts with (t-BuO)(Ph$_3$CO)Si(OH)(OAc) (formed from **MDA5** and water) to form directly **BS2** and acetic acid. The free energy of formation of **BS2** is more than twice that of **BS1** (-35.04 vs. -16.28 kcal·mol^{-1}).

This reaction pathway can also be used to explain why in the case of 3-hydroxyphenylboronic acid only compound **BS3** with the eight-membered ring is formed. First, the solubility of the 3-hydroxyphenylboronic acid is even lower than that of the phenylboronic acid, and even though the free energy of formation of compound **G** is only 2.6 kcal·mol^{-1} lower than that of **BS1**, the reaction of **G** with water is quite exergonic (-10.62 kcal·mol^{-1}). That is more than twice that for the analogous reaction of **BS1** (-4.49 kcal·mol^{-1}).

The same situation is valid also for the reaction of (t-BuO)(Ph$_3$CO)Si(OH)(OAc) with **BS1** (-12.43 kcal·mol^{-1}) or **G** (-18.53 kcal·mol^{-1}), respectively. This difference can be attributed to the electronic effects of the OH group in the meta position to the boron atom as it increases the acidity of the B(OH)$_2$ protons and thus decreases the stability of the B–O–B bridge towards

hydrolysis. Therefore, the compounds **BS1** and **G** are the kinetic products, while **BS2** and **BS3** are the thermodynamic species. Finally, this also explains why compounds with the six-membered B_2SiO_3 ring have not been observed in reactions between boronic acids and silanols, as these usually proceed under reflux and large quantities of water and silanols are present. [143,144,150]

4.1.5 Thermal stability

The thermogravimetric analysis of compounds **BS1**–**BS5** under a nitrogen atmosphere revealed that all compounds are stable up to 200 °C, but a partial mass loss of 5.7% and 8.4% respectively, was observed for compounds **BS3** and **BS4** at approximately 100 °C and is attributed to the loss of lattice solvent. Their presence was confirmed by ^1H and ^{13}C NMR spectra and by X-Ray crystallography (*vide supra*) [**Fig**. 4.9].

The highest thermal stability was observed for compound **BS4** as it presents a weight loss of 48.7% at 310 °C. Furthermore, compound **BS2** with $B_2Si_2O_4$ borosilicate ring decomposes at 275 °C, that is slightly higher than the decomposition temperature observed for compound **BS1** with the six-membered B_2SiO_3 ring (250 °C).

Interestingly, compound **BS3**, which differs from compound **BS2** only by the presence of a 3-OH group on the phenyl ring of the boronic acid, decomposes readily at 200 °C. Finally, compound **BS5** presents one stage decomposition (87.3% weight loss) above 300 °C leaving a B_2O residue. [159] In compounds **BS1**–**BS4**, the weight loss corresponds to a partial or total elimination of organic groups attached to silicon leaving PhB_2O_3Si (% calc = 29.8; % found = 32.3) for **BS1**, $(PhBSiO_2)_2$ (% calc = 30.5; % found = 28.7) for **BS2**, $[(C_6H_4OH)BSiO_2]_2OC(Ph)_3$, (% calc = 45.7; % found = 48.8) for **BS3**, and $(PhBSiO_3)_4O_2$ (% calc = 37.2; % found = 42.9) for **BS4**; respectively.
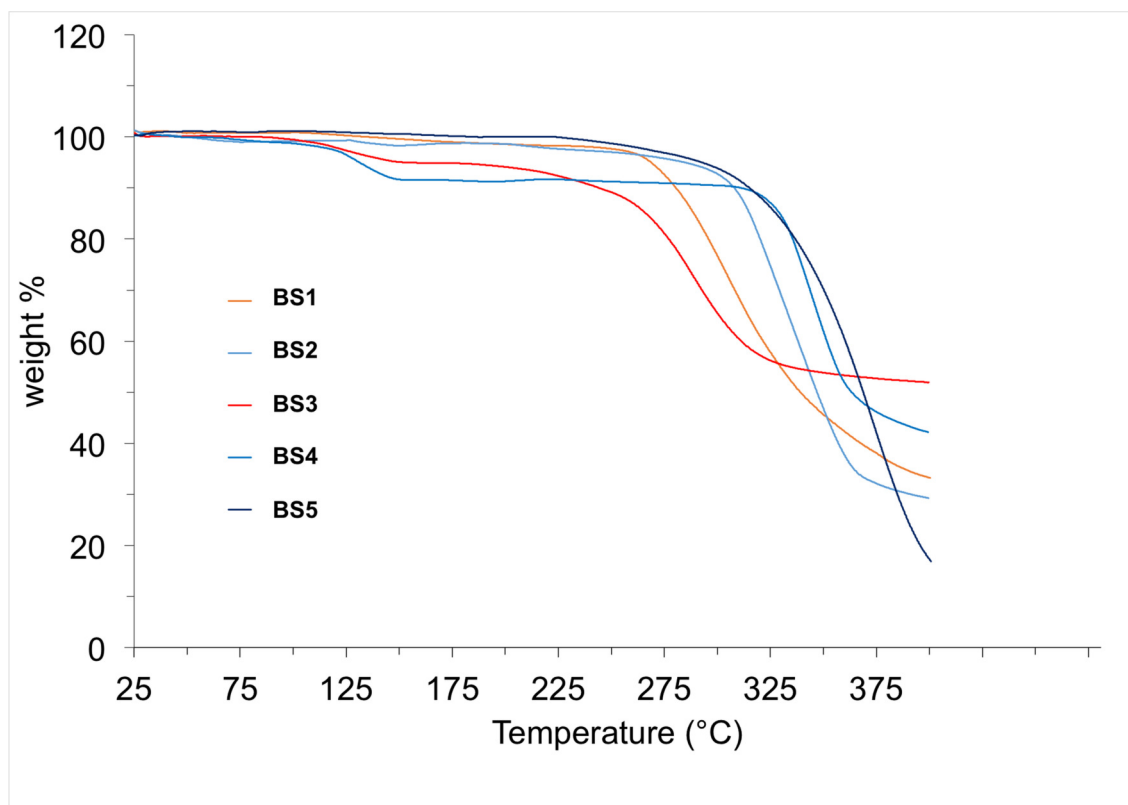
Figure 4.9. TGA trace for compounds **BS1**–**BS5**.

4.2 Conclusions

An easy method for the synthesis of cyclic borosilicate compounds with different ring size under mild conditions is presented. The method starts form substituted silicon acetates and organoboronic acids and allows for an easy modulation of the final inorganic core.

The major advantage of the method is the large diversity of possible silicate precursors eliminating the main restriction of current synthetic methods, which is the very limited availability of silanol precursors stable at high temperatures. In this case, the silicon acetates are easily synthesized from silicon tetraacetate and alcohols, and this reaction pathway allows for a straightforward modification of the properties of the silicate precursor. Moreover, this study enriches the morphological variety of borosilicate-based molecular clusters applied as models in the structural characterization of covalent-bonded extended networks.

Furthermore, although the vast majority of chemical reactions are done in borosilicate glass-

ware, compounds **BS1**–**BS4** are the first structurally characterized examples of molecular compounds with borosilicate rings containing SiO_4 units.

4.3 Experimental section

4.3.1 General methods

NMR spectroscopic data were recorded on a Bruker Avance III 300 MHz and Varian NMR Systems 500 MHz spectrometers and referenced to residual signals of the deuterated solvent for ^{1}H and ^{13}C nuclei, or TMS and $F_3B \cdot OEt_2$, respectively, as external standards for the ^{29}Si and ^{11}B spectra. Electron impact mass spectrometry (EI-MS) were carried on a Shimadzu GCMS-QP2010 Plus using direct injection in the detection range 20–1090 m/z. FT-IR spectra were recorded on a Bruker ALPHA FTIR spectrometer placed inside a glove-box using the ATR technique with a diamond window in the range of $\tilde{\nu}$ 500–4000 cm^{-1}. Melting points were measured in sealed capillaries on Büchi B-540 melting point apparatus. Elemental analyses (C, H, N) were determined on an Elementar MicroVario Cube analyzer. For all compounds, the experimental value for carbon content was lower than calculated, which is common in compounds with boron and silicon due to the formation of silicon and boron carbides difficult to pyrolyze.

4.3.2 Synthesis of borosilicates

(*t*-BuO)(Ph₃CO)Si{(μ-O)BPh}₂(μ-O) (BS1): In a Schlenk flask, diacetyloxysilylalkoxide **MDA5** (0.20 g, 0.42 mmol) and phenylboronic acid (0.10 g, 0.83 mmol) (1:2 ratio) were dissolved in toluene (20 mL) and stirred overnight. Afterwards, all volatiles were removed under reduced pressure. Crystals of compound **BS1** were grown by a slow evaporation (1 week) of saturated hexane solution at room temperature. **Yield**: 0.18 g, 0.31 mmol, 75%. **M.p.** 143–144 °C. **Elemental analysis** (%) Calcd for $C_{35}H_{34}B_2O_5Si$ (584.35 g·mol^{-1}): C 71.94, H 5.86; Found: C 68.71, H 5.88. **FT-IR (ATR) (cm^{-1})** $\tilde{\nu}$ 2963 (w, CH₃), 1259 (s, B–O), 1017 (s, Si–O). **^{1}H NMR** (300.53 MHz, CDCl₃): δ (ppm) 1.40 (s, 9H, CC*H₃*), 7.15–7.83 (m, 25H, C*H* of Ph). **^{13}C{^{1}H} NMR** (75.57 MHz, CDCl₃): δ (ppm) 31.6 (C*C*H₃), 75.2 (*C*CH₃), 86.7 (*C*Ph₃), 127.4, 127.7, 127.9, 128.6, 131.8, 135.4, 145.7 (p, m, o, i, *C* of Ar, the signal for the ipso carbon

bound to the boron atom was not observed). **^{29}Si NMR** (59.63 MHz, CDCl$_3$): δ (ppm) –93.5. **^{11}B NMR** (96.25 MHz, CDCl$_3$): δ (ppm) 28.9. **EI-MS**: m/z (%) 584 (25) [M]$^+$.

{(t-BuO)(Ph$_3$CO)Si(μ-O)BPh(μ-O)}$_2$ (BS2): In a Schlenk flask, diacetyloxysilylalkoxide **MDA5** (0.20 g, 0.42 mmol) and phenylboronic acid (0.05 g, 0.42 mmol) (1:1 ratio) were dissolved in toluene (20 mL) and stirred overnight. Then, all the volatiles were removed under reduced pressure. Crystals of compound **BS2** were grown by slow evaporation form hexane at room temperature. **Yield**: 75% of aprox. 70% purity (0.15 g, 0.15 mmol). Repeated recrystallizations from hexane led to a 95% pure sample. **M.p.** 187–189 °C. Due to the contamination by aprox. 5% of compound **BS1**, the elemental analysis was not performed. **FT-IR (ATR) (cm^{-1})** $\tilde{\nu}$ 2962 (w, CH$_3$), 1259 (s, B–O), 1014 (s, Si–O). The following NMR data contain only signals for compound **BS2**. All signals for **BS1** are omitted. **^{1}H NMR** (300.53 MHz, CDCl$_3$): δ (ppm) 1.18 (s, 18H, CCH_3), 7.13–7.41 (m, 40H, CH of Ph). **^{29}Si NMR** (59.63 MHz, CDCl$_3$): δ (ppm) –106.7, 107.1 **^{11}B NMR** (96.25 MHz, CDCl$_3$): δ (ppm) 26.1. **EI-MS**: m/z (%) 945 (4) [M–Me]$^+$.

{(t-BuO)(Ph$_3$CO)Si(μ-O)B(3-HOPh)(μ-O)}$_2$ (BS3): Compound **BS3** was obtained following the methodology described for compound **BS2**, using 3-hydroxyphenylboronic acid (0.056 g; 0.42 mmol) instead of phenylboronic acid. **Yield**: 1.49 g, 0.15 mmol, 72%. **M.p.** 208–210 °C. **Elemental analysis** (%) Calcd for C$_{58}$H$_{58}$B$_2$O$_{10}$Si$_2$ (992.87 g·mol^{-1}): C 70.16, H 5.89; Found: C 68.11, H 5.89. **FT-IR (ATR) (cm^{-1})** $\tilde{\nu}$ 3352 (w, O–H), 2973 (w, CH$_3$), 1311 (s, B–O), 1074 (s, Si–O). **^{1}H NMR** (300.53 MHz, CDCl$_3$): δ (ppm) 1.19 (s, 18H, CCH_3), 4.32 (s, 2H, OH), 6.61–7.83 (m, 38H, CH of Ph). **^{13}C{^{1}H} NMR** (75.57 MHz, CDCl$_3$): δ (ppm) 31.4 (CCH$_3$), 74.0 (CCH$_3$), 86.1 (CPh$_3$), 118.0, 121.8, 125.3, 126.8, 127.6, 128.2, 128.6, 129.0, 146.2, 154.6 (p, m, o, i, C of Ar).

[{(Ph$_3$CO)Si(μ-O)BPh(μ-O)}$_2$(μ-O)]$_2$ (BS4): **Method A**: In a Schlenk flask, triacetyloxysilylalkoxide **MTA5** (0.50 g, 1.10 mmol) and phenylboronic acid (0.20 g, 1.61 mmol) (2:3 stoichiometric ratio) were dissolved in toluene (20 mL) and stirred overnight. Then, all the volatiles were removed under reduced pressure and the remaining solid was washed with hexane to give white solid. Crystals of **BS4** were grown using a mixture of dichloromethane/hexane 1:1 at room temperature. **Yield**: 0.37 g, 0.22 mmol, 83%. **Method B**: In a Schlenk flask, triacetyloxysilylalkoxide **MTA5** (0.30 g, 0.646 mmol) and phenylboronic acid (0.08 g, 0.646

mmol) (1:1 stoichiometric ratio) were dissolved in toluene (20 mL), the reaction mixture was stirred for 2 h. Afterwards one equivalent of water was added (0.01 g, 0.646 mmol) and stirred overnigh. Then, all the volatiles were removed under reduced pressure and the remaining solid was washed with hexane to give white solid. **Yield**: 0.12 g, 0.073 mmol, 43%. **M.p.** 270–272 °C. **Elemental analysis** (%) Calcd for $C_{100}H_{80}B_4O_{14}Si_4 \cdot 2CH_2Cl_2$ (1831.09 g·mol^{-1}): C 66.90, H 4.62; Found: C 66.68, H 4.71. **FT-IR (ATR) (cm^{-1})** $\tilde{\nu}$ 2962 (w, CH$_3$), 1304 (s, B–O), 1068 (s, Si–O). **^{1}H NMR** (300.53 MHz, CDCl$_3$): δ (ppm) 6.72–7.46 (m, 38H, CH of Ph). **^{13}C{^{1}H} NMR** (75.57 MHz, CDCl$_3$): δ (ppm) 86.3 (CPh$_3$), 126.8, 127.1, 127.9, 128.5, 130.9, 135.8, 145.8 (p, m, o, i, C of Ar, the signal for the ipso carbon bound to boron was not observed). **^{29}Si NMR** (59.63 MHz, CDCl$_3$): δ (ppm) –106.9 **^{11}B NMR** (96.25 MHz, CDCl$_3$): δ (ppm) 29.6.

$(\mu\text{-O})(\text{PhB})_2(\mu\text{-O,O'-OAc})_2$ **(BS5)**: In a Schlenk flask, silicon tetraacetate (1.00 g, 3.78 mmol) and phenylboronic acid (0.46 g, 3.77 mmol) were suspended in toluene (20 mL) and the mixture was stirred overnight. All the volatiles were removed under reduced pressure and the remaining solid was washed with hexane to remove the oily silicon subproducts. Compound **BS5** was isolated as a white solid. Crystals were grown from a saturated solution in THF at –36 °C. **Yield**: 0.47 g, 1.51 mmol, 80%. **M.p.** > 220 °C (dec). **Elemental analysis** (%) Calcd for $C_{16}H_{16}B_2O_5$ (309.92 g·mol^{-1}): C 62.01, H 5.20; Found: C 58.82, H 5.04. **FT-IR (ATR) (cm^{-1})** $\tilde{\nu}$ 2962 (w, CH$_3$), 1258 (s, B–O). **^{1}H NMR** (300.53 MHz, CDCl$_3$): δ (ppm) 2.35 (s, 6H, CCH_3), 7.38 (m, 6H, p, m, CH of Ph), 7.78 (m, 4H, o, CH of Ph). **^{13}C{^{1}H} NMR** (75.57 MHz, CDCl$_3$): δ 22.7 (CCH$_3$), 127.6, 128.4, 131.6, 138.8 (C of Ph), 184.1 (COO). **^{11}B NMR** (96.25 MHz, CDCl$_3$): δ (ppm) 5.9. **EI-MS**: m/z (%) 312 (100) [M]$^+$.

4.3.3   Single-crystal X-ray diffraction analysis

Single crystals were mounted on a Bruker APEX DUO diffractometer equipped with an Apex II CCD detector at 100 K. Frames were collected using omega scans and integrated with SAINT.[125] Multi-scan absorption correction (SADABS)[125] was applied. The structures were solved by direct methods (SHELXT)[127] and refined using full-matrix least-squares on F^2 with SHELXL[128] using the ShelXle GUI.[128] Weighted R factors, R_w and all goodness-of-fit indicators, are based on F^2. All non-hydrogen atoms were refined anisotropically. The hydrogen

atoms of the C–H bonds were placed in idealized positions. The disordered groups and solvent molecules (**BS2**, 2 x Ph, 1 x *t*-Bu; **BS4**·2CH$_2$Cl$_2$, 1 x CH$_2$Cl$_2$) were refined using geometry (DFIX, SADI, SAME) and U_{ij} restraints (SIMU, RIGU) implemented in SHELXL.[128] The sum of the three refined positions of the dichloromethane molecule in **BS4**·2CH$_2$Cl$_2$ was controlled using the SUMP instruction. The molecular graphics were prepared using GRETEP, POV-RAY, and GIMP.[129–131]

4.3.4 Computational methods

The DFT and QTAIM were performed at M06-2X[160]/SDD theoretical level. For the calculations of the thermochemistry, all compounds were fully optimized.[160] The molecular optimizations and thermochemistry calculations were performed with Gaussian 09[161] program, and the local properties of electron density of compound **BS1** were obtained with the AIMAll software.[162]

Crystal data and structure refinement details of the obtained compounds

	BS1	BS2	BS4·2CH$_2$Cl$_2$	BS5
Chemical formula	C$_{35}$H$_{34}$B$_{12}$O$_5$Si	C$_{58}$H$_{58}$B$_2$O$_8$Si$_2$	C$_{102}$H$_{84}$B$_4$Cl$_4$O$_{14}$Si$_4$	C$_{16}$H$_{16}$B$_2$O$_5$
Fw (g·mol^{-1})	584.33	960.84	1831.09	309.91
crystal system	orthorhombic	triclinic	triclinic	orthorhombic
space group	$P2_12_12_1$	$P\bar{1}$	$P\bar{1}$	$Pca2_1$
a/Å	8.7153(2)	8.7999(2)	10.8389(8)	20.5418(2)
b/Å	18.9158(5)	11.4802(3)	14.9049(11)	8.04382(8)
c/Å	19.0191(5)	13.6929(4)	15.0276(11)	9.31580(9)
α/deg	90	73.7832(6)	109.3549(13)	90
β/deg	90	81.3008(6)	90.0269(15)	90
γ/deg	90	72.0887(6)	97.9839(15)	90
V/Å^3	3135.4(1)	1260.67(6)	2265.5(3)	1539.29(3)
Z	4	1	1	4
T/K	100(2)	100(2)	100(2)	100(2)
λ/Å	0.71073	0.71073	0.71073	1.54178
μ/mm^{-1}	0.116	0.127	0.250	0.793
ρ_{calcd} /g·cm^{-3}	1.238	1.266	1.342	1.337
$F(000)$	1232	508	952	648
crystal size/mm^3	0.236x0.129x0.086	0.280x0.130x0.080	0.357x0.139x0.136	0.274x0.116x0.077
θ Range/°	1.518 to 26.372	1.924 to 27.102	1.900 to 27.445	4.304 to 67.722
Limiting indices	$-10 \le h \le 10$	$-11 \le h \le 11$	$-14 \le h \le 14$	$-22 \le h \le 24$
	$-23 \le k \le 18$	$-14 \le k \le 14$	$-19 \le k \le 19$	$-9 \le k \le 9$
	$-23 \le l \le 23$	$-17 \le l \le 17$	$-19 \le l \le 19$	$-11 \le l \le 11$
Reflections collected	21342	23789	41614	18718
Unique reflections (R_{int})	6383 (0.0269)	5583 (0.0187)	10324 (0.0362)	2754 (0.0160)
No. of data / restraints / parameters	6383 / 0 / 391	5583 / 972 / 467	10324 / 200 / 634	2754 / 1 / 210
Goodness of fit on F^2	1.077	1.027	1.050	1.048
R_1,[a] wR_2[b] ($I > 2\sigma(I)$)	0.0343, 0.0907	0.0321, 0.0840	0.0360, 0.0896	0.0231, 0.0623
R_1,[a] wR_2[b] (all data)	0.0384, 0.0931	0.0356, 0.0870	0.0412, 0.0931	0.0232, 0.0625
Residual electron density/e·Å^{-3}	0.297 / -0.301	0.372 / -0.343	0.409 / -0.383	0.180 / -0.160
Flack parameter	0.08(4)	–	–	0.02(3)
CCDC	1551306	1551307	1551308	1551309

[a] $R_1 = \Sigma||F_o| - |F_c||/\Sigma|F_o|$. [b] $wR_2 = [\Sigma w(F_o^2 - F_c^2)^2/\Sigma w(F_o^2)^2]^{1/2}$.

Table 4-2. Crystal data and structure refinement details for compounds **BS1**, **BS2**, **BS3**, **BS4** and **BS5**.

General Conclusions

Acetylsilylalkoxides (ASA) offer a straightforward, scalable and cost-efficient synthetic pathway towards molecular hybrid organosilicates and organosilanols. Such pathway eliminates the main disadvantages of the current synthetic methods, such as: large quantities of organic solvent, the use of a base, and long reaction times.

This synthetic method permits a stepwise tuning of the steric and electronic environment of the silicate centers and consequently their hydrogen bonding capabilities. Therefore, their organocatalytic properties can be easily tailored, as observed in the cycloaddition of CO_2 with styrene oxide, to form styrene carbonate in the presence of TBAI. Furthermore, we demonstrated that such catalytic systems combine the advantages of both homogeneous and heterogeneous catalysis, since they feature a high efficiency under mild reaction conditions and can be easily recycled through filtration.

Additionally, it was demonstrated that the hydrogen-bonding interactions between organobis(silanols) and diamine molecules allow the formation of Hydrogen-bonded organic frameworks (HOFs) with modulated porosity.

Finally, we demonstrated the use of acetoxylsilylalkoxides compounds in the synthesis of a series of ring- and cage-like molecular borosilicates containing SiO_4 units, where the structure of the borosilicate core was easily modulated using two strategies: blocking of condensation sites and controlling the stoichiometry of the reaction.

Appendix A

Appendix

The results derived from this research work was published in two research papers in indexed journals, and one more is progress.

[1] Velásquez-Hernández, M. de J.; Torres-Huerta, A.; Hernández-Balderas, U.; Martínez-Otero, D.; Núñez-Pineda, A.; Jancik, V. *Polyhedron* **2017**, *122*, 161–171. *Our paper was featured on the font cover of Polyhedron*

[2] Torres-Huerta, A.; Velásquez-Hernández, M. de J.; Ramírez-Palma, L. G.; Cortés-Guzmán, F.; Martínez-Otero, D.; Hernández-Balderas, U.; Jancik, V. *Inorg. Chem.* **2017**, *56*, 10032–10043.

[3] Torres-Huerta, A.; Velásquez-Hernández, M. de J.; Martínez-Otero, D.; Höpfl H.; Jancik, V. *Cryst. Growth Des.* **2017**, *17*, 2438–2452.

[4] Velásquez-Hernández, M. de J.; Torres-Huerta, A.; Martínez-Otero, D.; Sánchez-González, E.; Ibarra, I. A.; Jancik, V. *Manuscript in preparation.*

Volume 122, 28 January 2017   ISSN 0277-5387
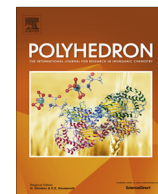
ELSEVIER

POLYHEDRON

THE INTERNATIONAL JOURNAL FOR RESEARCH IN INORGANIC CHEMISTRY

CO_2

Regional Editors
G. Christou & C.E. Housecroft

Available online at www.sciencedirect.com

ScienceDirect

Novel route to silanetriols and silanediols based on acetoxysilylalkoxides

Miriam de J. Velásquez-Hernández, Aarón Torres-Huerta, Uvaldo Hernández-Balderas,
Diego Martínez-Otero, Alejandra Núñez-Pineda, Vojtech Jancik *

Centro Conjunto de Investigación en Química Sustentable UAEM-UNAM, Carr. Toluca-Atlacomulco km 14.5, 50200 Toluca, Estado de México, Mexico

ARTICLE INFO

ABSTRACT

An easy and versatile method for the preparation of molecular alkoxysilanols as molecular organosilicates based on acetoxysilylalkoxides (ASA, $(RO)(tBuO)_nSi(OAc)_{3-n}$ or $(AcO)_{3-n}(tBuO)_nSi$-O-R-O-Si$(OtBu)_n(OAc)_{3-n}$, R = organic group; $n = 0$ or 1) is presented. These ASA precursors are prepared from silicon tetraacetate and suitable alcohols and are cleanly hydrolyzed in water to the corresponding alkoxysilanols in the absence of a base or organic solvents. The compounds were characterized by common spectroscopic methods including X-ray structural analysis. Alkoxysilanols were tested in the catalytic conversion of CO_2 to styrene carbonate and show quantitative conversion within 15 h at 60 °C and 1 atm of CO_2.

© 2016 Elsevier Ltd. All rights reserved.

1. Introduction

Organosilanols combine in their molecule $Si(OH)_n$ ($n = 1$–3) moiety, which provides remarkable hydrogen-bonding capabilities and tunable acidity, with an organic residue providing structural modularity and solubility [1–3]. Thus their final properties can be easily adjusted according to the desired application. Therefore, it is not surprising that they have found many applications in both academia and industry. The most significant are cross-coupling reactions, synthesis of hybrid organic–inorganic materials with long-range order [4–9], molecular recognition [10–12], environmentally friendly surfactants based on organosilanetriols [13]; as well as unique bioisosteres, that do not have stable carbon analogues, and are used in improving the advance of new therapeutic agents [14–19]. Furthermore, discrete alkoxysilanols $(RO)_nSi(OH)_{4-n}$ ($n = 2$, 3) with a silicon atom immediately coordinated to four oxygen atoms as in silica materials, have been used in the preparation of molecular models to understand the local active sites on the surface of heterogeneous catalysts [20–22]. More recently organosilanediols have been applied in enantioselective hydrogen-bond donor catalysis (HBD) [23–26] and the binary catalytic system silanediol/TBAI has been described by Cokoja et al. [27] as a "potential metal-free system that bridges the gap between metal containing and organic catalysts".

Despite the above-mentioned promising applications, wider use of organosilanols is hampered by the available synthetic methods

[1–3,28,29]. The most important are based on the hydrolysis of organochlorosilanes [2,3,28] or organoalkoxysilanes [29,30] ($R_nSiCl_{(4-n)}$ and $R_nSiOR'_{(4-n)}$; R' = Me, Et, $n = 1$–3 respectively), synthesized from $SiCl_4$ or tetramethoxy- or tetraethoxysilanes and organometallic reagents. Eventually, they can also be prepared using catalytic hydrosilylation of dienes, starting from $HSiCl_3$ or $HSi(OR)_3$ (R = Me, Et) [31]. These precursors are converted to the corresponding silanols by hydrolysis. However, each precursor type has its disadvantages. The hydrolysis of the chlorosilanes produces HCl, which causes condensation of the silanols and thus it has to be trapped using stoichiometric amounts of a base such as aniline or pyridine. However, an excess of the base can also cause decomposition of the products [2,3,28]. The hydrolysis of alkoxysilanes produces alcohols that by themselves do not accelerate the condensation of the silanols, but this hydrolysis requires acidic catalysis and long reaction times (up to 34 days!), which always results in a partial condensation and thus product loss [29,30]. Finally, both methods require, especially in the case of silanols with two or three OH groups, large quantities of organic solvent to dilute the reagents and thus protect the silanols from condensation. In addition, the synthesis of alkoxysilanols $(RO)_nSi(OH)_{4-n}$ starts from the respective chloro derivatives $(RO)_nSiCl_{4-n}$ and is even more problematic than the synthesis of silanols with Si–C bonds, due to the low stability of the Si–OR bond under the synthetic conditions [32]. However, they feature higher potential as a catalyst for HBD due to the higher acidic character of their OH groups [33].

These facts prompted us to pursue a new sustainable synthetic pathway, which would afford stable alkoxysilanols $(RO)_nSi(OH)_{4-n}$

Synthesis of Cyclic and Cage Borosilicates Based on Boronic Acids and Acetoxysilylalkoxides. Experimental and Computational Studies of the Stability Difference of Six- and Eight-Membered Rings

Aarón Torres-Huerta,[†,§] Miriam de J. Velásquez-Hernández,[†,§] Lillian G. Ramírez-Palma,[‡]
Fernando Cortés-Guzmán,*[,‡] Diego Martínez-Otero,[†] Uvaldo Hernández-Balderas,[†]
and Vojtech Jancik*[,†]

[†]Centro Conjunto de Investigación en Química Sustentable UAEM-UNAM. Carretera Toluca-Atlacomulco, km. 14.5, 50200 Toluca, Estado de México México

[‡]Instituto de Química, Ciudad Universitaria, Universidad Nacional Autónoma de México Circuito Exterior s/n, 04510 CDMX, México

Ⓢ *Supporting Information*

ABSTRACT: A series of borosilicates was synthesized, where the structure of the borosilicate core was easily modulated using two strategies: blocking of condensation sites and controlling the stoichiometry of the reaction. Thus, on the one hand, the condensation of phenylboronic or 3-hydroxyphenylboronic acid with diacetoxysilylalkoxide [(^{t}BuO)(Ph$_3$CO)-Si(OAc)$_2$] led to the formation of borosilicates (^{t}BuO)-(Ph$_3$CO)Si{(μ-O)BPh}$_2$(μ-O) (**1**), [{(^{t}BuO)(Ph$_3$CO)Si(μ-O)BPh(μ-O)}$_2$] (**2**), and [{(^{t}BuO)(Ph$_3$CO)Si(μ-O)B(3-HOPh)(μ-O)}$_2$] (**3**) with a cyclic inorganic B$_2$SiO$_3$ or B$_2$Si$_2$O$_4$ core, respectively. On the other hand, the reaction of phenylboronic acid with triacetoxysilylalkoxide (Ph$_3$CO)Si-(OAc)$_3$ in 3:2 ratio resulted in the formation of a cagelike structure [{(Ph$_3$CO)Si(μ-O)$_2$BPh(μ-O)}$_2$] (**4**) with B$_4$Si$_4$O$_{10}$ core, while the reaction of the boronic acid with silicon tetraacetate generated an unusual 1,3-bis(acetate)-1,3-diphenyldiboraxane PhB(μ-O)(μ-O,O′-OAc)$_2$BPh (**5**). Additionally, compound **1** was used to evaluate the possibility to form N→B donor−acceptor bond between the boron atom in the borosilicates and a nitrogen donor. Thus, coordination of **1** with piperazine yielded a tricyclic [{(^{t}BuO)(Ph$_3$CO)Si(OBPh)$_2$(μ-O)}$_2$·C$_4$H$_{10}$N$_2$] compound **6** with two borosilicate rings bridged by a piperazine molecule. Finally, the processes involved in the formation of the six- and eight-membered rings (B$_2$SiO$_3$ and B$_2$Si$_2$O$_4$) in compounds **1** and **2** were explored using solution ^{1}H NMR studies and density functional theory calculations. These molecules represent to the best of our knowledge first examples of cyclic molecular borosilicates containing SiO$_4$ units.
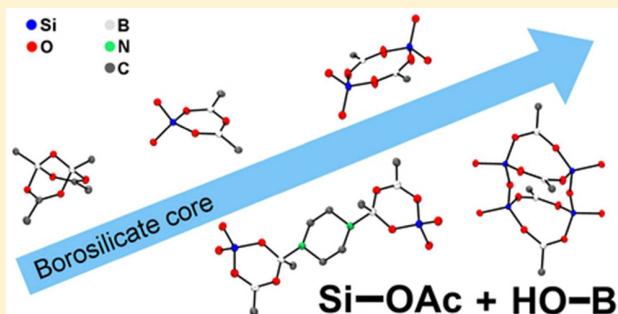
■ INTRODUCTION

The borosilicates are solid tridimensional materials with characteristic properties such as chemical resistance, thermal stability, catalysis, ion exchange, and optoelectronic properties, and they are used for encapsulating organic molecules and fabrication of different sorts of glasses.[1−6] The main component in the borosilicate glasses is silicon oxide in the form of the tetrahedral SiO$_4$ unit, and in a smaller amount B$_2$O$_3$, Na$_2$O, Al$_2$O$_3$, and CaO, where the B$_2$O$_3$ content is between 5 and 30%.[7,8] The presence of the boron atoms is fundamental for the resulting properties of the material, due to its Lewis acid character and thus the possibility to change its coordination number and the geometry from trigonal planar to tetrahedral in the presence of basic oxides, nucleophiles, or Lewis bases.[9,10] Despite the properties and applications of these materials there are very few examples of molecular borosilicates,[11−15] and to the best of our knowledge, reports of structurally characterized borosilicates containing SiO$_4$ units are limited to few acyclic

derivatives of [{(^{t}BuO)$_3$SiO}$_2$BOH].[16−18] Molecular borosilicates are usually obtained from boronic acids and either silanediols, dichlorosilanes, or dialkoxysilanes and contain 6-, 8-, 10-, or 12-membered cyclic cores based on B−O−Si units, where the eight-membered rings are the most common.[19−26] On the one hand, it is noteworthy that the formation of the smaller or bigger rings requires the use of predesigned precursors such as ClSi(R)$_2$OSi(R)$_2$Cl or HOSi(R)$_2$OSi-(R)$_2$OSi(R)$_2$OH.[23,24] However, only a handful of such compounds have been reported. On the other hand, few cagelike structures with B$_2$Si$_6$O$_9$, B$_3$Si$_2$O$_6$, and B$_4$Si$_4$O$_{10}$ cores are also known and are based either on boric acid (B(OSiPh$_2$OSiPh$_2$O)$_3$B) or boronic acids (^{t}BuSi{O(BR)-O}$_3$Si^{t}Bu or (^{t}BuSi)$_4$(BR)$_4$O$_{10}$; R = organic group).[27−29] Also, despite the fact that borosilicate scaffolds are suitable

Structural Induction via Solvent Variation in Assemblies of Triphenylboroxine and Piperazine—Potential Application as Self-Assembly Molecular Sponge

Aaron Torres-Huerta,[†] Miriam de Jesús Velásquez-Hernández,[†] Diego Martínez-Otero,[†] Herbert Höpfl,[‡] and Vojtech Jancik*,[†]

[†]Centro Conjunto de Investigación en Química Sustentable UAEM-UNAM, Carretera Toluca-Atlacomulco, km. 14.5, Toluca, México, 50200, México

[‡]Centro de Investigaciones Químicas, Instituto de Investigación en Ciencias Básicas y Aplicadas, Universidad Autónoma del Estado de Morelos, Av. Universidad 1001, Cuernavaca, Morelos, 62209, México

S *Supporting Information*

ABSTRACT: This study examined the direct effect of solvent on the chemical composition and structure of supramolecular assemblies formed from triphenylboroxine ($(PhBO)_3$) and piperazine (ppz) through N→B bonds. Oxygen-containing solvents with a molecular size smaller than 4.1 Å produce 1D polymeric structures (1:1 boroxine/piperazine) of compositions $\{(PhBO)_3(ppz)\}_n \cdot nTHF$ (**1a·THF**) and $\{(PhBO)_3(ppz)\}_n \cdot n$Acetone (**1a·Acetone**), in which the boroxine B_3O_3 rings are linked through N→B bonded piperazine molecules in a *cis*-conformation. In both cases, a pseudocavity is generated between two polymer chains, which is occupied by a solvent molecule interacting through bifurcated N−H···O···H−N hydrogen bonds with one of the chains. In contrast, oxygen-based solvents with a size larger than 6.3 Å give rise to discrete 2:1 assemblies, $\{(PhBO)_3\}_2(ppz) \cdot 2$Ethyl acetate (**2·AcOEt**) and $\{(PhBO)_3\}_2(ppz) \cdot 2$Pentanone (**2·Pentanone**), with the piperazine molecule bridging two B_3O_3 rings and interacting with two solvent molecules via N−H···O hydrogen bonds. In chloroform or dichloromethane 2:3 adducts, $\{(PhBO)_3\}_2(ppz)_3 \cdot 4CHCl_3$ (**3·CHCl₃**) and $\{(PhBO)_3\}_2(ppz)_3 \cdot 2.09CH_2Cl_2$ (**3·CH₂Cl₂**), were obtained, with N−H···N interactions formed between the piperazine molecules directing the crystal lattice. Finally, unlike with THF and acetone, the presence of two coordination sites in dioxane gives rise to a 1D polymeric 1:1 clathrate-type assembly with *trans*-conformation, $\{(PhBO)_3(ppz)\}_n \cdot 3.5n$Dioxane (**1b·Dioxane**). In accordance with the structural characterization, the thermogravimetric analysis of compounds **1−2** evidenced relatively high decomposition (solvent elimination) temperatures for the inclusion complexes derived from oxygen-containing solvents (T_{peak} = 76.4 to 145.4 °C). On the contrary, solvates based on halogenated solvents (**3·CHCl₃** and **3·CH₂Cl₂**) or 1,4-dioxane started to decompose already at room temperature. In view of potential applications for the storage and structural characterization of volatile or highly reactive reagents, a final inclusion experiment was carried out with racemic 1,2-epoxybutane. As expected, the resulting N→B bonded inclusion complex exhibited a 1:1 *cis*-polymeric structure, in which the guest molecules were bonded by bifurcated N_{pip}−H···O_{epoxy}···H−N_{pip} hydrogen bonds.
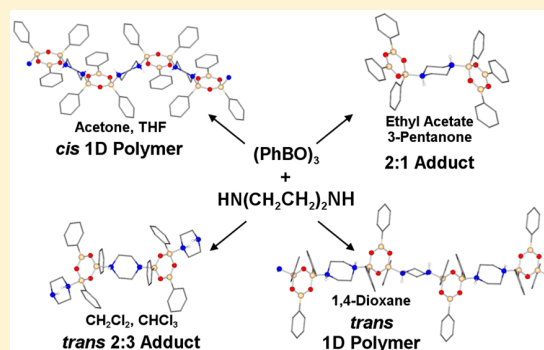
1. INTRODUCTION

Nowadays, there is growing interest in the design and synthesis of macrocycles, molecular cages, coordination polymers, and three-dimensional systems using self-assembly processes.[1−4] The success of the self-assembly approach lies in its proficiency to form periodic systems with high dimensionality using a minimum number of simple building units. This reduces the number of reaction steps and increases yields.[5−8] Additionally, systems based on coordinative bonds present the advantage of possible self-healing due to the reversibility of the construction processes favoring the thermodynamic product.[9−14] Besides, the relatively low thermodynamic stability of coordinative bonds increases the structural diversity of the products obtained from a set of building blocks upon changing the reaction conditions.[15−18] Currently, one of the main remaining challenges in crystal engineering is the development of effective synthetic procedures to achieve the desired target structure and properties of the coordination polymer. Even though a plethora of self-assembly systems have been studied, the processes involved in the formation of molecular aggregates and supramolecular synthons to consolidate the crystal structure are often not clear. This fact is evidenced by phenomena such as supramolecular isomerism,[19,20] polymorphism,[21,22] and solvatomorphism.[23] Important factors that influence the

Bibliography

[1] Kickelbick, G. *Hybrid Materials Synthesis, Characterization, and Applications*; Wiley-VCH, 2007.

[2] Sanchez, C.; Belleville, P.; Popall, M.; Nicole, L. *Chem. Soc. Rev.* **2011**, *40*, 696–753.

[3] Ciriminna, R.; Fidalgo, A.; Pandarus, V.; Béland, F.; Ilharco, L. M.; Pagliaro, M. *Chem. Rev.* **2013**, *8*, 6592–6620.

[4] Hurkes, N.; Ehmann, H. M. A.; List, M.; Spirk, S.; Bussiek, M.; Belaj, F.; Pietschnig, R. *Chem. Eur. J.* **2014**, *20*, 9330–9335.

[5] Kondo, S.-i.; Bie, Y.; Yamamura, M. *Org. Lett.* **2013**, *15*, 520–523.

[6] Kondo, S.-i.; Harada, T.; Tanaka, R.; Unno, M. *Org. Lett.* **2006**, *8*, 4621–4624.

[7] Madsen, J. L. H.; Andersen, T. L.; Santamaria, S.; Nagase, H.; Enghild, J. J.; Skrydstrup, T. *J. Med. Chem.* **2012**, *55*, 7900–7908.

[8] Mutahi, M. W.; Nittoli, T.; Guo, L.; Sieburth, S. M. *J. Am. Chem. Soc.* **2002**, *124*, 7363–7375.

[9] Sieburth, S. M.; Chen, C.-A. *Eur. J. Org. Chem.* **2006**, 311–322.

[10] Yamamura, M.; Kondo, S.-i.; Unno, M. *Tetrahedron Lett.* **2014**, *55*, 646–649.

[11] Diemoz, K. M.; Hein, J. E.; Wilson, S. O.; Fettinger, J. C.; Franz, A. K. *J. Org. Chem.* **2017**, *82*, 6738–6747.

[12] Hardman-Baldwin, A. M.; Mattson, A. E. *ChemSusChem* **2014**, *7*, 3275–3278.

[13] Schafer, A. G.; Wieting, J. M.; Fisher, T. J.; Mattson, A. E. *Angew. Chem. Int. Ed.* **2013**, *52*, 11321–11324.

[14] Tran, N. T.; Wilson, S. O.; Franz, A. K. *Org. Lett.* **2012**, *14*, 186–189.

[15] Wieting, J. M.; Fisher, T. J.; Schafer, A. G.; Visco, M. D.; Gallucci, J. C.; Mattson, A. E. *Eur. J. Org. Chem.* **2015**, 525–533.

[16] Kuroda, K.; Shimojima, A.; Kawahara, K.; Wakabayashi, R.; Tamura, Y.; Asakura, Y.; Kitahara, M. *Chem. Mater.* **2014**, *26*, 211–220.

[17] Alauzun, J.; Mehdi, A.; Reyé, C.; Corriu, R. J. P. *J. Mater. Chem.* **2005**, *15*, 841–843.

[18] Carlos, L. D.; de Zea Bermudez, V.; Amaral, V. S.; Nunes, S. C.; Silva, N. J. O.; Sá Ferreira, R. A.; Rocha, J.; Santilli, C. V.; Ostrovskii, D. *Adv. Mater.* **2007**, *19*, 341–348.

[19] Cerveau, G.; Chappellet, S.; Corriu, R. J. P.; Dabiens, B.; Le Bideau, J. *Organometallics* **2002**, *21*, 1560–1564.

[20] Cerveau, G.; Chappellet, S.; Corriu, R. J. P. *J. Mater. Chem.* **2003**, *13*, 2885–2889.

[21] Wakabayashi, R.; Kuroda, K. *Chempluschem* **2013**, *78*, 764–774.

[22] Brinker, C. J.; Scherer, G. W. *Sol-Gel Sci.*; Academic Press: Boston, MA, 1990; p 912.

[23] Shea, K. J.; Loy, D. a.; Webster, O. *J. Am. Chem. Soc.* **1992**, *114*, 6700–6710.

[24] Hunt, J. R.; Doonan, C. J.; LeVangie, J. D.; Côté, A. P.; Yaghi, O. M. *J. Am. Chem. Soc.* **2008**, *130*, 11872–11873.

[25] Mehdi, A.; Reye, C.; Corriu, R. *Chem. Soc. Rev.* **2011**, *40*, 563–574.

[26] Baney, R. H.; Itoh, M.; Sakakibara, A.; Suzuki, T. *Chem. Rev.* **1995**, *95*, 1409–1430.

[27] Creff, G.; Pichon, B. P.; Blanc, C.; Maurin, D.; Sauvajol, J. L.; Carcel, C.; Moreau, J. J. E.; Roy, P.; Bartlett, J. R.; Wong Chi Man, M.; Bantignies, J. L. *Langmuir* **2013**, *29*, 5581–5588.

[28] Oviatt, H. W.; Shea, K. J.; Small, J. H. *Chem. Mater.* **1993**, *5*, 943–950.

[29] Boury, B.; Valerie, L. S.; Corriu, R. J. P.; Delord, P.; Nobili, M. *Angew. Chem. Int. Ed.* **1999**, *38*, 3172–3175.

[30] Corriu, R. J. P.; Morea, J. J. E.; Thepot, P.; Chi Man, M. W. *Chem. Mater.* **1992**, *4*, 1217–1224.

[31] Hobson, S. T.; Shea, K. J. *Chem. Mater.* **1997**, *9*, 616–623.

[32] Zvonkina, I.; Soucek, M. *Curr. Opin. Chem. Eng.* **2016**, *11*, 123–127.

[33] Loy, D. A.; Carpenter, J. P.; Myers, S. A.; Assink, R. A.; Small, J. H.; Greaves, J.; Shea, K. J. *J. Am. Chem. Soc.* **1996**, *118*, 8501–8502.

[34] Loy, D. A.; Russick, E. M.; Yamanaka, S. A.; Baugher, B. M.; Shea, K. J. *Chem. Mater.* **1997**, *9*, 2264–2268.

[35] Vashist, S. K.; Lam, E.; Hrapovic, S.; Male, K. B.; Luong, J. H. T. *Chem. Rev.* **2014**, *114*, 11083–11130.

[36] Shea, K. J.; Loy, D. A. *Chem. Mater.* **2001**, *13*, 3306–3319.

[37] Jia, X.; Huang, Z. *Nat Chem* **2016**, *8*, 157–161.

[38] Marciniec, B. *Coord. Chem. Rev.* **2005**, *249*, 2374–2390.

[39] Holwell, A. J. *Platin. Met. Rev.* **2008**, *52*, 243–246.

[40] Brondani, D. J.; Corriu, R. J. P.; Ayoubi, S. E.; Moreau, J. E.; Wong, M.; Man, C. *J. Organomet. Chem.* **1993**, *451*, C1–C3.

[41] Harrison, P. G. *J. Organomet. Chem.* **1997**, *542*, 141–183.

[42] Tillmann, J.; Meyer, L.; Schweizer, J. I.; Bolte, M.; Lerner, H. W.; Wagner, M.; Holthausen, M. C. *Chem. Eur. J.* **2014**, *20*, 9234–9239.

[43] Liu, H.; Zheng, S.; Nie, K. *Macromolecules* **2005**, *38*, 5088–5097.

[44] Ye, Q.; Zhou, H.; Xu, J. *Chem. Asian J.* **2016**, *11*, 1322–1337.

[45] Bassindale, A. R.; Liu, Z.; MacKinnon, I. A.; Taylor, P. G.; Yang, Y.; Light, M. E.; Horton, P. N.; Hursthouse, M. B. *Dalton Trans.* **2003**, 2945–2949.

[46] El Aziz, Y.; Bassindale, A. R.; Taylor, P. G.; Horton, P. N.; Stephenson, R. A.; Hursthouse, M. B. *Organometallics* **2012**, *31*, 6032–6040.

[47] Kannan, R. Y.; Salacinski, H. J.; Butler, P. E.; Seifalian, A. M. *Acc. Chem. Res.* **2005**, *38*, 879–884.

[48] Laine, R. M. *J. Mater. Chem.* **2005**, *15*, 3725–3744.

[49] Tereshchenko, T. a. *Polym. Sci. Ser. B* **2008**, *50*, 249–262.

[50] Oguri, N.; Egawa, Y.; Takeda, N.; Unno, M. *Angew. Chem. Int. Ed.* **2016**, *55*, 9336–9339.

[51] Kawahara, K.; Hagiwara, Y.; Kuroda, K. *Chem. Eur. J.* **2011**, *17*, 13188–13196.

[52] Liu, H.; Kondo, S.-i.; Takeda, N.; Unno, M. *J. Am. Chem. Soc.* **2008**, *130*, 10074–10075.

[53] Smet, S.; Verlooy, P.; Duerinckx, K.; Breynaert, E.; Taulelle, F.; Martens, J. A. *Chem. Mater.* **2017**, *29*, 5063–5069.

[54] Quadrelli, E. A.; Basset, J.-M. *Coord. Chem. Rev.* **2010**, *254*, 707–728.

[55] Pinkert, D.; Limberg, C. *Chem. Eur. J.* **2014**, *20*, 9166–9175.

[56] Chan, K. L.; Sonar, P.; Sellinger, A. *J. Mater. Chem.* **2009**, *19*, 9103–9120.

[57] Chemtob, A.; Belon, C.; Croutxé-Barghorn, C.; Brendlé, J.; Soulard, M.; Rigolet, S.; Le Houérou, V.; Gauthier, C. *New J. Chem.* **2010**, *34*, 1068–1072.

[58] Graffion, J.; Cojocariu, A. M.; Cattoën, X.; Ferreira, R. A. S.; Fernandes, V. R.; André, P. S.; Carlos, L. D.; Wong Chi Man, M.; Bartlett, J. R. *J. Mater. Chem.* **2012**, *22*, 13279–13285.

[59] Zhang, C.; Zhang, C.; Sun, J.; Ding, R.; Zhang, Q.; Xu, Y. *RSC Adv.* **2015**, *5*, 56998–57005.

[60] Liu, X.; Maegawa, Y.; Goto, Y.; Hara, K.; Inagaki, S. *Angew. Chem. Int. Ed.* **2016**, *55*, 7943–7947.

[61] Cerveau, G.; Chappellet, S.; Corriu, R. J. P.; Dabiens, B. *Silicon Chem.* **2002**, *1*, 321–331.

[62] Inagaki, S.; Guan, S.; Ohsuna, T.; Terasaki, O. *Nature* **2002**, *416*, 304–307.

[63] Chandrasekhar, V.; Boomishankar, R.; Nagendran, S. *Chem. Rev.* **2004**, *104*, 5847–5910.

[64] Murugavel, R.; Voigt, A.; Walawalkar, M. G.; Roesky, H. W. *Chem. Rev.* **1996**, *96*, 2205–2236.

[65] Schmidt, M. W.; Truong, P. N.; Gordon, M. S. *J. Am. Chem. Soc.* **1987**, *109*, 5217–5227.

[66] Chen, C. A.; Sieburth, S. M.; Glekas, A.; Hewitt, G. W.; Trainor, G. L.; Erickson-Viitanen, S.; Garber, S. S.; Cordova, B.; Jeffry, S.; Klabe, R. M. *Chem. Biol.* **2001**, *8*, 1161–1166.

[67] Franz, A. K.; Wilson, S. O. *J. Med. Chem.* **2013**, *56*, 388–405.

[68] Copéret, C.; Comas-Vives, A.; Conley, M. P.; Estes, D. P.; Fedorov, A.; Mougel, V.; Nagae, H.; Núñez-Zarur, F.; Zhizhko, P. A. *Chem. Rev.* **2016**, *116*, 323–421.

[69] Genevieve, C.; Corriu, R. J. P.; Dabiens, B.; Bideau, J. L. *Angew. Chem. Int. Ed.* **2000**, *39*, 4707–4711.

[70] Buttrus, N. H.; Damja, R. I.; Eaborn, C.; Hitchcock, P. B.; Lickiss, P. D. *J. Chem. Soc. Chem. Commun.* **1985**, 1385–1386.

[71] Suzuki, J.; Shimojima, A.; Fujimoto, Y.; Kuroda, K. *Chem. Eur. J.* **2008**, *14*, 973–980.

[72] Taylor, M. S.; Jacobsen, E. N. *Angew. Chem. Int. Ed.* **2006**, *45*, 1520–1543.

[73] Phipps, R. J.; Hamilton, G. L.; Toste, F. D. *Nat. Chem.* **2012**, *4*, 603–614.

[74] Cokoja, M.; Wilhelm, M. E.; Anthofer, M. H.; Herrmann, W. A.; Kühn, F. E. *ChemSusChem* **2015**, *8*, 2436–2454.

[75] Hoffmann, F.; Cornelius, M.; Morell, J.; Fröba, M. *Angew. Chem. Int. Ed.* **2006**, *45*, 3216–3251.

[76] Mellot-Draznieks, C.; Cheetham, A. K. *Nat. Chem.* **2016**, *9*, 6–8.

[77] Laeri, F.; Schuth, F.; Simon, U. *Host-Guest Systems Based on Nanoporous Crystals*; Wiley-VCH, 2003.

[78] Ruren, X.; Wenqin, P.; Jihong, Y.; Qisheng, H.; Chen, J. *Chemistry of Zeolites and Related Porous Materials: Synthesis and Structure*; Wiley and Sons, 2007.

[79] Long, J. R.; Yaghi, O. M. *Chem. Soc. Rev.* **2009**, *38*, 1213–1214.

[80] Tranchemontagne, D. J.; Mendoza-Cortés, J. L.; O'Keeffe, M.; Yaghi, O. M. *Chem. Soc. Rev.* **2009**, *38*, 1257–1283.

[81] Uemura, N. K. S., Takashi Yanai *Chem. Soc. Rev.* **2009**, *38*, 1228–1236.

[82] Brunet, P.; Simard, M.; Wuest, J. D. *J. Am. Chem. Soc.* **1997**, *119*, 2737–2738.

[83] Adachi, T.; Ward, M. D. *Acc. Chem. Res.* **2016**, *49*, 2669–2679.

[84] Yang, W.; Li, B.; Wang, H.; Alduhaish, O.; Alfooty, K.; Zayed, M. A.; Li, P.; Arman, H. D.; Chen, B. *Cryst. Growth Des.* **2015**, *15*, 2000–2004.

[85] Hu, F.; Liu, C.; Wu, M.; Pang, J.; Jiang, F.; Yuan, D.; Hong, M. *Angew. Chem. Int. Ed.* **2017**, *56*, 2101–2104.

[86] Li, P.; He, Y. B.; Zhao, Y. F.; Weng, L. H.; Wang, H. L.; Krishna, R.; Wu, H.; Zhou, W.; O'Keeffe, M.; Han, Y.; Chen, B. L. *Angew. Chem. Int. Ed.* **2015**, *54*, 574–577.

[87] Wen, H.-M.; Li, B.; Wang, H.; Wu, C.; Alfooty, K.; Krishna, R.; Chen, B. *Chem. Commun.* **2015**, *51*, 5610–5613.

[88] Mouchaham, G.; Roques, N.; Khodja, W.; Duhayon, C.; Coppel, Y.; Brand?s, S.; Fodor, T.; Meyer, M.; Sutter, J.-P. *Chem. Eur. J.* **2017**, *23*, 11818–11826.

[89] Galli, E.; Quartieri, S.; Vezzalini, G.; Alberto, A.; Franzini, M. *Am. Mineral* **1997**, *82*, 423–429.

[90] Tranchemontagne, D. J.; Hunt, J. R.; Yaghi, O. M. *Tetrahedron* **2008**, *64*, 8553 – 8557.

[91] Li, P.; He, Y.; Arman, H. D.; Krishna, R.; Wang, H.; Weng, L.; Chen, B. *Chem. Commun.* **2014**, *50*, 13081–13084.

[92] Raatikainen, K.; Rissanen, K. *Chem. Sci.* **2012**, *3*, 1235–1239.

[93] Bajpai, A.; Natarajan, P.; Venugopalan, P.; Moorthy, J. N. *J. Org. Chem.* **2012**, *77*, 7858–7865.

[94] Bialek, M. J.; Zareba, J. K.; Janczak, J.; Zon, J. *Cryst. Growth Des.* **2013**, *13*, 4039–4050.

[95] Zareba, J. K.; Bialek, M. J.; Janczak, J.; Zon, J.; Dobosz, A. *Cryst. Growth Des.* **2014**, *14*, 6143–6153.

[96] Pietschnig, R.; Spirk, S. *Coord. Chem. Rev.* **2016**, *323*, 87–106.

[97] Prabusankar, G.; Murugavel, R.; Butcher, R. J. *Organometallics* **2004**, *23*, 2305–2314.

[98] Waller, P. J.; Gándara, F.; Yaghi, O. M. *Acc. Chem. Res.* **2015**, *48*, 3053–3063.

[99] Uribe-Romo, F. J.; Hunt, J. R.; Furukawa, H.; Klöck, C.; O'Keeffe, M.; Yaghi, O. M. *J. Am. Chem. Soc.* **2009**, *131*, 4570–4571.

[100] Cote, A. P.; Benin, A. I.; Ockwig, N. W.; OKeeffe, M.; Matzger, A. J.; Yaghi, O. M. *Science* **2005**, *310*, 1166–1170.

[101] El-Kaderi, H. M.; Hunt, J. R.; Mendoza-Cortes, J. L.; Cote, A. P.; Taylor, R. E.; OKeeffe, M.; Yaghi, O. M. *Science* **2007**, *316*, 268–272.

[102] Doonan, C. J.; Tranchemontagne, D. J.; Glover, T. G.; Hunt, J. R.; Yaghi, O. M. *Nat. Chem.* **2010**, *2*, 235–238.

[103] Foucher, D. A.; Lough, A. J.; Manners, I. *Inorg. Chem.* **1992**, *31*, 3034–3043.

[104] Thieme, K.; Bourke, S. C.; Zheng, J.; MacLachlan, M. J.; Zamanian, F.; Lough, A. J.; Manners, I. *Can. J. Chem. Can. Chim.* **2002**, *80*, 1469–1480.

[105] O'Dowd, A. T.; Spalding, T. R.; Ferguson, G.; Gallagher, J. F.; Reed, D. *Chem. Commun.* **1993**, *634*, 1816–1817.

[106] Fujdala, K. L.; Tilley, T. D. *Zeitschrift fur Anorg. und Allg. Chemie* **2005**, *631*, 2619–2622.

[107] Fujdala, K. L.; Oliver, A. G.; Hollander, F. J.; Tilley, T. D. *Inorg. Chem.* **2003**, *42*, 1140–1150.

[108] Kinetics and Mechanism of Aqueous Hydrolysis and Condensation of alkyltrialkoxysilanes. In Molecular characterization of composite interfaces. 1985.

[109] Velásquez-Hernández, M. J. Síntesis de compuestos tipo organosilicato con relevancia en la formación de materiales híbridos. M.Sc. thesis, UNAM, 2013.

[110] Suzuki, J.; Shimojima, A.; Fujimoto, Y.; Kuroda, K. *Chem. Eur. J.* **2008**, *14*, 973–980.

[111] Shklover, V. E.; Dubchak, I. L.; Struchkov, Y. T.; Khinku, E. S.; Zhdanov, A. *J. Struc. Chem.* **1981**, *22*, 225–229.

[112] Wendler, C.; Reinke, H.; Kelling, H. *J. Organomet. Chem.* **2001**, *626*, 53–58.

[113] Rulkens, R.; Coles, M.; Tilley, T. *J. Chem. Soc., Dalton Trans.* **2000**, 627–628.

[114] Spirik, S.; Nieger, M.; Rechberger, G. N.; Pietschnig, R. *Appl. Organomet. Chem.* **2006**, *20*, 683–686.

[115] Wang, J.; Leong, J.; Zhang, Y. *Green Chem.* **2014**, *16*, 4515–4519.

[116] Wang, J. Q.; Kong, D. L.; Chen, J. Y.; Cai, F.; He, L. N. *J. Mol. Catal. A: Chem.* **2006**, *249*, 143–148.

[117] Dharman, M. M.; Choi, H. J.; Kim, D. W.; Park, D. W. *Catal. Today* **2011**, *164*, 544–547.

[118] Takahashi, T.; Watahik, T.; Kitazume, S.; Yasuda, H.; Sakakura, T. *Chem. Commun.* **2006**, 1664–1666.

[119] Balthis, J. H.; Rochow, E. G. In *Inorganic Syntheses*; Bailar, J., Ed.; Wiley and Sons: NJ, 2007; Vol. 4.

[120] McQuade, D. T.; Kim, J.; Swager, T. M. *J. Am. Chem. Soc.* **2000**, *122*, 5885–5886.

[121] Mortier, J.; Vaultier, M.; Carreaux, F.; Jean-Marc, D. *J. Org. Chem.* **1998**, *63*, 3515–3516.

[122] Jacobs, A.; Nassimbeni, L. R.; Silwana, N.; Bathori, N. B.; Weber, E. *CrystEngComm* **2011**, *13*, 7014–7018.

[123] Nassimbeni, L. R.; Su, H.; Weber, E.; Skobridis, K. *Cryst. Growth Des.* **2004**, *4*, 85–88.

[124] Seebach, D.; Beck, A. K.; Heckel, A. *Angew. Chem. Int. Ed.* **2001**, *40*, 92–138.

[125] SAINT and SADABS, Bruker AXS Inc., Wisconsin, USA, 2007.

[126] Hübschle, C. B.; Sheldrick, G. M.; Dittrich, B. *J. Appl. Cryst.* **2011**, *44*, 1281–1284.

[127] Sheldrick, G. M. *Acta Cryst. A* **2015**, *71*, 3–8.

[128] Sheldrick, G. M. *Acta Cryst. C* **2015**, *71*, 3–8.

[129] d Heres, M. LMGP-Suite Suite of Programs for the interpretation of X-ray Experiments, J. Laugier, B. Bochu, ENSP/Laboratoire des Materiaux et du Genie Physique, BP 46. 38042 Saint http://www.inpg.fr/LMGP and http://www.ccp14.ac.uk/tutorial/lmgp/.

[130] Persistence of Vision Raytracer (Version 3.6), Persistence of Vision Pty. Ltd. (2004) http://www.povray.org.

[131] GIMP 2.8: The GNU Image Manipulation Program. http://www.gimp.org.

[132] Kawakami, Y.; Sakuma, Y.; Wakuda, T.; Nakai, T.; Shirasaka, M.; Kabe, Y. *Organometallics* **2010**, *29*, 3281–3288.

[133] Nandi, S.; Chakraborty, D.; Vaidhyanathan, R. *Chem. Commun.* **2016**, *52*, 7249–7252.

[134] Park, I. H.; Medishetty, R.; Kim, J. Y.; Lee, S. S.; Vittal, J. J. *Angew. Chem. Int. Ed.* **2014**, *53*, 5591–5595.

[135] Durka, K.; Jarzembska, K. N.; Lulin, S. *Cryst. Growth Des.* **2012**, *12*, 3720–3734.

[136] Kutyła, S. E.; Stepien, D. K.; Jarzembska, K. N.; Kaminski, R.; Dobrzycki, L.; Ciesielski, A.; Boese, R.; Mlochowski, J.; Cyranski, M. K. *Cryst. Growth Des.* **2016**, *16*, 7037–7050.

[137] Hix, G. B.; Caignaert, V.; Rueff, J.-m.; Pluart, L.; Warren, J. E. *Cryst. Growth Des.* **2007**, *7*, 30–33.

[138] Zareba, J. K.; Bialek, M. J.; Janczak, J.; Zon, J.; Dobosz, A. *Cryst. Growth Des.* **2014**, *14*, 6143–6153.

[139] Mercury CSD 3.9 (Build RC1) Copyright CCDC 2001-2016, http: www.ccdc.cam.ac.uk/mercury/.

[140] Desiraju, G. R. *J. Am. Chem. Soc.* **2013**, *135*, 9952–9967.

[141] Tran, N. T.; Wilson, S. O.; Franz, A. K. *Chem. Commun.* **2014**, *50*, 3738–3740.

[142] Dizman, B.; Elasri, M. O.; Mathias, L. J. *Journal of Applied Polymer Science* **2004**, *94*, 635–642.

[143] Beckett, M. A.; Rugen-Hankey, M. P.; Sukumar Varma, K. *Polyhedron* **2003**, *22*, 3333–3337.

[144] Murphy, D.; Sheehan, J. P.; Spalding, T. R.; Ferguson, G.; Loughb, A. J.; Gallagher, J. F. *J. Mater. Chem.* **1993**, *3*, 1275–1283.

[145] Dal-Negro, A.; Ungaretti, L.; Perotti, A. *J. Chem. Soc., Dalton Trans.* **1972**, 1639–1643.

[146] Mitu, S.; Baird, M. C. *Organometallics* **2006**, *25*, 4888–4896.

[147] Schafer, A.; Saak, W.; Haase, D.; Muller, T. *Angew. Chem. Int. Ed.* **2012**, *51*, 2981–2984.

[148] Brisdon, B. J.; Mahon, M. F.; Molloy, K. C.; Schofield, P. J. *J. Organomet. Chem.* **1992**, *436*, 11–22.

[149] Foucher, D. A.; Lough, A. J.; Manners, I. *Inorg. Chem.* **1992**, *31*, 3034–3043.

[150] Thieme, K.; Bourke, S. C.; Zheng, J.; MacLachlan, M. J.; Zamanian, F.; Lough, A. J.; Manners, I. *Can. J. Chem. Can. Chim.* **2002**, *80*, 1469–1480.

[151] Koller, H.; Chen, C. Y.; Zones, S. I. *Top. Catal.* **2015**, *58*, 451–479.

[152] Avent, A. G.; Lawrence, S. E.; Meehan, M. M.; Russell, T. G.; Spalding, T. R. *Collect. Czech. Chem. Commun.* **2002**, *67*, 1051–1060.

[153] Pascu, M.; Ruggi, A.; Scopelliti, R.; Severin, K. *Chem. Commun.* **2013**, *49*, 45–47.

[154] Liu, W.; Pink, M.; Lee, D. *J. Am. Chem. Soc.* **2009**, *131*, 8703–8707.

[155] Neville, L. A.; Spalding, T. R.; Ferguson, G. *Angew. Chem. Int. Ed.* **2000**, *39*, 3598–3601.

[156] Zones, S. I.; Benin, A.; Hwang, S. J.; Xie, D.; Elomari, S.; Hsieh, M. F. *J. Am. Chem. Soc.* **2014**, *136*, 1462–1471.

[157] Tokunaga, Y.; Ueno, H.; Shimomura, Y.; Seo, T. *Heterocycles* **2002**, *57*, 787–790.

[158] Kua, J.; Iovine, P. *J. Phys. Chem. A* **2005**, *109*, 8938–8943.

[159] Li, Q.; Chen, W.; Xia, Y.; Liu, Y.; Wang, H.; Wang, H.; Ma, Y. *Diam. Relat. Mater.* **2011**, *20*, 501–504.

[160] Jani, M.; Power, P. P.; M., T. H. *Inorg. Chem.* **2010**, *49*, 10992–11000.

[161] Gaussian 09, Revision D.01, Frisch, M. J.; Trucks, G. W.; Schlegel, H. B.; Scuseria, G. E.; Robb, M. A.; Cheeseman, J. R.; Scalmani, G.; Barone, V.; Mennucci, B.; Petersson, G. A.; Nakatsuji, H.; Caricato, M.; Li, X.; Hratchian, H. P.; Izmaylov, A. F.; Bloino, J.; Zheng, G.; Sonnenberg, J. L.; Hada, M.; Ehara, M.; Toyota, K.; Fukuda, R.; Hasegawa, J.; Ishida, M.; Nakajima, T.; Honda, Y.; Kitao, O.; Nakai, H.; Vreven, T.; Montgomery, Jr., J. A.; Peralta, J. E.; Ogliaro, F.; Bearpark, M.; Heyd, J. J.; Brothers, E.; Kudin, K. N.; Staroverov, V. N.; Kobayashi, R.; Normand, J.; Raghavachari, K.; Rendell, A.; Burant, J. C.; Iyengar, S. S.; Tomasi, J.; Cossi, M.; Rega, N.; Millam, J. M.; Klene, M.; Knox, J. E.; Cross, J. B.; Bakken, V.; Adamo, C.; Jaramillo, J.; Gomperts, R.; Stratmann, R. E.; Yazyev, O.; Austin, A. J.; Cammi, R.; Pomelli, C.; Ochterski, J. W.; Martin, R. L.; Morokuma, K.; Zakrzewski, V. G.; Voth, G. A.; Salvador, P.; Dannenberg, J. J.; Dapprich, S.; Daniels, A. D.; Farkas, O.; Foresman, J. B.; Ortiz, J. V.; Cioslowski, J.; Fox, D. J. Gaussian, Inc., Wallingford CT, 2009.

[162] AIMAll (Version 15.05.18), Keith, T. A. TK Gristmill Software, Overland Park KS, USA, 2015 (aim.tkgristmill.com).